

A Curved Compliant Differential Mechanism with Neutral Stability

For the use in Exoskeleton Design

R. Mak

A Curved Compliant Differential Mechanism with Neutral Stability

For the use in Exoskeleton Design

by

R. Mak

to obtain the degree of Master of Science
at the Delft University of Technology,
to be defended publicly on Friday August 27, 2021 at 12:30.

Student number: 4380533
Project duration: Dec 1, 2020 – August 27, 2021
Thesis committee: Prof. dr. ir. J. L. Herder, TU Delft, Supervisor
Ir. A. Amoozandeh Nobaveh, TU Delft, Daily Supervisor
Dr. Ir. G. Radaelli, TU Delft, Daily Supervisor

This thesis is confidential and cannot be made public until August 27, 2023.

An electronic version of this thesis is available at <http://repository.tudelft.nl/>.

Preface

After a strange year with a lot of corona related restrictions and working from home, I am proud to be finishing my thesis project, and simultaneously my life as a student. While both my final thesis and my study in general have been at times difficult and stressfull, I have thoroughly enjoyed it. Before I make my next step as an engineer, I would like to thank a few people who have helped me along the way.

First of all, Ali, Thank you for our weekly meetings, insights, help and for always making time for my questions. Furthermore, I would like to thank Giuseppe for his knowledge during the weekly group and progress meetings. Additionally, I would like to thank all students in the shellskeleton research group for all discussions and various off-topic Zoom calls. Big thank you to all the support staff at 3ME for their help with my prototypes and experiments, in particular to Patrick van Holst and Jurriaan van Slingerland. Furthermore, I would like to thank Laevo for providing me with their expertise and help during my thesis project.

And last but definitely not least, my family, friends, and girlfriend. Thanks to my family for their love, help and support during my entire educational life, without them I would never have been where I am today. Thanks to my friends for all the fun moments, study sessions, long discussions, fun getaways, and of course support during my entire study and thesis project. And finally, Meike, who has been vital this last year, for her help, graphical knowledge, reviewing, and most importantly for always being there to support when needed.

*Robin Mak
Delft, August 2021*

In the final weeks of my graduation my beloved grandmother sadly passed away. I would like to dedicate a part of this thesis to her, to thank her for her unconditional love and support. She will be dearly missed by all.

†Alida Divera Mak-Vriend

Summary

People in healthcare, warehousing, and the agriculture sector all have one thing in common. They require labour which can be demanding on the human body, this could lead to problems in the long term. A way to alleviate these problems is to use a passive exoskeleton. While passive exoskeletons can have a variety of different use cases and types of support, this thesis will focus on a wearable passive back support. A company specialising in these passive wearable back supports is Laevo[1]. They have their own version of such a mechanism using torsional springs which are attached to the upper torso and legs. This ensures that when bending the mechanism provides support. However when walking, these springs are also activated and make walking more difficult and require more energy. A way to solve this problem is to use a differential mechanism. Such a mechanism can be quite complex and bulky and comprised of a lot of parts. A solution could be found in the world of compliant mechanisms.

The goal of this project is to create and analyse a compliant differential mechanism for use in passive exoskeleton design. As a basis for a design, the proposed mechanism by Maurice Valentijn[2] was used. The two main challenges were the location of the rotational axis and a relatively low stiffness ratio between the bending and walking scenario. While this mechanism showed potential as a compliant differential mechanism, it did have some problems which needed to be overcome before the use in a passive exoskeleton would be feasible.

The proposed design to solve these challenges consists of a thin-walled beam, with an H-shaped cross section, which has two curves forming a U-shape. By applying constraints on the sides the rotational axis of the mechanism could be changed to align with the rotational axis of the hip joint. This mechanism in combination with reintroduction of potential energy using springs to lower the stiffness of the mechanism when walking. This allowed for a design which could be used as a compliant differential mechanism in the use of exoskeleton design. To investigate the proposed design for a compliant differential mechanism, the mechanism first needs to be modelled and optimised to meet the requirements needed for the use in an exoskeleton. For the optimisation, a framework is proposed which integrates the use of a simulated Ansys model in combination with a Matlab optimisation problem. With this optimised model the behaviour of the mechanism can be analysed. The behaviour of the mechanism is investigated in the paper in Chapter 4. In this paper the simulated model is validated using an experimental setup. This paper is the main contribution of this thesis.

Findings of the paper show that the stiffness of the mechanism can be significantly reduced by reintroducing potential energy into the system to compensate the stored potential elastic energy in the material during walking. This caused the mechanism to have different types of behaviour: positive stiffness, zero stiffness, and negative stiffness. These stiffnesses depend on the initial preload of the springs, more initial preload means more energy is stored in the springs and releases more energy for the same displacement. This changes the overall potential energy to have these three aforementioned stiffness states. Zero stiffness is the most interesting for exoskeleton design, this minimises the amount of work required while walking without having bistable behaviour in the mechanism.

Finally, As a proof of concept for the mechanism a wearable exoskeleton prototype has been created to get a practical understanding of the mechanism and to find problems with the implementation of the mechanism for future works. The wearable exoskeleton prototype showed a lot of potential, the behaviour of the mechanism in the experimental setup was transferred to the prototype and low stiffness while walking was achieved without effecting the bending support.

Contents

1	Introduction	1
1.1	Compliant mechanisms	2
1.2	Exoskeleton.	2
2	Problem definition	3
2.1	Research aim	3
2.2	Requirements.	4
3	Project Layout	5
3.1	Concept design	5
3.1.1	Manufacturing of the mechanism	6
3.2	Simulated model	7
3.3	Optimisation Framework	7
3.3.1	User-based parameter optimisation	8
3.3.2	Behaviour optimisation	8
3.4	Analysis of the mechanism.	8
4	Paper	9
5	Discussion	21
5.1	Behaviour	21
5.2	Optimisation	22
5.3	Exoskeleton Prototype	22
5.4	Future Works	23
6	Conclusion	25
A	Literature Report	29
B	Concept Generation	43
B.1	Concept A.	43
B.2	Concept B.	44
B.3	Concept C	44
B.3.1	Concept C1	45
B.3.2	Concept C2	45
B.3.3	Concept C3	46
C	Additional Results	47
C.1	Linear spring validation.	47
C.2	Kinematic Performance Ratio	47
C.3	Stress concentrations	48
C.4	Result unwelded mechanism	49
C.5	Parameter variation	50
D	Exoskeleton Prototype Design	51
E	Ansys Parametric Design Language	55
E.1	Initialisation	55
E.2	Model	55
E.3	Actuation	56
E.4	Data Storage	56

F	Optimisation Framework	57
F.1	Matlab and Ansys Integration	57
F.1.1	Initialisation	57
F.1.2	Running Ansys model	57
F.1.3	Post processing.	58
F.2	Optimisation	58
G	Ansys Parametric Design Language Code	59
H	Matlab and Ansys APDL integration codes	67
H.1	Run_ANSYS.m	67
H.2	Setup_Directories.m	69
H.3	Set_Parameters_True_Scale.m	70
H.4	RUN_Scenario.m	72
H.5	Write_Parameters_ANSYS.m	73
H.6	Run_ANSYS_Batch.m	74
H.7	Load_Store_Results.m	75
H.8	Analysis.m	78
I	Optimisation Code	79
I.1	Run_ANSYS_Optimisation_bh_bw_F0.m	79
I.2	Optimization_bh_bw_same.m	81
I.3	OBJ_FUNC_Run_ANSYS_bh_bw_same.m	82
I.4	Optimization_F0.m	83
I.5	OBJ_FUNC_Run_ANSYS_F0.m	84

1

Introduction

People in healthcare, warehousing, and the agriculture sector all have one thing in common. They require labour which can be demanding on the human body. This could be by constantly having to bend over a patient during an hours-long surgery or having to lift heavy equipment in a warehouse or military cargo plane. All these cases cause stress and strain on the upper and lower back, which in the long-term could lead to chronic back problems. A way to alleviate these problems is to use an exoskeleton. While exoskeletons can have a variety of different use cases and types of support, this thesis will focus on a wearable back support.

Within these kinds of exoskeletons there are more distinctions in the way of assistance. Exoskeletons generally use either active or passive assistance methods[3]. Active assistance methods could use, for example, DC motors which require a source of energy. Passive assistance methods do not require any external power and use, for example, material compliance to provide gravity compensation. The latter is especially interesting because the lag of external energy means less weight to carry, more manoeuvrability and less maintenance such as charging.

A company specialising in these passive wearable back supports is Laevo[1]. They have their own version of such a mechanism using torsional springs which are attached to the upper torso and legs. This ensures that when bending the mechanism provides support, as can be seen by the angular displacement when bending in Figure 1.1. However an angular displacement can also be seen when walking. This means these springs are also activated and make walking more difficult and require more energy. A way to solve this problem is to use a differential mechanism. Such a mechanism could have high stiffness when the angular displacement for both legs move in the same direction, bending, while having low stiffness when the angular displacement opposes each other, walking. Such differential mechanisms can be quite complex and bulky mechanisms consisting of a lot of individual parts. A solution could be found in the world of compliant mechanisms. These compliant mechanisms are mechanisms that use elastic deformation to accomplish something useful[4]. When using a compliant differential mechanism the part count could be reduced by having a monolithic structure, which could also result in a smaller size, lower weight, and lower cost. At the time of writing, research into compliant differential mechanism is limited. Therefore, this thesis will try to create a compliant differential mechanism for use in a wearable back support. This use case does introduce some more challenges such as a rotational axis which aligns with the human body and specific loads and degrees of freedom associated with the human body.

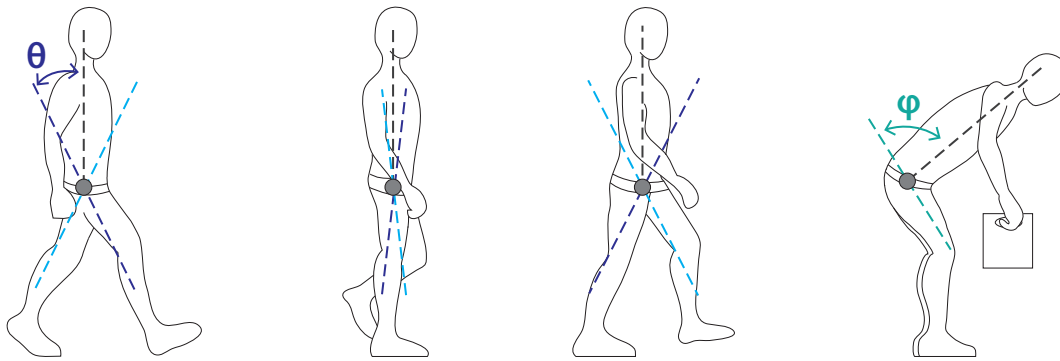


Figure 1.1: The passive exoskeleton requires a low stiffness when walking, however when bending the mechanism should provide high stiffness to support the user.

1.1. Compliant mechanisms

Compliant mechanisms are mechanisms that use elastic deformation to accomplish something useful[4]. Traditionally, when designers need movement within a mechanism, they will use stiff rigid bodies connected with hinges and sliding joints. However, when looking at nature, much more flexibility in movement can be seen, think of bee wings, elephant trunks, eels, seaweed, spines, and blooming of flowers. Very compact mechanisms using this flexible behaviour can be seen in nature. Compliant mechanisms have a lot of advantages such as significantly lower cost due to fewer parts and monolithic construction, increased precision due to reduced wear and eliminated backlash, no need for lubrication, and generally a reduction in mass and size. However, compliant mechanisms also introduce some challenges such as more difficult designing process of simultaneous design for motion and force behaviour, fatigue life needs to be addressed, the motion is often more limited than traditional rigid-link mechanisms with no continuous rotation possible, there are higher stress concentrations, and most importantly energy is stored during movement due to elastic deformation.[5].

1.2. Exoskeleton

As mentioned before assistive devices such as exoskeletons can be used in multiple situations to give mechanical benefits to the user. These mechanical benefits could be used for medical purposes for people with paralysis with complete or partially functional failure of muscular function, these exoskeletons could help or influence functional limitations or even replace lost function. They could also be used to promote muscular activity or even regain it. However, there are other uses in other sectors such as military, civilian, or industry applications. For these use cases the mechanical benefits that are provided by the exoskeleton improves the strength and endurance of the user. It can furthermore relieve the person of stresses and strains on the human body, to prevent problems later in life in, for example, the lower-back. Examples of uses of exoskeletons could be for lifting of heavy equipment for fire fighters or rescue-workers or for surgeons who have to bend over a patient during a long surgery. For exoskeletons there are generally two types of assistance, either active or passive assistance methods[3]. The first method with active assistance use, for example, DC motors, pneumatics, levers or hydraulics. All of these methods require a type of external power source. Examples of such an active exoskeleton are made by the company Atoun[6], their exoskeletons were, for example, used by volunteer at the hammer throwing and weightlifting competitions at the 2020 Tokyo Olympics. This exoskeleton uses motors and batteries to reduce the workload for the wearer. Secondly, passive assistance methods do not require any external power and use, these could for example use material compliance to provide gravity compensation. This last category is especially interesting because if used correctly, they can be much more compact, lightweight and convenient to use due to the lag of external power required. A passive exoskeleton currently on the market is one of the companies Laevo[1]. They have designed a wearable passive chest and back support for heavy labour. Their exoskeleton uses springs and pads on the legs and chest to relieve the spine and back muscles from stresses and strains. This is done by storing energy while bending and utilising this energy while standing back up. Their exoskeleton focuses on industries such as a agriculture, warehousing, healthcare, and the military.

2

Problem definition

The goal of this project is to create a compliant differential mechanism for use in passive exoskeleton design. As a basis for a design, the proposed mechanism by Maurice Valentijn[2] was used. He investigated a compliant differential mechanism using warping in thin-walled structures. When this mechanism would be actuated from one side, the mechanism would have a low stiffness and transfer an opposite angle to the other side of the mechanism, as would be required when walking. However, when the mechanism was actuated on both sides in the same direction, a much higher stiffness was observed, as would be required when bending. While this showed potential as a compliant differential mechanism, it did have some problems which needed to be overcome before the use in a passive exoskeleton would be feasible. The two main challenges were the location of the rotational axis and a relatively low stiffness ratio between the bending and walking scenario. The rotational axis around which the differential mechanism worked was located in the axial axis in the middle of the beam, this means that the mechanism would have to be inside of the human body to properly align with the rotational axis of the hip joint, this will of course not be feasible in practice. The second challenge was that while the mechanism showed a much lower stiffness in the walking scenario compared to the bending scenario, there was still significant stiffness in the mechanism for the walking scenario. In the optimal situation, the walking scenario would have zero stiffness while not effecting the stiffness of the bending scenario.

2.1. Research aim

When a design for the aforementioned challenges has been found, it has to be validated and optimised to work as a compliant differential mechanism for the use in an exoskeleton. To achieve this, the design first needs to be modelled and simulated. This simulated model can then be used to create an optimisation framework which optimises the design to be able to meet the requirements and dimensions of the intended user. This intended user could be an individual or a more general target group. When an optimal design has been found, it needs to be tested to validate its behaviour. Finally, when the design is optimised and tested, it has to be implemented in a passive exoskeleton as a proof of concept. To conclude, the research aim of this thesis is formulated as:

"Create and analyse a design for a compliant differential mechanism for the use in passive exoskeleton design"

To achieve this research aim, four research objectives are required. These objectives are defined as:

1. Find a design for a compliant differential mechanism for the use in exoskeleton design.
2. Create a framework for optimising the proposed design for the use in exoskeleton design.
3. Analyse the behaviour of the compliant differential mechanism using simulations and an experimental setup.
4. Create a physical wearable exoskeleton prototype to serve as a proof of concept.

2.2. Requirements

To realise a design, there first has to be set some requirements. These requirements are mainly obtained from Laevo and their exoskeletons, however additional literature has also been used. The first requirement is in the range of motion of the mechanism, the mechanism should be able to undergo an angular displacement while bending and walking. For walking the range of motion should be between -25° and 25° [7]. For bending, this angle is more subjective, furthermore the Moment-Angle curve is more complex due to desired nonlinear support. To achieve this nonlinear Moment-Angle behaviour, an additional mechanism is required in series with the differential mechanism. Therefore, the range of motion is less important, because this can be extended using the additional mechanism. Therefore the minimum required moment is much more important. The range of motion when bending is set to 20° , this is set as a feasible range of motion the mechanism should be able to deform. The second requirement for the mechanism focuses on the required moment for both the walking and bending scenario. For the walking scenario, the desired moment should be as low as possible. This is because due to this moment, work has to be done while walking, which costs energy and is not desirable. According to Laevo the maximum desirable moment while walking is 5 N m within the aforementioned range of motion while walking. For the bending scenario, this is the moment that generates the support while bending, this is the moment after an angular displacement of 20° . This minimum bending moment should be within 25 N m and 50 N m and is based on personal preference. For this design, the chosen minimum bending moment is set to 30 N m, at 20° degrees of angular displacement. Another requirement is that the rotational axis of the mechanism is aligned with the rotational axis of the human hip-joint. This ensures that the mechanism works properly with the human body and no discomfort is caused by misalignment of the exoskeleton.

Finally, the requirement for the size of the mechanism depends on the human sizes. Measurements from an individual can be used to for the optimisation to optimise the mechanism for the preferred bending moment. The most important measurements are the hip breadth and hip depth, which can be used as input parameters to optimise the mechanism. Therefore, it is required that the mechanism is wider and deeper than the measured hip breadth and hip depth, for the mechanism to be outside of the body. Furthermore, the size of the mechanism should be as compact as possible to not hinder the user in their movement.

Besides these requirements there were a few more factors which needed to be considered for the design. One of these considerations is regarding manufacturing of the mechanism. Compliant mechanisms can be challenging to produce, therefore this needs to be considered for the design. It would be preferred that the mechanism would be manufactured with conventional fabrication methods and be able to be produced on a relatively large scale and for a reasonable cost. This would for example, exclude additive or subtractive manufacturing, such as 3D printing and CNC machining, as fabrication methods due to their high cost and slow process.

3

Project Layout

This chapter will explain the layout of the project. The main contribution of this thesis is the investigation into the behaviour of a compliant differential mechanism. However, to investigate the behaviour first a mechanism needs to be developed, modelled and finally optimised to have the desired behaviour. These factors will briefly be explained in this chapter with more information in the appendices. Finally the behaviour of the mechanism will be analysed using a combination of simulations and an experimental test setup. This analysis can be found in the paper in Chapter 4.

3.1. Concept design

To find a suitable design which fulfilled the requirements set in Chapter 2 multiple designs have been considered, a selection of these concepts can be found in Appendix B. While a few concepts showed potential, one mechanism was chosen as the final design for solving all challenges and showing great potential for user-based parameter optimisation and manufacturability. The chosen design for a compliant differential mechanism for the use in exoskeleton design can be split-up into two sub-solutions. The first sub-solution consists of a solution to change the rotational axis of the differential mechanism proposed by Maurice Valentijn. A solution for this could lay in compliant remote center of motion mechanisms, these mechanisms were further investigated in Appendix A. The final solution to change the rotational axis is to implement two curves in the mechanism to make the mechanism wrap around the human body. To ensure the rotational axis aligns with the hip joint, a constraint is applied on the two sides which are in line with the hip joint. These constraints allow translation on the same axis as the rotational axis of the hip joint. This allows the mechanism to rotate around the same axis as the human hip joint as can be seen in Figure 3.1 and Figure 3.3a. The second sub-solution reduces the stiffness of the walking scenario of the mechanism. This is solved by reintroducing energy to compensate for the storage of potential elastic strain energy in the mechanism during actuation. This reintroduction of

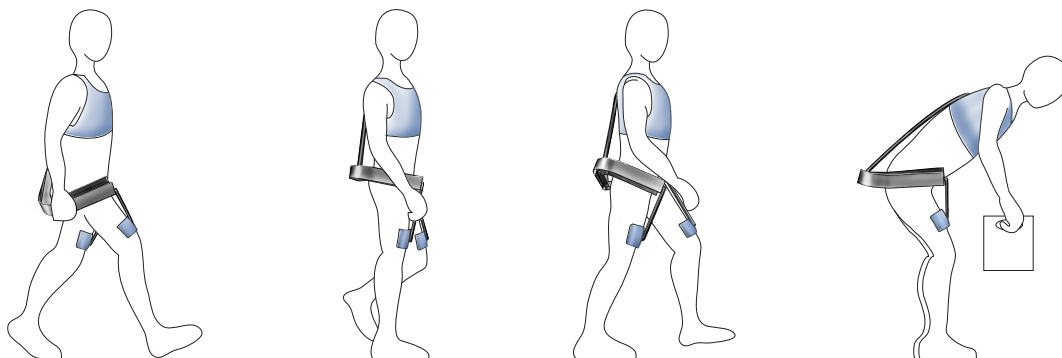


Figure 3.1: The proposed compliant differential mechanism used as a passive exoskeleton, it can be observed that the rotational axis of the mechanism aligns with the rotational axis of the hip joint.

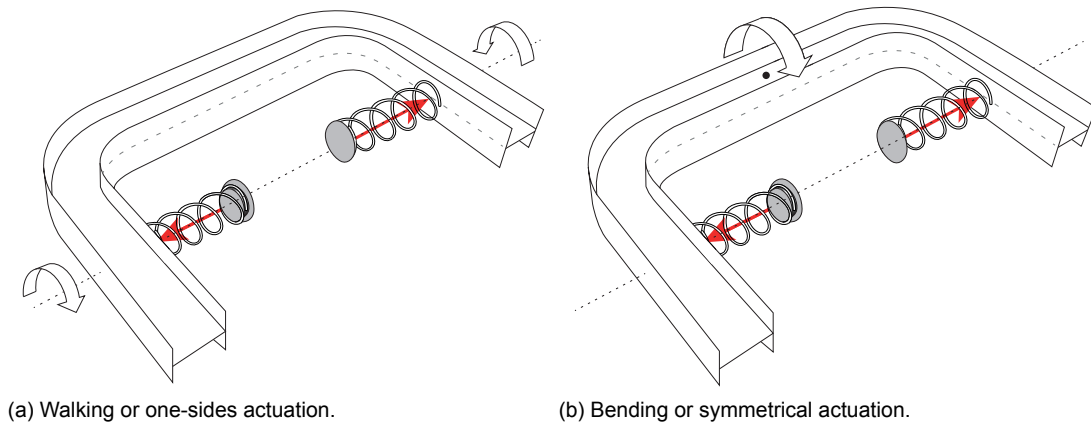


Figure 3.2: The two different scenarios for actuation of the mechanism.

energy requires a source of potential energy, the proposed solution is to use springs. These springs could be prestressed and placed on the inside of the mechanism as shown in Figure 3.2. When the mechanism is asymmetrically actuated, as shown in Figure 3.2a, the springs will be decompressed and will release potential energy into the system to compensate for the potential elastic strain energy of the mechanism. If this reintroduced energy matches the stored potential elastic strain energy in the system, the mechanism will have a constant potential energy while actuating. This will make the system neutrally stable and have zero stiffness. For the bending scenario, the springs' decompression is negligible and therefore not releasing potential energy. This concept of reintroduction of potential energy will be further explained in the paper of Chapter 4.

These two sub-solutions create a design which consists of a symmetrical thin-walled beam with an H-profile cross section with two curves, as can be seen in Figure 3.2. The behaviour of the mechanism is investigated in the paper, found in Chapter 4.

3.1.1. Manufacturing of the mechanism

Manufacturing of compliant mechanisms can be challenging due to their often complex form factor and specific requirements for material properties. This was also the case for this compliant differential mechanism. For the manufacturing of the mechanism, it was important that it would be fabricated from a material with a high yield strength to allow for the large deformations which the mechanism experiences. Furthermore, it was desired to use relatively simple fabrication methods with a low cost. As discussed in the requirements, manufacturing methods like adaptive manufacturing or subtractive manufacturing were not an option due to their high cost and lag of scalability for larger production numbers. Therefore the complexity of the mechanism was also limited to traditional manufacturing methods. The fabrication method which showed the most promise was a combination of using spring-steel sheets and lasercutting. This method allowed the web and flanges of the mechanism to be cut from a flat sheet of spring-steel. Then the curves in the flanges needed to be made, these are created by plastically deforming the flat flanges to make sure no residual stresses are present in the material. These residual stresses could interfere with the behaviour of the mechanism. For the connection between the web and the flanges, two methods are used. The first fixation method uses slits and wedges in the web and flanges, this allows for correct alignment and forms a fairly rigid connection. This method was sufficient for the walking scenario, however this was not a sufficient connection for the bending scenario. For this reason spot-welds are introduced between the web and the flanges, this creates a rigid connection while minimising the amount of added material and limiting the heat affected zones created by the high temperature of the welds. However a method like laserwelding would have been preferred due to its localised heat and minimising the amount of added material while having a continuous connection. This fabrication method of a combination between lasercutting and welding would be a viable method of production for this compliant differential mechanism on a larger scale due to the efficient material use and common production methods.

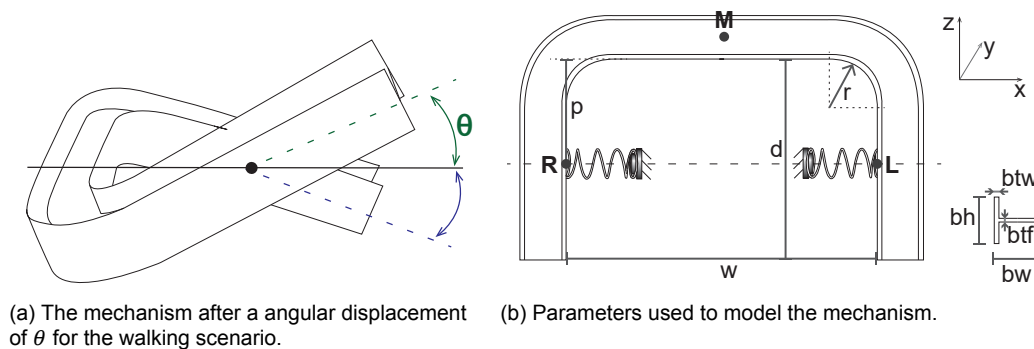


Figure 3.3

3.2. Simulated model

With the chosen design the next step can be taken. For the validation of the behaviour of the mechanism, user-based parameter optimisation, behaviour optimisation of the mechanism, a model needs to be created to simulate the behaviour of the mechanism for different parameters. The software chosen to model and simulate the behaviour of the mechanism is Ansys Parametric Design Language (APDL). The main advantage of APDL is that the mechanism can be modelled using a scripting language and can be made parametric. This ensures maximum control over the simulations and allows for running the simulation with different parameters using Matlab, which is required for optimisation. The Ansys model can be found in Appendix E.

As mentioned the simulated model is constructed to be fully parametric and in the Ansys Parametric Design Language. The parameters of the parametric model are directly controlled from Matlab, this allows for the optimisation using the model. The parameters which can be varied are shown in Figure 3.3b. For the simulated model, a static analysis with large deflection effects included is used in combination with a shell model to simulate the behaviour of the mechanism. A shell model was chosen because a beam model was deemed not suitable due to the geometry and highly non-linear behaviour of the mechanism. Furthermore, a solid model was too computationally expensive for the use in an optimisation problem. The shell is meshed using 8-nodal SHELL281 elements, these elements consist of 8 nodes with each 6 degrees of freedom and is well-suited for linear, large rotation and/or large strain nonlinear applications. 8-nodal SHELL282 elements gave more consistent results than its 4-nodal SHELL181 elements counterpart and was therefore used. The model is modelled by sweeping the cross section around a path, which forms 3 surfaces. These surfaces can be converted to shells by inputting the shell-thicknesses, direction of the thickness and the offset from the surfaces. The constraints are applied to the nodes at the locations of points R, L, and M. The actuation for the walking scenario of the mechanism is preformed by adding a rotation to the centerline of nodes around point R. The preloading of the mechanism is applied by having two forces on points R and L in opposite directions, the force on point R in the positive X direction, and the force on point L in the negative X direction. This force can either be constant or simulating a linear spring in accordance with Hooke's law based on the U_x displacement of points R and L.

3.3. Optimisation Framework

One of the objectives was to create a framework which can be used to optimise various properties of the mechanism, by implementing a method of using Matlab and Ansys together to optimise using Matlab and use Ansys for simulating the behaviour. This framework for both optimisations are the same and works by varying the parameters of the Ansys simulation in an optimisation problem in Matlab. This framework is further explained in Appendix F. The optimisation of the mechanism can be divided into two separate optimisation problems. The first optimisation is the user-based parameter optimisation, this optimisation optimises the mechanism to have the desired fit and behaviour for the user. The second optimisation for behaviour optimisation is to optimise the preloaded spring in such a way that the mechanism is tuned to be neutrally stable and have zero stiffness, and thus minimise the energy required when walking. For the optimisation problem in Matlab the `fmincon` function is used, this

function is for finding the minimum of constrained nonlinear multi-variable problems. The algorithm used for this problem is interior-point. The main difference between the two preformed optimisations is the difference in design parameters and objective functions. These optimisation problems are run independent and sequentially. The input parameters for both optimisations are the same, they consist of the hip breadth, hip depth, and desired bending moment.

3.3.1. User-based parameter optimisation

Exoskeletons are used by a variety of people with different sizes, needs, and preferences, therefore it is required that a method of user-based parameter optimisation is created. This method can optimise the mechanism to have correct dimensions to fit a specific user or a specific target-group with similar sizes and needs. In this optimisation problem, the bending moment is optimised. The design parameters for this problem are bw and bh , these parameters can be used to change the bending behaviour of the mechanism. The objective function for the mechanism is a weighted function of both the root-mean-square error (RMSE) of the walking moment and a penalty function for the required bending moment. The RMSE is used to approximate zero stiffness at $\theta = 0$. A penalty function is used to constrain the lifting moment to fit the desired bending moment. This method minimises the required energy during walking while being constrained to the required minimum bending moment.

3.3.2. Behaviour optimisation

The second optimisation is regarding the stiffness of the mechanism, by optimising the springs to minimise the stiffness of the mechanism during walking. This optimisation is performed after the user-based parameter optimisation and optimises the prestress in the springs to control the reintroduction of the potential energy for the optimised mechanism. This optimisation used the same simulated model and framework to optimise. As the objective function, the RMSE to approximate zero stiffness at $\theta = 0$ was used, the initial preload of the spring was used as a design parameter. This initial preload of the spring corresponds to the initial prestress of the spring and thus the amount of stored potential energy, this also regulates the amount of energy released for a given angular displacement.

3.4. Analysis of the mechanism

With the found design and supplementary optimisation framework it is possible to create a mechanism with desired dimensions and behaviour. The validation and analysis of the behaviour of the mechanism is preformed in a paper format. This paper will focus on the mechanism itself without the focus on the use in exoskeleton design. In the paper the parameters used to optimise the mechanism are based on anthropometric data from DINED[8] with dataset "Dutch adults, dined2004". Input parameters for hip depth and hip breadth arbitrarily chosen around 50 percentile of age group 20-60 years. The used parameters and the optimised values for the mechanism can be found in the paper. In the paper the behaviour of the mechanism will be analysed using the simulated model from Ansys APDL and an experimental test setup. The paper for the analysis of the mechanism can be found in Chapter 4.

4

Paper

In this chapter, the main contribution of this thesis is presented in a paper format. This paper will analyse the behaviour of the found design for a compliant differential mechanism. The paper can be viewed as a stand-alone research for a wider range of applications. The parameters used for the design are however chosen for the research purpose of this thesis with the accompanied requirements. The mechanism will be investigated using both simulations using Ansys and an experimental test results. In the discussion, in Chapter 5, of this thesis the findings of this paper will be linked to the use in exoskeleton design.

A Curved Compliant Differential Mechanism with Neutral Stability

Robin Mak¹, Ali Amoozandeh Nobaveh, Giuseppe Radaelli and Just Herder

Abstract—A compliant differential mechanism is presented, using the reintroduction of potential energy to compensate for the potential elastic strain energy stored in the material when actuated. This mechanism has a high rotational stiffness when the mechanism is symmetrically actuated, while having a low rotational stiffness when actuated on one side. For the storage of potential energy, two linear springs were used. The rotational stiffness of the one-sided actuation stage around the neutral position of the compliant differential mechanism is hypothesised to be adjustable to have positive stiffness, zero stiffness, and negative stiffness. This would indicate that the mechanism can have neutral stability and bistability. The hypothesis is tested using a simulated model in Ansys Parametric Design Language using optimised parameters to achieve the desired stiffness for the mechanism. The simulated model is validated using an experimental setup for both the one-sided and symmetrical actuation stage. The experimental results showed a high correlation between the simulations and the experimental tests. The mechanism showed near zero stiffness and neutral stability for an optimised initial preload for a range of 16° . Negative stiffness and bistability was found for initial preloads higher than the aforementioned optimised initial preload. A linear trend was found between the initial preload of the springs and the rotational stiffness at $\theta = 0$. Furthermore, a kinematic performance ratio above 0.97 was found for the simulated results, with the experimental results showing a kinematic performance ratio of 0.95. The analysed mechanism met all requirements and showed high potential as a compliant differential mechanism.

Index Terms—Compliant Differential Mechanisms, Exoskeleton, Neutral stability, Bistability, Zero Stiffness

I. INTRODUCTION

The first recorded instance of a differential mechanism being used in a mechanism has been over 2000 years ago in the Antikythera Mechanism using differential gears[1]. The differential mechanism was used to determine the angle between the ecliptic positions of the sun and moon. Other uses for differential mechanisms in history are for the use as a compass around 250 AD by engineer Ma Jun[2], or by Clockmaker Joseph Williamson in a clock mechanism. One of the most known uses for differential mechanism are as an automobile differential which was invented by the Onésiphore Pecquer in 1827[3]. In this long history of differential mechanism, only conventional mechanisms using predominately gear were found. Only one compliant differential mechanism by Valentijn was found. He used a thin-walled warping beam to create differential behaviour in his mechanism[4]

Compliant mechanisms are mechanisms that use elastic deformation to accomplish something useful[5]. Traditionally, when designers need movement within a mechanism, they will use stiff rigid bodies connected with hinges and sliding joints. However, when looking at nature, much more flexibility in movement can be seen, think of bee wings, elephant trunks, eels, seaweed, spines, and blooming of flowers. Very compact mechanisms using this flexible behaviour can be seen in nature. Compliant mechanisms have a lot of advantages such as significantly lower cost due to fewer parts and monolithic construction, increased precision due to reduced wear and eliminated backlash, no need for lubrication, and generally a reduction in mass and size. However, compliant mechanisms also introduce some challenges such as more difficult designing process of simultaneous design for motion and force behaviour, fatigue life needs to be addressed, the motion is often more limited than traditional rigid-link mechanisms with no continuous rotation possible, there are higher stress concentrations, and most importantly energy is stored during movement due to elastic deformation[6]. The last point also means that energy is required to move the mechanism, which is not preferred in most cases.

A way to have the benefits of a compliant mechanism but eliminate the stored energy during movement is to make the mechanism neutrally stable. A method of making a mechanism neutrally stable is to reintroduce energy into the energy stream between the input and output of the system[7]. If the input and output energy of the mechanism are the same over a range of motion, the potential energy will be constant with initial assumption that the system is isolated and conservative[8]. Another way to describe this behaviour is a mechanism undergoing elastic deformation without requiring external work[9]. Several equivalent descriptions for this behaviour exist, such as, neutral stability, continuous equilibrium, constant potential energy or zero stiffness[9]. However the zero stiffness description is only valid if the potential energy in the system is constant along a certain trajectory. Only having zero stiffness over a certain trajectory is not a sufficing condition because zero stiffness also represents systems with a constant force, which has a linear potential energy function[8]. Stiffness is the second derivative of the potential energy or the first derivative of the force-displacement or Moment-Angle curve. When looking at the stiffness of a mechanism there are three different cases, firstly there is positive stiffness, this is the behaviour expected for an elastically deforming structure without any compensation, more displacement generates more potential elastic strain energy. Secondly, there is zero stiffness,

¹Department of Mechanical Engineering at Delft University of Technology
r.mak@student.tudelft.nl

as discussed previously for this case a constant force is required to elastically deform the mechanism. Finally, there is negative stiffness, in this case there is an unstable equilibrium point. This is a peak in the potential energy curve and is also accompanied by two local minima, this indicates bistable behaviour.

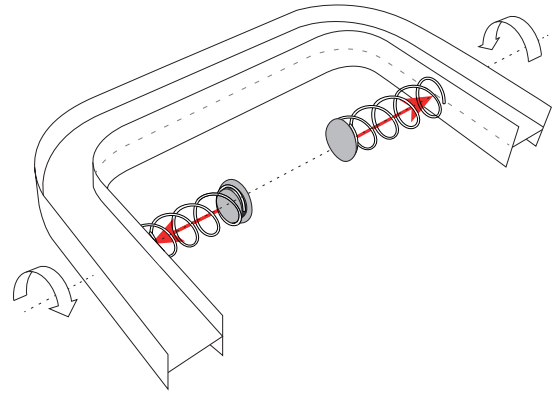
There are multiple ways to store the potential energy in a system to compensate the elastic strain energy. This could be by creating prestresses in the material, prestressing an added compliant element or by adding an external prestressed compensation device using conventional features such as links and springs[10]. An example of prestress in the material of the mechanism itself has been done by Lachenal et al., he prestressed the flanges of an I-beam to store potential elastic strain energy in the material[11]. A mechanism which uses an external prestressed compensation device is proposed by Herder and van den Berg, he added a rolling-link spring mechanism to a compliant laparoscopic grasper to eliminate the stiffness in this compliant grasper[10]. This idea was further developed by Stapel and Herder he proposed preloaded compliant flexures to reduce the stiffness of the aforementioned compliant laparoscopic grasper[12]. While storage and reintroduction of potential energy find zero stiffness has been used before, it has not been used in a compliant differential mechanism.

This paper will try to fill the gap of research into compliant differential mechanisms. A compliant differential mechanism is purposed in combination with stiffness reduction by reintroduction energy to compensate the potential elastic strain energy storage during actuation. The reintroduction of energy changes the stiffness of the mechanism from positive stiffness to zero stiffness or negative stiffness. The behaviour of the mechanism will be analysed and tested using optimisation and simulations. Furthermore the simulated results will be validated using an experimental setup with a physical prototype.

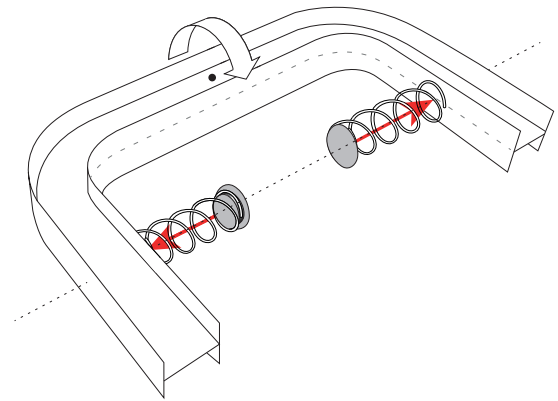
In Section II the working principle and intended application of the mechanism will be explained. In Section III the used model is explained and how the experiment to validate this model was executed and how the model is created to simulate the expected behaviour. In Section IV the results from both the simulations and experimental setup will be shown and will be discussed in Section V. Finally in Section VI a conclusion will be drawn from the results.

II. WORKING PRINCIPLE

The compliant differential mechanism this paper will focus on can be seen in Fig. 1. The mechanism works by having 2 springs pushing outwards on the inside of the U-shaped open section thin-walled beam. While actuating the mechanism on one side, a opposite rotation on the other side of the mechanism is generated. This one-sided actuation can be seen in Fig. 1a and Fig. 2. During this actuation the springs are decompressed and transferring the potential spring energy into the mechanism. The springs are aligned with the rotational axis of the mechanism, in this way the springs only experience compression and decompression without any translation or



(a) One-sided actuation scenario.



(b) Symmetrical actuation scenario.

Fig. 1: A schematic view of the researched solution for a compliant differential mechanism with energy compensation to reach zero stiffness and neutrally stable behaviour. The dotted line indicates the rotational axis of the mechanism and the arrows show the opposite rotation around this axis for the one-sided actuation scenario.

bending in other directions. The transfer of energy causes the energy required to actuate the mechanism to be lower, and in that way lowers the rotational stiffness of the mechanism while being actuated only on one side. The other behaviour is a high rotational stiffness when the mechanism undergoes symmetrical actuation. This symmetrical actuation can be seen in Fig. 1b. This mechanism has the interesting behaviour of working like a differential mechanism with a low stiffness transfer of motion from one side of the mechanism to the other, while having a high stiffness when the mechanism is actuated from both sides in a symmetrical way.

The mechanism is hypothesised to work in a way where the potential elastic strain energy is compensated with a source of potential energy. When the mechanism is one-sided actuated the springs are decompressed, the potential spring energy is released and transferred into the mechanism due to the conservation of energy in an isolated and conservative mechanical system [8]. This changes the total potential energy

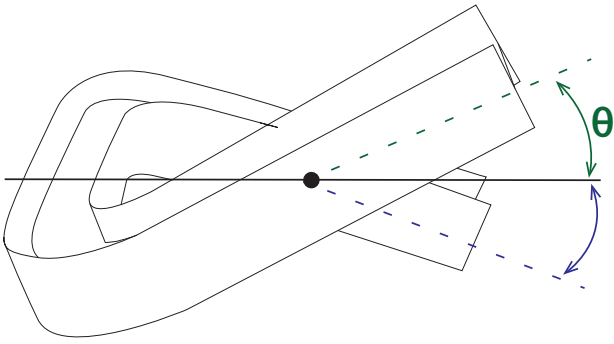


Fig. 2: A side view of the one-sided actuation, θ indicates the angular displacement of the input. The transfer of motion can also be observed on the opposite side of the mechanism.

of the mechanism. If the system is assumed to have these conditions, the total potential elastic energy of all components would then be expected to look like Fig. 3, the green line is the potential elastic strain energy of the mechanism, the blue line is the potential spring energy of the two springs, the total potential energy can be found by the summation of both the potential energy of the beam and the potential energy of both springs, the total potential energy is illustrated by the red line, for which a constant total potential energy can be observed for a range of motion. This constant potential energy can be categorised as neutral stability. The second derivative of the potential energy is the stiffness, thus when the potential energy is constant, the stiffness and actuation force of the mechanism will be zero. This makes the mechanism a zero stiffness mechanism. Due to the constant potential energy, the work required over this range would also be zero.

If the source of potential releases more energy than required to compensate potential elastic strain energy a different behaviour will be observed, this will create a peak in the potential energy with two minima on each side. This behaviour would be classified as a bistable system, with two stable equilibriums at the two local minima and an unstable equilibrium at the peak of the potential energy. This unstable equilibrium indicates a negative stiffness when the potential energy is differentiated twice. This bistability can be used to lower the overall required work to actuate the mechanism over a larger range.

This would indicate that three different states can be achieved. A state with positive stiffness when no or non-sufficient energy compensation is used. A state with zero stiffness and neutral stability when a constant potential energy is reached when the potential elastic strain energy is perfectly compensated. And lastly, a state with negative stiffness and bistability, when the stored potential energy released is larger than the potential elastic strain energy required to actuate the mechanism. The released energy is a function of the initial preload and the decompression of the spring. If outward deformations of the mechanism due to the preload force are small compared to the displacement of the mechanism due to actuation, it can be concluded that the rotational stiffness of the

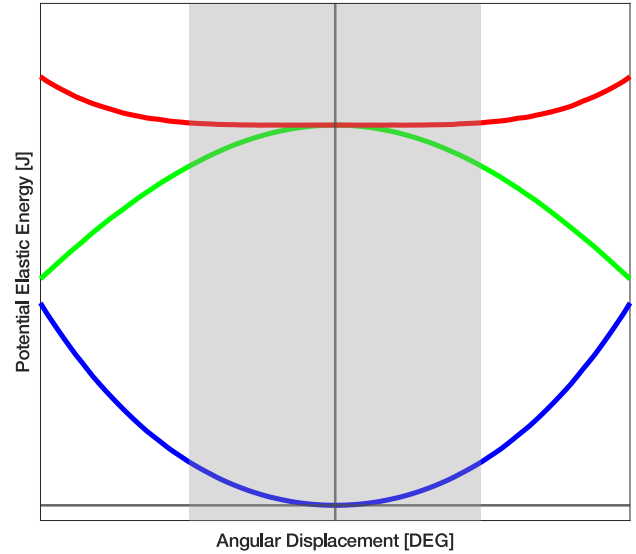


Fig. 3: The hypothesised total potential elastic energy of the mechanism (Red) for the neutral stable mechanism, this is a summation of the preloaded elastic energy of the beam (Blue) and potential spring energy of the springs (Green). The range of motion with a constant total potential energy is shown in gray.

mechanism is a direct function of initial preload of the springs. Because the energy released is a function of the decompression of the spring and the initial preload of the spring.

This behaviour of varying the stiffness of the mechanism and especially the zero stiffness of neutrally stable state will be further investigated in this paper and will be tested on a physical prototype. The two interesting parts of this behaviour are the ability to vary the stiffness of the mechanism and create neutral stability and zero stiffness.

The original design purpose of this compliant differential mechanism was for the use in a passive exoskeleton as a back support. For this use case, it is required that the mechanism has low stiffness when walking, or one sided actuation, but has a high stiffness when bending for the needed support. A mechanism which can be used to create this behaviour is a differential mechanism. The bending scenario is when a person bends, and thus actuates both sides, a symmetrical actuation. Furthermore, for this use case, it is required that the mechanism would wrap around the human body but still have a rotational axis which aligns with the rotational axis of the human hip joint. Therefore, a U-shaped beam is chosen with constrains on the side of the human hip to create a rotation axis around these constrains. In this research this application was chosen as basis for all parameter, requirements and optimised values. The parameters are therefore arbitrarily chosen around human-sizes and can be changed to suit other applications as needed.

III. METHOD

The mechanism which will be examined consists of a thin-walled beam, with an H-shaped cross section, which has two bends forming a U-shape geometry. The mechanism can be found in Fig. 1 and Fig. 4. A Force is applied to the inside of the mechanism at points L and R using two springs. The goal is to research and analyse the neutral stability and bistability behaviour of the mechanism, and the variability of stiffness due to the reintroduction of potential energy. Furthermore, to find the characteristics and performance of this mechanism as a compliant differential mechanism. This will be analysed using simulations and experimental results for various initial preloads.

A. Requirements

The mechanism is subjected to the requirements which are set for the aforementioned case of a passive exoskeleton. For this case, the one-sided actuation is used for walking and the symmetrical actuation is used as a support for bending. In this research, the minimum moment for symmetrical actuation is set to 30 N m after 20° of angular displacement. For the one-sided actuation scenario, the maximum moment should be lower than 5 N m with a range of motion of 50°, between -25° and 25°. Furthermore, the mechanism should be as compact and lightweight as possible to not limit the user of the passive exoskeleton in its movement.

B. Geometry

The geometry of the mechanism can be found in Fig. 4, the mechanism consists of a U-shaped beam with an H-shaped cross section. The cross section of the beam was chosen to be an H-shaped, this cross section was chosen for its relatively low torsional stiffness and high bending stiffness, these two combined were found to be best suited. A C-shaped and I-shaped cross section were considered, but were found to be less reliable in simulations and seemed to perform less in general. Some tests were performed on a cross section with a warping constant which approaches zero, a closed box section, however this did not show the desired behaviour. Because of this, it was concluded that a cross section was required which had a low torsional stiffness, a high bending stiffness, and a high warping constant. A H-shaped cross section met these criteria. The mechanism is constraint at only 3 points which each constraining 2 degrees of freedom, thus a total of 6 degrees of freedom are constraint, which makes the mechanism iso-constrained. The location of the constraints are symmetrical and located at points R, L and M as seen in Fig. 4. Points R and L both constrain the mechanism to move in the Y and Z direction and thus only allow translation in the X direction while allowing rotation around all axes. Point M is constrained in the Y and X directions and thus allows translation in the Z direction while allowing rotation around all axes. These constraints are the same for all scenarios. The preload force is applied to points R and L in opposite directions in the X direction. The preload force is created by a compressed linear spring.

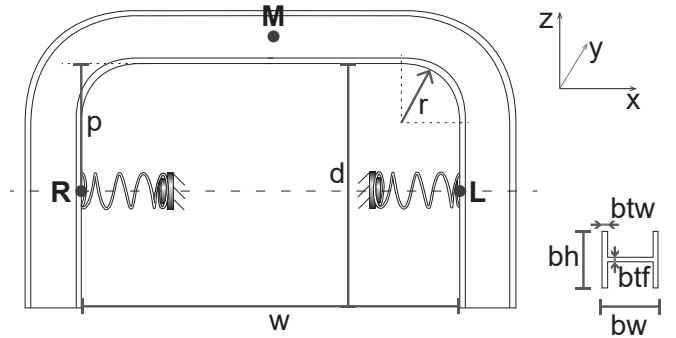


Fig. 4: The compliant differential mechanism investigated in this research is shown with the used parameters. The location of the applied spring force is also shown.

C. Parameters

The parameters used for this research have been chosen for the use in a passive exoskeleton and are stated in Table I. They have been chosen based on literature and optimisation using simulations in Ansys, with finite element solvers. The width and depth of the mechanism have been obtained using anthropometric data from DINED[13] with dataset "Dutch adults, dined2004". w was obtained by taking a hip breadth of 400 mm plus two times 25 mm for the preloaded springs. p was obtained by taking half of the abdominal depth, which is chosen to align with the rotational axis of the hip joint. The hip breadth and abdominal depth was arbitrarily chosen around 50 percentile of age group 20-60 years. These could be approximated because the goal of the project was to optimise the mechanism for these two input parameters. For radius of the two curves, R , early tests found its contribution to the behaviour of the beam to be rather small and outside of the scope of the research. Therefore R was not varied in this research, and has been arbitrarily chosen to follow the shape of the human body. bw and bh are the height and width of the H-profile cross section. These were obtained using an optimisation problem in Matlab, which will be further explained in section III-D2. For this research, the thickness of the web and flanges have been chosen to be equal. The thickness has been found by manual optimisation with readily available stock material thicknesses. A thickness of 0.8 mm was found to be best suited for the chosen design parameters and requirements. Finally, the spring used to apply the preload to the mechanism is also chosen by having a spring which would be able to apply the required force F_n , free length L_n and a spring constant c which is as high as possible to approximate a constant force. A spring which met the right condition was chosen.

For the material AISI 301 or EN 1.4310, which is a hardened austenitic chromium-nickel stainless steel. The spring steel used in this research has a Youngs modulus E of around 190 GPa with an ultimate tensile strength between 1300-1500 N mm⁻².

TABLE I: Parameters used in this research.

Parameter	Symbol	Value
Inside Width	w	450 mm
Inside Depth	d	160 mm
	p	125 mm
Curve radius	r	25 mm
H profile height	bh	34 mm
H profile width	bw	34 mm
Web Thickness	btw	0.8 mm
Flange Thickness	btf	0.8 mm
Density	ρ	7880 kg m ⁻³
Poisson ratio	ν	0.275
Youngs modulus	E	190 GPa
Free spring length	L ₀	86.6 mm
Maximum spring force	F _n	102 N
Spring constant	c	1.49 N mm ⁻¹

D. Modelling

For modelling the mechanism Ansys Parametric Design Language (APDL) is used. The main advantage of this program is that the mechanism can be modelled using a scripting language and can be made a parametric model. This ensures maximum control over the simulations and allows for running the simulation with different parameters using Matlab. By using an integration of Ansys and Matlab, it is possible to run the Ansys model in an optimisation problem to optimise the model for given input parameters and requirements of the mechanism.

The model is simulated in Ansys Parametric Design Language using Finite Element Modelling(FEM). The model is fully parametric and is fully constructed in the APDL scripting language. For the simulation, a static analysis with large deflection effects included is used. A shell model is used to simulate the behaviour of the beam. A shell model was chosen because a beam model was deemed not suitable due to the geometry and highly non-linear behaviour of the mechanism. The solid model was too computationally expensive for the use in an optimisation problem. The shell is meshed using 8-nodal SHELL281 elements.

The constraints are as aforementioned and applied to the nodes at the locations of points R, L, and M on the shell. The preloading of the mechanism is performed by having two forces on points R and L in opposite directions, the force on point R in the positive X direction, and the force on point L in the negative X direction. This force can either be constant or simulating a linear spring in accordance with Hooke's law based on the U_x displacement of points R and L.

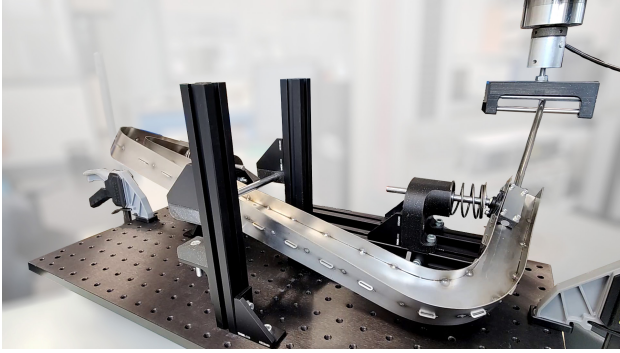
1) *Measurement:* The modelled mechanism can be actuated in two different ways for the one-sided actuation and the symmetrical actuation scenario. For the one-sided actuation scenario, a rotation is applied to a line of nodes on the left inside of the mechanism, this line of nodes spans 25 mm in both directions of the Z-axis with point R in the middle. For the symmetrical actuation scenario, a line of nodes spanning a line in the Z direction at point M in the web. For both scenarios the rotation is around the X-axis. To obtain the Moment-Angle and Potential Energy-Angle curves, the required moment to actuate the mechanism a predefined angle has to be calculated.

This will be performed for both the one-sided actuation and symmetrical actuation scenario. The one-sided actuation moment is calculated in the simulations by measuring the reaction forces on point M. With the known distance from point R to M, this accounts for a change in distance in the deformed state, the moment around the rotational axis between points R and L can be calculated. For the symmetrical actuation scenario, a similar approach is taken, however for this scenario the reaction forces on point R and L are measured and converted to a moment around point M. The reaction forces can directly be exported from the simulations. To calculate the potential energy at a given angle, a cumulative trapezoidal numerical integration is used. This approximates the area under the Moment-Angle graph to approximate the potential energy in the mechanism calculated from the neutral position at $\theta = 0$. The rotational stiffness of the mechanism is calculated by differentiating the Moment-Angle curve, the focus of this rotational stiffness will mainly be on the rotational stiffness at $\theta = 0$. The compliant differential mechanism has a difference in input angle and output angle, where the input angle is the actuated side of the mechanism and the output angle is the angle of the unactuated side, as can be seen in Fig. 2. In this research, the ratio between input and output angle will be defined as the kinematic performance ratio. To calculate this kinematic performance ratio of the compliant differential mechanism, the angle of both the actuated side and the unactuated side are measured. These angles are plotted against each other to find the correlation. From these data points, a linear regression is taken, for which the slope of this linear regression approximates the average kinematic performance ratio over the complete range of motion.

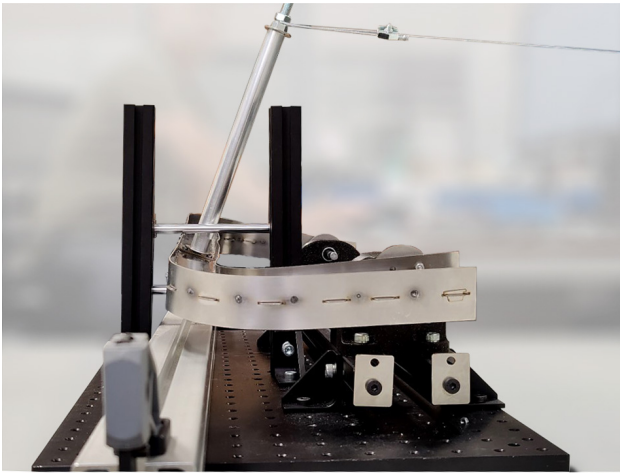
2) *Optimisation:* As discussed previously, the values of bw , bh and the initial preload to achieve neutral stability are found using optimisation in Matlab. This was performed by Matlab running the Ansys model with different parameters. As the objective function a weighted function of both the root-mean-square error (RMSE) of the one-sided actuation moment and a penalty function for the required symmetrical actuation moment is used. The RMSE is used to approximate zero stiffness at $\theta = 0$. The penalty function is used to constrain the lifting moment to fit the desired symmetrical actuation moment. Sequentially, the initial preload of the spring was optimised using the same RMSE to find the initial preload for which zero stiffness is achieved and thus neutral stability.

E. Experimental Validation

1) *Physical Prototype:* The physical prototype is constructed with a hardened stainless steel spring steel with the properties mentioned in section III-C. The thickness and properties of the material are in accordance with the simulated model. The material is laser cut with slits and wedges in the web and flanges to allow for alignment and fixation of the web and flanges. While this gives a fairly rigid connection, it does not fully fixate the web and the flanges similar to the model. Therefore spot-welds are introduced to fixate the web and the flanges. A fully welded connection between the web



(a) Experimental setup for one-sided actuation.



(b) Experimental setup for symmetrical actuation.

Fig. 5: The experimental setup used to validate the simulated results for both the symmetrical actuation and one-sided actuation scenario.

and flanges was not chosen because of several reasons, such as the added material with different material properties and the change of the material properties in the heat affected zone of the welded locations. Therefore the spot-welds were chosen to minimise the added material and heat affected zone.

2) *Experimental setup:* The experimental setup in Fig. 5 consists of the mechanism attached to two axes on linear sliders which constrain the translation in the Y and Z direction of point R and L. To make sure the constraint points are still allowed to freely rotate in all directions, a ball joint is used at the contact point between the axis and the inside flange of mechanism. The preload force is applied to the mechanism using 2 springs which are attached to the two axes, this applies the force directly to the ball joint to match the simulated model as close as possible. The constraint at point M is only constrained in the Y Direction, contrary to the simulated model which was also constrained in the X direction. However this constraint was not required for the experimental setup due to the springs constraining the mechanism, which restricted point M from moving in the X direction.

3) *Measurement:* To measure the Moment-Angle curve a tensile testing machine is used to actuate one side of the mechanism using a rod attached to the flanges and the web on one side of the mechanism, as shown in Fig. 5a. The tensile testing machine operates at a speed of 200 mm min^{-1} . The measurement is performed by actuating the mechanism to 25° and then to -25° before returning to 25° . The cycle is repeated 2 times for both sides of the mechanism to check for repeatability and to get more data-points for a smoother and more accurate result. The measured force and displacement can be converted to a moment and angle with the known length and displacement of the actuation rod. The potential energy required can be calculated with the same method as for the simulated results. The effect of the weight of the actuation rod can be compensated for in the data processing with the known length, weight, and angle of the rod. Due to the coulomb friction in the constraints such as the ball joint and the linear bearings, there is a hysteresis loop which centres around the predicted Moment-Angle curve, as can be seen in Fig. 6 in gray. The predicted true Moment-Angle curve can be subtracted from the hysteresis loop by averaging the higher and lower moments of the loop for each angle, this should be a close estimation if the mechanism is symmetrical and friction in both directions is assumed to be the same. To measure the symmetrical actuation scenario a rod is attached to the middle of the web at point M. A force is applied to this rod which causes a moment on the beam at the point of attachment, this force is applied using the tensile testing machine and a cable, as can be seen in Fig. 5b. This force and displacement can be converted to a moment and angle respectively. The springs used are also tested to see if the springs are similar to the modelled linear springs following Hooke's law, this test is performed using a tensile testing machine. Finally to calculate the kinematic performance, an extra rod is attached to the unactuated side of the mechanism to better visualise its angle. A camera and video analysis software is used to measure both the input and output angle to calculate the kinematic performance ratio of the mechanism. This calculation was performed using the same method as the simulated results by finding the slope of the linear regression.

F. Experiments

In this research, 4 different scenarios are considered. The first 3 scenarios are variations of the initial preload of the springs. The first no preload of 0 N. The second has a preload which makes the mechanism neutrally stable, which has an initial preload of 70 N, the spring is compressed by 47 mm to achieve this initial preload. The last of these scenarios is where the mechanism shows bistable behaviour, which has an initial preload of 95 N, the spring is compressed by 64 mm. for the fourth scenario, a rotation is applied to point M, the symmetrical actuation scenario. For this case, the preload effect is negligible and therefore not considered in the tests.

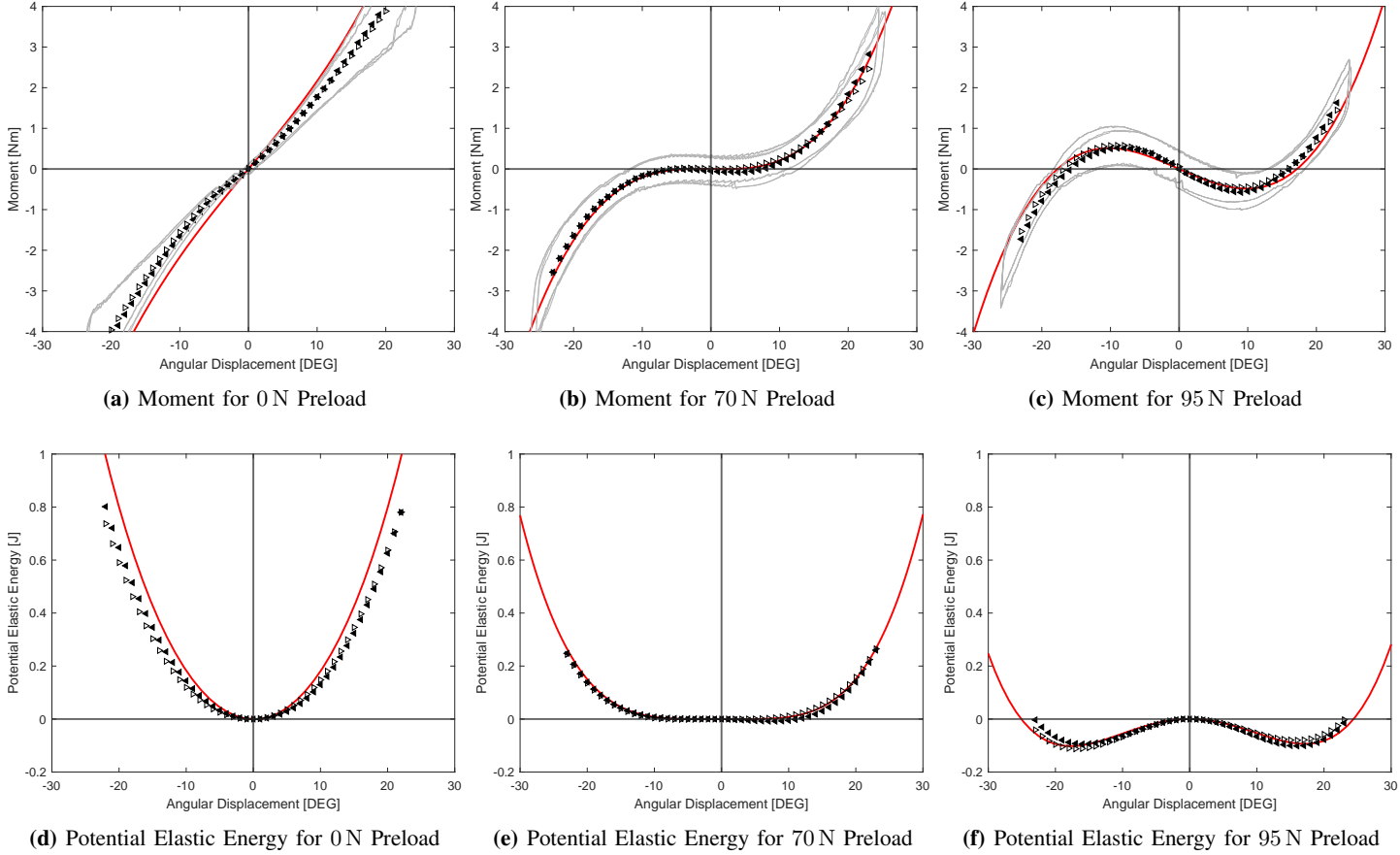


Fig. 6: These figures show the results for the moments and potential energies of different initial preloads against the angular displacement. Both the simulated results (Red) and the experimental results (Gray) are shown. Finally the \blacktriangleleft and \blacktriangleright symbols show the friction compensated results for the left and right side respectively.

IV. RESULTS

Fig. 6a to 6c shows with the red line the resulting simulated moments for one-sided actuation for no initial preload, neutral stable initial preload, and an initial preload which results in bistability. These moments are plotted against the angular displacement in degrees. The experimental results are shown with \blacktriangleleft and \blacktriangleright symbols for the left and right side actuation respectively. In light gray the raw measured results are shown, these results show a hysteresis loop due to the friction in the experimental setup. As discussed in Sec. III-E3 the friction in the experiment results is compensated for by averaging the moments, and thereby sampling the experimental results.

Fig. 6d to 6f show the simulated potential energy in joules measured from the mechanism with the red line. Both of these cases are plotted against the angular displacement of one of the two actuated sides of the mechanism. The experimental results are shown with \blacktriangleleft and \blacktriangleright symbols for the left and right side actuation respectively. Because the potential energy is calculated from the sampled Moment-Angle curve, the friction in the results is already compensated.

For the neutrally stable or zero stiffness scenarios, the results are shown in Fig. 6b and Fig. 6e. The results in Fig. 6b

show a near constant moment within -0.1 Nm and 0.1 Nm within a range of motion of 16° between -8° and 8° . The results in Fig. 6e show a near constant potential elastic energy below 0.003 J within a range of motion of 16° between -8° and 8° . The constant potential energy and a slope of zero indicate zero stiffness at $\theta = 0$. The experimental results show a strong correlation with the simulated results for both the Moment-Angle curve and the Potential Energy-Angle curve. The results from the right-sided and left-sided actuation show minimal differences for both the friction compensated results as well as the uncompensated results. Furthermore, the results show consistency between cycles and sides of the mechanism.

For the bistable scenarios, the results are shown in Fig. 6c and Fig. 6f. The results in Fig. 6c show a local minimum and a maximum at -10° and 10° respectively. There are three locations at which the moment is zero at: -17° , 0° and 17° , which are the equilibrium points. The results in Fig. 6f show potential elastic energy with two local minima at -17° and 17° , which corresponds to the equilibrium points in Fig. 6c. Furthermore, the negative slope through $\theta = 0$ indicates negative stiffness. The experimental results show the same behaviour as the simulated results, but there is a slight

difference. After the peaks the experimental results seem to have a steeper angle which indicates more stiffness, this can be observed in both the Moment-Angle curve and Potential Elastic Energy-Angle curve.

For the not preloaded scenarios, the results are shown in Fig. 6a and Fig. 6d. The results in Fig. 6a show almost linear behaviour going through the origin, which indicates an almost constant positive stiffness over the entire range of motion. While the experimental results show similar behaviour as the simulated results, there is a deviation. However, the experimental results show a similar slope of the line and similar linear behaviour after 5° .

Fig. 7 shows the moment for the symmetrical actuation scenario, the red line is the simulated moment for the symmetrical actuation scenario. these results show a linear relation with the angular displacement from 0 N m to the optimised value of 30 N m. The experimental results for the symmetrical actuation scenario are shown with \square symbol. These experimental results show a deviation from the experimental results after 5° , after this point a steeper slope can be observed which indicates a higher stiffness for the symmetrical actuation scenario.

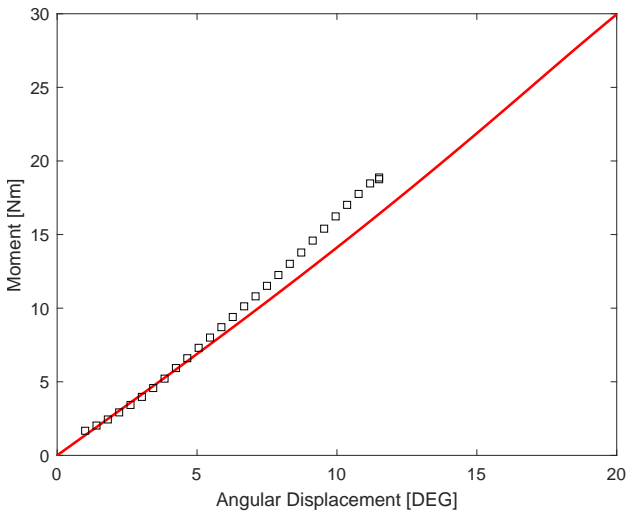


Fig. 7: The moment required for the symmetrical actuation case, both the simulated results (Red) and the experimental results are shown. The experimental results are shown with the \square symbol.

Fig. 8 shows the behaviour of the variable stiffness of the mechanism which was observed. Within the tested initial preloads the mechanism shows a linear relationship between the initial preload and the stiffness of the mechanism at $\Theta = 0$. The linear relationship is shown in Eq. 1, where k_ψ is the rotational stiffness and F_p is the initial preload of the springs.

$$k_\psi = -0.1673 * F_p + 11.6153 \quad (1)$$

This means that the initial preload is negatively correlated with the stiffness, a higher initial preload results in a lower stiffness. This behaviour can also be observed for negative

preloads, a force pulling inwards instead of a force pushing outwards. For initial preloads at 70 N zero stiffness is observed, which indicates neutral stability. While for initial preloads higher than 70 N negative stiffness is observed, which indicates bistability. The experimental results are shown with the calculated stiffness using the \blacksquare symbol.

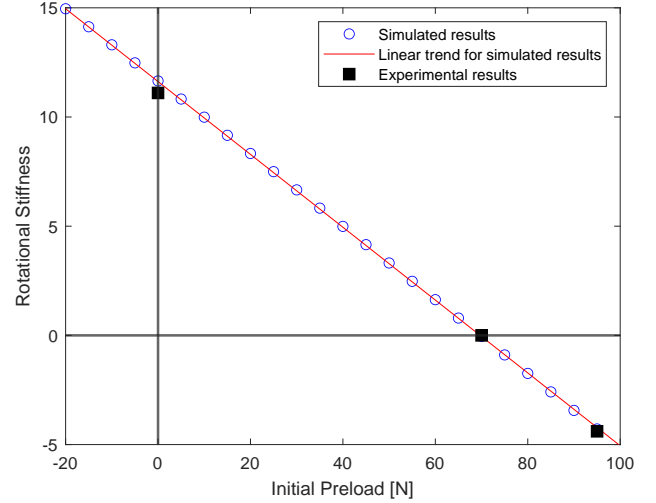


Fig. 8: The effect of the initial preload of the springs on the rotational stiffness of the mechanism.

Fig. 9 shows the kinematic performance ratio of the different initial preloads from simulations. The red line shows a linear trend between the kinematic performance ratio and the initial preload. The kinematic performance ratio show a linear trend between 0.96 and 0.98 for the simulations. The experimental results for the neutrally stable scenario which is shown with the \blacksquare symbol in the same figure, which is 0.95 for a 70 N initial preload, the error bar indicate the 95% confidence range.

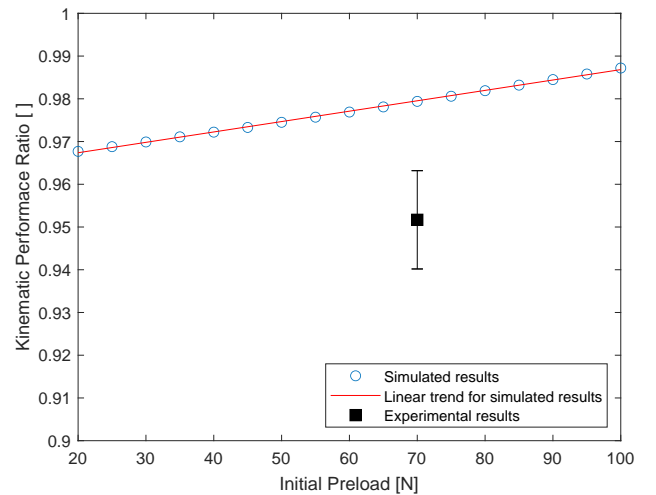


Fig. 9: Kinematic performance ratio for different initial preloads are shown with a linear trend between them, the ratio is also shown for the experimental results.

The linear approximation for the springs according to Hooke's law has been tested. The compression test has been performed on the springs used in the experimental setup. The springs showed the same linear behaviour as the simulated springs, with the same spring stiffness of 1.49 N mm^{-1} .

V. DISCUSSION

The expected behaviour of neutral stability was found in both the simulated and experimental results for the optimised initial preload. This indicates that the used method of reintroduction of potential energy to manipulate the stiffness was successful. Furthermore, for the increased reintroduction of potential energy, a higher initial preload will lead to the expected bistable behaviour. This bistable behaviour was observed in both the simulated and experimental results.

The experimental results of the neutrally stable scenario almost perfectly matches the simulated results, the bistable scenario and not preloaded scenario do show some deviation from the simulated results in the experimental results. This could be due to the experimental setup, for example, the tool used to actuate the mechanism required a few millimetres of backlash to work properly, this is also the case for the fixation at point M. This backlash could cause a shift in the final processed results. This will be most pronounced in the not preloaded scenario due to the steeper slope. This backlash could be removed by creating better and more complex fixations, however for this research the current setup was sufficient to show the observed behaviour. Another discrepancy that could explain differences between the simulations and the experimental results is the difference in actuation. The simulated model is actuation by only applying an angular displacement, which differs from the applied linear displacement. This introduces forces into the system instead of only a pure moment. Another difference between simulations and the experimental setup is the connection between the web and flanges, in the simulations this is a uniform continuous rigid connection. In the experimental setup this was not feasible and a connection using spot-welds was used, this gave the mechanism a rigid connection while minimally effecting the material properties at connection. A way to better approximate the simulations would be to use laser-welding to create a fixation between the web and the flanges, this minimises added material and only has very localised heating which would be beneficial. For this research, this was not a feasible method of construction, therefore spot-welds were chosen and deemed sufficient.

For the symmetrical actuation scenario, the optimisation to reach 30 N m at 20° was successful and that the rotational stiffness of the symmetrical actuation is independent of the angular displacement, this means a linear behaviour of the moment angle curve with a constant rotational stiffness. The experiments did however show a deviation of the simulations after 5° , after this point the experimental results show a higher rotational stiffness of the beam. This deviation could be caused by the difference in application of the moment. In the simulated model, a pure rotation is applied to the web, while

in the experimental setup a rod with a force applied to it is used, which is converted to a moment in the results analyses. A way to fix this problem would be to extend the actuation rod downwards, so 2 forces could be symmetrically applied.

For the symmetrical actuation scenario, the full 20° of angular displacement could not be achieved due to buckling in the flanges, this buckling was observed after about 7° . The simulations also showed buckling, however this only occurred at deformations higher than the 20° used in this research. The buckling at smaller deformations could be caused by the spot-weld which caused a non-uniform connection with the web, the spot-welds also caused some slight imperfections in the flanges which could also cause the buckling. Due to this buckling, the experiment was stopped after 12° of angular displacement. A solution could again be to use laser-welding, for a more uniform connection.

The kinematic performance ratio for the simulated results is around 2% to 3% lower than the ideal ratio of 1. The measured experimental results show only a 2% difference with a 95% transfer of motion. This is a high percentage and considered a good result. This deviation between experiments and the simulated kinematic performance ratio can be seen in Fig. 9. This could be explained by a few factors, first of all, friction in the experimental setup could cause losses in the transfer of motion from the input to the output angle. Secondly, a camera was used to calculate the difference in angle between the actuated and unactuated arm, therefore a difference in perspective or possible lens distortion could alter the results. Finally, the accuracy of measurement was to a maximum of 1° accurate. A way to get more accurate measurements could be to use a laser measurement sensor on both sides, these could measure displacements in height which could be converted to angular displacements with a higher degree of accuracy.

An important metric of this differential mechanism is the ratio between the rotational stiffness of the one-sided actuation and the symmetrical actuation. For the mechanism used in this research, the ratio of moment required to move an angle of 20° for both the one-sided and symmetrical actuation for the neutrally stable scenario:

$$\frac{\text{Symmetrical actuation}}{\text{One - sided actuation}} = \frac{30}{1.76} = 17.01 \quad (2)$$

This is almost 3 times higher ratio than for the not preloaded mechanism, for which this ratio is $\frac{30}{5.09} = 5.89$. This shows a significant increase in the difference in rotational stiffness by reintroducing energy to lower the overall rotational stiffness of the mechanism. The ratio could be even higher if the bistability of the mechanism was utilised, however this bistability is not always desired.

It was found that the stresses in the mechanism show that the main contribution of the behaviour of the mechanism is located at the straight back section of the mechanism. This indicates that the sides of the mechanism could be reduced in size. The curves itself showed high stresses at the inside connection between the flanges and the web, this could be lowered by having a larger radius, however this would alter

the behaviour of the mechanism because it would shorten the straight back section if the width of the mechanism is kept constant.

Now that the expected behaviour has been found and verified, more research can be done into this mechanism. The design used for this proof of concept has been kept simple and uniform to find the behaviour with as little variables as possible. In future research into the mechanism, a variation in the width and height of the beam could be investigated, for example, the bw and bh of the beam could be optimised separately to see if the mechanism could be made more compact or have a wider range of motion with neutral stability and zero stiffness. Another interesting thing to look into is varying the thickness of the web and flanges separately, a lower thickness web could, for example, lower the stiffness of the mechanism while impacting the warping of the beam less. Furthermore, the two side sections around point R and L were found to be less important for behaviour of the mechanism and show much lower stresses than the straight back section. More narrow and more compact dimensions could most likely be chosen in this area.

Besides the dimensions, the cross section itself could also be changed. While in initial testing a C-shaped and I-shaped cross section seemed to perform less than the H-shaped cross section, it could be further examined, especially if other parts of the mechanism are also altered. Cross sections like open circular sections or T-profile which have not been looked into at all could show different and interesting behaviour.

A recommendation for future work is to change the potential energy storage of the mechanism, the potential energy stored in the springs could be replaced by prestresses in the mechanism itself. A similar approach to Lachenal et al.[11] with prestressed flanges could be interesting to look into. Another approach would be to change the parts around point R and L to allow some flex, this could then be used to store the potential energy in a similar fashion as the external springs used in this research.

VI. CONCLUSION

In this paper, a compliant differential mechanism with near zero stiffness is presented. The mechanism showed the ability to manipulate the rotational stiffness by reintroducing energy to compensate for the storage of potential elastic strain energy in the mechanism. Three different initial preloads of the springs have been tested, no initial preload, 70 N initial preload which makes the mechanism have zero stiffness and be neutrally stable, and finally 95 N initial preload which causes the mechanism to have negative stiffness and be bistable. It was found that for the optimised value of 70 N a range of motion of 16° was observed for which the potential energy was near constant. Furthermore, it is shown that the initial preload of the spring had a linear relationship with the stiffness at its neutral position at $\Theta = 0$. This was even the case for negative stiffnesses for initial preload higher than 70 N, this allowed for bistability of the mechanism.

The requirements of the mechanisms were all met. The maximum absolute moment between -25° and 25° for the one-sided actuation was 3.6 N m which is lower than the set requirement of 5 N m, this was for the optimised initial preload of 70 N m. For the symmetrical actuation, the mechanism was successfully optimised for the minimum required moment of 30 N m at 20° . Due to the optimisation of the mechanism, the dimensions of the mechanism were minimised while fulfilling the requirements.

The mechanism performed well as a compliant differential mechanism with a high stiffness while being symmetrically actuated and having a low stiffness when actuated from one side. The required moment after 20° of actuation was 17 times higher for the symmetrical actuation compared to the one-sided actuation. Furthermore a high kinematic performance ratio was observed for the one-sided actuation of more than 0.97 in the simulated results, with the experimental results showing a kinematic performance ratio of only 2% lower.

It can be concluded that this compliant differential mechanism can be optimised to have a range of motion for which the potential energy can be near constant and that the stiffness outside of this range is also reduced significantly. This was validated using both simulations and experimental tests. Furthermore, the mechanism can be easily optimised to fit specified requirements for a chosen application. This application could be for the use in exoskeleton design, for which the mechanism can be optimised for a specific user. Furthermore, due to the scalability and proposed optimisation framework, the mechanism can be used in other applications which require a compliant differential mechanism.

REFERENCES

- [1] M. T. Wright, "The Antikythera Mechanism reconsidered," *Interdisciplinary Science Reviews*, vol. 32, no. 1, pp. 27–43, 3 2007.
- [2] M. Santander, "The Chinese South-Seeking chariot: A simple mechanical device for visualizing curvature and parallel transport," pp. 782–787, 9 1992.
- [3] V. V. Vantsevich, *Advanced Autonomous Vehicle Design for Severe Environments*, V. V. Vantsevich and M. V. Blundell, Eds., 10 2015.
- [4] M. C. Valentijn, "Thin-walled Warping Beams for Differential Mechanism Applications," Delft University of Technology, Tech. Rep., 2020.
- [5] L. L. Howell, *Compliant Mechanisms*. John Wiley & Sons, 2001.
- [6] L. L. Howell, S. P. Magleby, and B. M. Olsen, *Handbook of Compliant Mechanisms*. Wiley, 2 2013.
- [7] J. A. Gallego, "Statically Balanced Compliant Mechanisms: Theory and Synthesis," Tech. Rep., 2013.
- [8] J. A. Gallego and J. Herder, "Criteria for the Static Balancing of Compliant Mechanisms," Tech. Rep., 2010.
- [9] M. Schenk and S. D. Guest, "On zero stiffness," pp. 1701–1714, 2014.

- [10] J. L. Herder and F. P. A. van den Berg, "Statically Balanced Compliant Mechanisms (SBCM'S): An Example and Prospects," 9 2000.
- [11] X. Lachenal, S. Daynes, and P. M. Weaver, "A non-linear stiffness composite twisting I-beam," vol. 25, no. 6, pp. 744–754, 4 2014.
- [12] A. Stapel and J. L. Herder, "Feasibility Study of a Fully Compliant Statically Balanced Laparoscopic Grasper," 2004.
- [13] "DINED." [Online]. Available: <https://dined.io.tudelft.nl/en>

5

Discussion

This chapter will discuss the findings of the paper and relate them to the context of the use in exoskeleton design and the requirements will be checked. The optimisation will also be discussed. Finally everything will be implemented into a wearable exoskeleton prototype to work as a proof of concept. Additional results can be found in Appendix C, some of these additional results are used as validation of the mechanism.

5.1. Behaviour

The behaviour analysed in the paper in Chapter 4 shows great potential. The paper analysed the compliant differential mechanism for a wider range of applications. However, the parameters used in the paper are applicable for the use in exoskeleton design.

Findings of the paper show that the stiffness of the mechanism can be significantly reduced by reintroducing potential energy into the mechanism to compensate the stored potential elastic energy in the material during walking. This caused the mechanism to have different types of behaviour: positive stiffness, zero stiffness, and negative stiffness. These stiffnesses depend on the initial preload of the springs, more initial preload means more energy is stored in the springs and means it releases more energy for the same displacement. This changes the overall potential energy to have these three aforementioned stiffness states. Zero stiffness or Neutral stability is the most interesting for exoskeleton design, this minimises the amount of work required while walking without having bistable behaviour in the mechanism. This bistable behaviour could also be used to minimise the amount of work required while walking, however this would cause undesirable forces on the legs while walking due to the negative stiffness. Therefore this has not been optimised for.

The maximum desired moment for the stiffness compensated mechanism while walking for the range of motion between -25° and 25° was found to be 3.6 N m. This is below the maximum desired moment of 5 N m set in the requirements. This is not the case for the non compensated mechanism, which had a maximum moment of almost twice as much at 7.1 N m. Furthermore the minimum desired moment while bending was also successfully met, the value was optimised to exactly hit the value of 30 N m after 20° degrees of bending. This bending moment linearly increased from 0° to 30° degrees. This behaviour while bending is not fully desired, the support required while bending is nonlinear and for a much larger range of motion. However, these types of large deformations are not possible for the current design, therefore the design needs to be altered or an additional mechanism needs to be designed which works in series with the current design to alter and extend the bending behaviour. Because of this reason, the minimum bending moment is much more important because the mechanism still has to support this moment.

To conclude, the reintroduction of potential energy did minimally effect the stiffness of the mechanism while bending. This gave the mechanism the property of supporting a 17 times higher moment at 20° while bending compared to walking at the same angular displacement. This is 3 times higher than without any stiffness compensation. Furthermore, the transfer of motion from one side to the other side was more than 97% in the simulations and more than 95% for the prototype tested in the experimental setup. The paper also found this transfer of motion to be dependent on the initial preload of

the springs, a higher initial preload resulted in a higher ratio between the input angle and the output angle. Furthermore, all above-mentioned behaviour was achieved around a rotational axis which can be aligned with the human hip joint

5.2. Optimisation

A framework for optimisation has been created and shows a lot of promise, and can be found in Appendix F. The integration of Matlab and Ansys worked reliably and the parametric model was reliable enough for the use in an optimisation problem. The framework was able to run the Ansys model from Matlab for hundreds of times in a row without issue while varying multiple parameters in a wide range. However there were a few combinations of parameters for which the mechanism did not run properly, however this was generally not a problem for future runs in the loop. For the optimisation itself, the user-based parameter optimisation and behaviour optimisation were created and shows promise. For the parameters used in the paper of Chapter 4, the bending moment was optimised to be 30 N m while minimising the required energy while walking. Furthermore, the mechanism was also successfully optimised to have zero stiffness or neutral stability around $\theta = 0$. While the optimisation did work, the focus of this thesis was not on the optimisation itself but the capability of being optimised. Because of this the optimisation is kept reliability basic. Improvements in efficiency and reliability should be made in the future. The optimisation was very computationally intensive and therefore quite slow, this could be improved by using better or more advanced algorithms with better boundary and stopping conditions. Furthermore, the reliability was lower than desired, the Ansys model was very robust and would successfully run around 98%. However, 2% of the time the simulated model would fail to find a solution, independent of the used parameters. The exact cause for this problem has not been found, but most likely has to do with a memory error in Ansys and not in the model itself. While the succesrate for the simulated model was high, the failed runs would interfere with the optimisation and therefore be less reliable. For future work, this will have to be improved to have a more reliable optimisation. The focus of this thesis was not on the optimisation but analysing the behaviour of the mechanism, for which optimisation was required. Therefore, the optimisation has not been further improved and only used to show that optimisation is possible. However, the framework for optimising the mechanism was successful. This framework can be further improved to be more efficient and reliable. It could then be used for personalisation of exoskeletons using this compliant differential mechanism.

5.3. Exoskeleton Prototype

As a proof of concept for the mechanism a wearable exoskeleton prototype has been created. The goal of this wearable exoskeleton prototype was to get a practical understanding of the mechanism and to find problems with the implementation of the mechanism for future works. For this prototype the mechanism itself is attached to a rigid frame which can be worn by the user, this rigid frame is required to allow for the constraints required to have the desired rotational axis. This rigid frame was furthermore required to absorb the load from the two springs on either side of the body, without this rigid frame these loads would cause discomfort for the user. The mechanism is attached to the frame using linear guides with springs, similar to the method used in the experimental setup in the paper of Chapter 4. Images of the wearable exoskeleton prototype can be found in Appendix D.

The wearable exoskeleton prototype showed a lot of potential, the behaviour of the mechanism in the experimental setup was transferred to the prototype. The low stiffness when walking was noticeable, while for bending the stiffness was much higher. For bending the mechanism did provide support to the user, however the provided support was linearly increasing with the angular displacement, which is not the optimal behaviour for support as discussed in section 5.1. In future works this needs to be further investigated and optimised. The effects of the exoskeleton on the range of motion of the user was minimal. Movements such as abduction and adduction of hip joint were not limited, and rotation and lateral flexion of the upper torso was minimally constrained.

These initial tests are however not conclusive and are only meant as a proof of concept. They do however show that the mechanism works as expected in real world scenario's and outside of a controlled experimental setup.

5.4. Future Works

For future works, a few things can be further explored. The first thing has been discussed already, the mismatch between the bending support provided by the mechanism and the desired nonlinear behaviour which is required as a support. This can be solved by altering the current design or by designing an additional device which changes the linear behaviour of the mechanism to a nonlinear behaviour over a larger range of motion.

Another factor which can be further explored is to make the mechanism monolithic, this could be done by removing the springs and try to prestress the material of the mechanism itself to create a source of potential energy. An interesting direction could be to use the working principles of Lachenal et al. he used prestressed flanges to create bistability inside of a twisting I-beam[9]. This could be implemented in a similar way as Concept C3 in Appendix B. Another method would be to design the sides of the mechanism in such a way that they could be used to store potential energy, for example an inwards angle of the sides with fixed constraints to not allow for any translation could be investigated, similar to Concept C2 in Appendix B. In the concept phase, this idea showed potential with bistable behaviour.

Furthermore, in this research the mechanism and optimisation itself has been kept relatively simple to investigate the behaviour of the mechanism with a small number of variables. Now that the behaviour is better understood, the shape and dimensions of the mechanism can be further optimised. For example, the beam width and height, bh and bw can be independently optimised. The shape and size of the two sides can be altered to be slimmer and more compact, this could be investigated because the main stresses in the mechanism were found to be on the back of the mechanism, as can be seen in the additional results in Appendix C. It would furthermore be interesting to more extensively investigate the different cross sections of the mechanism, while early testing showed that an H-shaped cross section would be best suited due to its simple form factor, relatively easy manufacturing and reliable results in simulations. However, other cross section could have interesting behaviour which could potentially increase the range of reduced stiffness.

Finally, while the wearable exoskeleton prototype shows a lot of potential and in a lot of ways work as expected, it is still a proof of concept. More rigorous testing needs to be performed and more elegant and robust constraints need to be implemented. As mentioned before, a solution needs to be found to alter the provided support for lifting to provide better support. Finally, the mechanism can be better optimised to be more compact and better fitted to the human body.

6

Conclusion

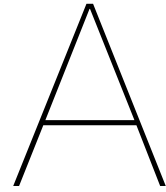
The research aim of this thesis was to create and analyse a compliant differential mechanism for the use in exoskeleton design. To achieve this research aim the four research objectives, found in Chapter 2, had to be achieved.

- The first research objective was to find a design for a compliant differential mechanism for the use in exoskeleton design. The found design consists of a thin-walled beam, with an H-shaped cross section, which has two bends forming a U-shape. By applying constraints on the sides, the rotational axis of the mechanism could be changed to align with the rotational axis of the hip joint. This mechanism in combination with the reintroduction of potential energy using springs allowed for a design which could be used as a compliant differential mechanism in the use of exoskeleton design.
- The second research objective was to create a framework for optimising the proposed design for the use in exoskeleton design. The framework was found to work as expected and could reliably run Ansys for various parameters using Matlab. The framework was also found to be reliable enough to be used for optimisation and was able to optimise the mechanism according to the requirements set for the use in exoskeleton design.
- The third research objective was to analyse the behaviour of the compliant differential mechanism using simulations and an experimental setup. This objective has been successfully achieved and can be found in Chapter 4. Zero stiffness and neutral stability have been found for the proposed design. The optimised mechanism according to the set requirements for the use in exoskeleton design showed near zero stiffness and neutral stability for a range of 16° between -8° and 8° . Furthermore, outside of this near zero stiffness range the mechanism showed a decrease in stiffness and required moment for actuation. The maximum moment within the range of motion between -25° and 25° is 3.6 N m which is well below the required 5 N m for the range of motion. Furthermore, the minimum desired moment while bending met at the optimised and required value of 30 N m after 20° .
- The fourth research objective was to create a wearable exoskeleton prototype to serve as a proof of concept. This final research objective was also met, an exoskeleton prototype has been developed which showed a lot of potential. The prototype was usable and showed very little resistance when walking while creating support when lifting. It furthermore minimally restricted the user in their movements such as abduction and adduction of the hip joint and rotation and lateral flexion of the upper torso.

With all research objectives successfully achieved, the main research aim of creating and analysing a design for a compliant differential mechanism for the use in passive exoskeleton design have been achieved.

Bibliography

- [1] "Laevo-Exoskeletons." [Online]. Available: <https://www.laevo-exoskeletons.com/en/home>
- [2] M. C. Valentijn, "Thin-walled Warping Beams for Differential Mechanism Applications," Delft University of Technology, Tech. Rep., 2020.
- [3] R. P. Matthew, E. J. Mica, W. Meinhold, J. A. Loeza, M. Tomizuka, and R. Bajcsy, "Introduction and initial exploration of an Active/Passive Exoskeleton framework for portable assistance," *IEEE International Conference on Intelligent Robots and Systems*, vol. 2015-Decem, pp. 5351–5356, 2015.
- [4] L. L. Howell, *Compliant Mechanisms*. John Wiley & Sons, 2001.
- [5] L. L. Howell, S. P. Magleby, and B. M. Olsen, *Handbook of Compliant Mechanisms*. Wiley, 2013.
- [6] "Atoun." [Online]. Available: <https://atoun.co.jp/en/>
- [7] F. Moissenet, F. Leboeuf, and S. Armand, "Lower limb sagittal gait kinematics can be predicted based on walking speed, gender, age and BMI," *Scientific Reports*, vol. 9, no. 1, 12 2019.
- [8] "DINED." [Online]. Available: <https://dined.io.tudelft.nl/en>
- [9] X. Lachenal, S. Daynes, and P. M. Weaver, "A non-linear stiffness composite twisting I-beam," vol. 25, no. 6, pp. 744–754, 4 2014.



Literature Report

The literature research into compliant remote center of motion mechanisms. Due to the lack of research into compliant remote center of motion mechanisms this report was created to guide in the search for a solution to change the rotational axis of a warping beam.

Categorisation of Compliant Remote Center of Motion Mechanisms

Robin Mak

*Department of Mechanical Engineering
Delft University of Technology
Delft, the Netherlands
r.mak@student.tudelft.nl*

Abstract—Remote Center of Motion is an important topic in exoskeleton design because the rotational axis of the mechanism, outside of the human body, needs to be aligned with the inner rotational axis of the human joints. While research has been done on Remote Center of Motion using traditional mechanisms, the research on Compliant Remote Center of Motion mechanisms is more limited. This literature study has collected, categorised, and rated the mechanisms found in the literature and determine which mechanisms would be best suited for use in exoskeleton design. The categorisation based on the type of compliance, the type of flexure, and configuration of the flexure has been found to include most of the mechanisms found in literature. The rating system based on the most useful criteria, for Compliant Remote Center of motion, found in literature showed the advantages and disadvantages of the found mechanisms and categories. It was found that curved leaf flexures showed the most potential for use in exoskeletons, due to their relatively high range of motion and compact form factor.

Index Terms—Remote Center of Motion, Compliant Mechanisms, Remote Center of Compliance, Exoskeleton

I. INTRODUCTION

Exoskeletons generally use either active or passive assistance methods[1]. Active assistance methods could use, for example, DC motors which require a source of energy. Passive assistance methods do not require any external power and use, for example, material compliance to provide gravity compensation. Both of these types of mechanisms have one thing in common, they both require a way to align the rotational axis of the human joint with the rotational axis of the joint of the exoskeleton. One of the ways to achieve this is to use a Remote Center of Motion mechanism.

A Remote Center of Motion is defined as "A remote fixed point, with no physical revolute joint over there, around which a mechanism or part of it can rotate"[2]. There are generally two ways to generate a Remote Center of Motion[3]. The first method uses a programmable or software constraint. This method generally uses a general-purpose robot to hold a tool which is rotated around a fixed point in space using control software, no real physical constraints are applied to the motion. This method is also referred to as a Virtual Remote Center of Motion. The second method consists of mechanically constrained kinematic structures. This method uses mechanisms that are kinematically constrained to have a

Remote Center of Motion. They can only rotate around that designed location and do not require complicated programs to compute the motion, they move by themselves around the Remote Center of Motion thus only simple actuation is necessary. This method is also referred to as a Real Remote Center of Motion. This report will not take the first method into account and will focus on the Real Remote Center of Motion. These Remote Center of Motion mechanisms have several applications in, for example, exoskeletons[4], Minimal Invasive Surgery[5] and parallel alignment[6]. The most common ways of creating a Remote Center of Motion mechanism are by using single-revolute-joints, circular-prismatic-joints, parallelogram-based synchronous-transmission-based, and instantaneous-center based[7]. While most of these mechanisms are composed of sliding joints, gears, revolute joints or other rigid-link mechanisms, there is potential in the use of compliant mechanisms.

Compliant mechanisms are mechanisms that use elastic deformation to accomplish something useful[8]. Traditionally, when designers need movement, they will use stiff rigid bodies connected with hinges and sliding joints. However, when looking at nature, much more flexibility in movement can be seen, think of bee wings, elephant trunks, eels, seaweed, spines, human joints, and blooming of flowers. Very compact mechanisms using this flexible behaviour can be seen in nature. Compliant mechanisms have a lot of advantages such as significantly lower cost due to fewer parts and monolithic construction, increased precision due to reduced wear and eliminated backlash, no need for lubrication, and generally a reduction in mass and size. However, compliant mechanisms also introduce some challenges such as more difficult designing process of simultaneous design for motion and force behaviour, fatigue life needs to be addressed, the motion is often more limited than traditional rigid-link mechanisms with no continuous rotation possible, energy is stored during movement and finally there are higher stress concentrations[9]. For exoskeleton design compliant mechanisms can be beneficial for replacing the often heavy, rigid and bulky solutions. Compliant versions can often overcome the drawbacks of rigid exoskeletons in terms of adaptability, comfort, safety, and efficiency[10]. Disadvantages of compliant exoskeletons

can mainly be found in range of motion and storage of energy. These advantages and disadvantages are on top of the advantages and disadvantages of compliant mechanisms in general.

When Remote Center of Motion and compliant mechanisms are combined, it results in Compliant Remote Center of Motion mechanisms. When talking about Compliant Remote Center of Motion mechanisms, the term Remote Center of Compliance[11] is equivalent to what is called the Elastic Center[12], at this point any force results in pure translation and any moment results in pure rotation. While this is not the same definition as the remote center of motion, it is generally equivalent for the purposes of this research. Compliant Remote Center of Motion mechanisms have the same advantages and disadvantages as compliant mechanisms. Such as a limited range of motion, in particular only a finite angle of rotation is possible, so no continuous rotation. Applications proposed for these mechanisms are, for example, parallel alignment[13], a hard disk drive arm[14] or in the use of a linear voice coil motor[15]. These mechanisms are commonly used in high precision applications, no mechanisms have been found which were specifically designed for exoskeleton use.

While quite some research has been done on categorising and classifying Remote Center of Motion using traditional mechanisms[2, 7, 16, 17], very little research has been found on categorising and classifying Compliant Remote Center of Motion Mechanisms. This literature study will categorise these Compliant Remote Center of Motion mechanisms and compare these mechanisms to each other using a rating system with the most useful criteria, for Compliant Remote Center of Motion, found in literature. Based on this categorisation and rating, a conclusion will be drawn on which types of mechanisms are best suited for use in exoskeletons.

Section II will start with categorising all mechanisms in Section II-B and the rating system will be explained in Section II-C. In Section III all mechanisms will be rated and explained. Then in Section IV the results will be discussed. Finally, in Section V this literature study will be concluded.

II. METHOD

This Section will explain the mechanism selection in Section II-A, the categorisation in Section II-B and the rating system in Section II-C chosen for the Remote Center of Motion mechanisms.

A. Mechanism selection

For the selection of the Compliant Remote Center of Motion mechanisms a few requirements are used. The first requirement is that it has to be a compliant mechanism. The second requirement is that the Remote Center of Motion has to be positioned outside of the body and thus be remote. While this seems arbitrary, there are some differences in literature of what is considered remote. For example, Fig. 1 shows two

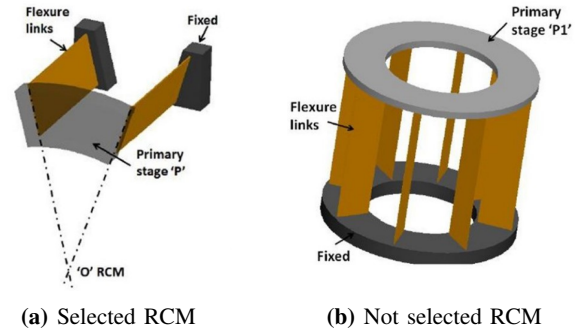


Fig. 1: A Compliant Remote Center of Motion Mechanisms by Gandhi et al. [14]

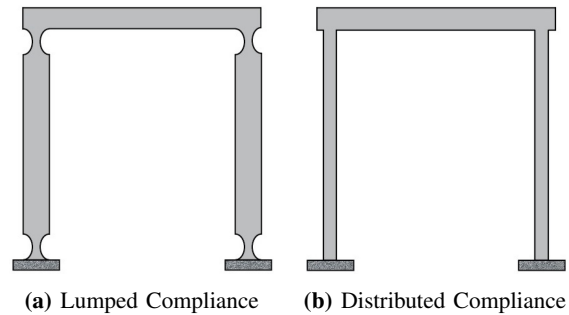


Fig. 2: Difference between lumped compliance and distributed compliance [18]

mechanisms which are classified as Remote Center of Motion mechanisms, however in Fig. 1b the Center of Motion is still enclosed by the mechanism. These kinds of mechanisms will not be considered in the categorisation and only mechanisms which have a Center of Motion not fully enclosed by the mechanism will be selected, so mechanisms similar to the mechanism in Fig. 1a. This distinction has been made because a fully enclosed mechanism will generally not be useful in exoskeleton use.

B. Categorisation

The categorisation is based on a tree diagram, with the found mechanisms at the end of each branch. The created categorisation can be found in Fig. 3. In compliant mechanisms two main types of compliance can be distinguished, lumped compliance and distributed compliance. In lumped compliant mechanisms the deformation occurs in a concentrated part of the constitutive elements, while in distributed compliant mechanisms the deformation occurs along a broader part on the constitutive elements[18], as can be seen in Fig. 2. This distinction has been made for the categorisation and forms the two main branches. The distributed compliance branch has been further separated by the type of flexures used in the mechanism. The two flexure types which were found in the Remote Center of Motion mechanisms were leaf flexures[19] and wire flexures[20]. Wire flexures are often referred to as slender rods. These two types of flexures can be

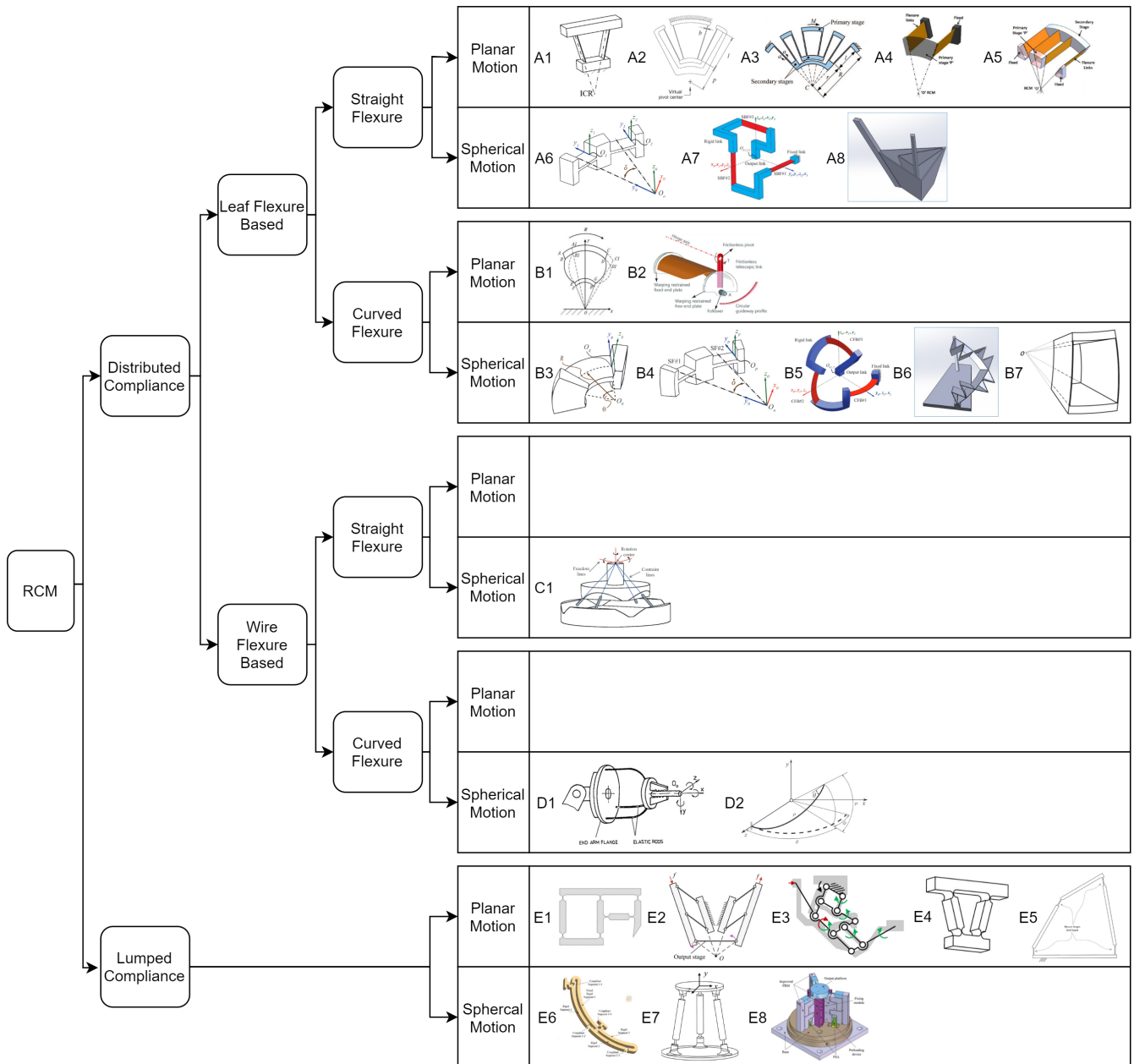


Fig. 3: Categorisation of Compliant Remote Center of Motion(RCM) mechanisms

used in two types of configurations. The first configuration is a straight flexure, the second type of configuration is an initially curved flexure[21]. For the lumped compliance branch, no separation between the types of flexures used has been made. These mechanisms were mainly based on the Rigid-Body-Replacement method[9] with different kinds of compliant joints. This was not taken into account because the objective for this research is not to differentiate between compliant joints, but between the mechanisms themselves. If the same mechanism was found with a different joint it will be mentioned in the text. Mechanisms which do not fit these

categories but are still Compliant Remote Center of Motion mechanisms have been added to an extra category which is called Special Cases. Finally, all branches can be further distinguished between two types of motion. The first motion is planar motion, this motion is defined as the output motion in a 2-Dimensional plane. This means the rotation will be around a single axis. The second type of motion is a spherical motion, which is defined as a motion in a 3-Dimensional space around a single point and therefore is a combination of rotations around multiple axes.

C. Rating

The most important criteria for a Compliant Remote Center of Motion are **Range Of Motion, Center shift, Distance of the Remote Center of Motion, Off-axis stiffness, Rotational stiffness, Compactness** and **Adaptability**. These criteria were chosen due to their prevalence in literature about Compliant Remote Center of Motion mechanisms and their usefulness in exoskeleton design. By these criteria the Compliant Remote Center of Motion mechanisms are rated relative to each other in Section II-C. A relative rating was chosen ranging from (- -) to (+ +) with (0) in the middle as neutral. All found mechanisms were designed for their intended application, this results in all mechanisms having to meet different design goals. For this reason, the mechanisms can not be directly compared to each other and an absolute rating would not be useful. Therefore, a relative rating was chosen, this means the rating was given for the mechanism's potential for the same design requirements. The chosen definition for the criteria are as follows:

Range of motion is one of the drawbacks for compliant mechanisms in general because the motion of compliant mechanisms are often more limited than traditional rigid-link mechanisms[9]. Compliant mechanisms always have a finite range of motion, in contrast to the traditional rigid-link mechanisms which do not have this constraint and can have continuous rotation. The range of motion of compliant mechanisms is limited by permissible stresses and strains in the material[22]. However, there is a large variety in the Range of Motion between different types of compliant mechanisms, therefore Range of Motion is chosen as a criterion. The rating for the Remote Center of Motion mechanisms will range from (- -) for a limited Range of Motion to (+ +) for large range of motion.

Center shift of mechanisms is defined as the axis shift of the Remote Center of Motion during rotation. This is a form of parasitic motion which is defined as the undesirable motion accompanying the desired motion. Axis shift is described as the difference between the actual revolute axis of a mechanism and the desired one regarding only location and not orientation[23]. Compliant mechanisms will always have some center shift in joints due to the lack of a fixed axis of rotation, like in physical revolute joints, but rather a deformation of the material. For Remote Center of Motion this will be even more pronounced due to the distance from the mechanism. Especially in high precision application this is an important metric for Compliant Remote Center of Motion mechanisms. The rating is chosen as (- -) for mechanisms with relatively small center shift to (+ +) for relatively large center shift.

Distance of Remote Center of Motion from the body is an important metric for Remote Center of Motion mechanisms. This metric shows how far the Remote Center

of Motion is located from the mechanism relative to the size of the body. The rating is chosen as (- -) for a Remote Center of Motion against the mechanism to (+ +) for a Remote Center of motion far from the body.

Off-axis stiffness will be defined as the ratio of the stiffness about an undesirable axis relative to the stiffness about the desirable axis of motion[9]. If this ratio is low the mechanism is more prone to move in undesirable directions under loading. A high ratio is often desirable for Remote Center of Motion mechanisms or compliant mechanisms in general to maintain precise motion. The rating is chosen as (- -) for mechanisms with relatively low off-axis stiffness and (+ +) for relatively high off-axis stiffness.

Rotational stiffness is defined as the stiffness around the desired (remote) axis of rotation. Compliant mechanisms will always have some stiffness in the moving direction due to the deformation of the materials in compliant mechanisms. The rating is chosen as (- -) for mechanisms with relatively low rotational stiffness and (+ +) for relatively large rotational stiffness.

Compactness is defined as how much space the mechanism takes up compared to the distance of the Remote Center of Motion and the range of motion. The rating is chosen as (- -) for mechanisms that are relatively large compared to the Remote Center of Motion distance and range of motion and (+ +) for mechanisms that are relatively small compared to the remote center of motion distance and range of motion.

Adaptability is defined as how easily a mechanism can be adapted to fit a particular design purpose. This includes aspects such as the scalability or how complex it is to change the location of the Remote Center of Motion. Generally a more complex mechanism will be more difficult to adapt than a single flexure mechanism. The rating is chosen as (- -) for mechanisms which are relatively difficult to adapt to a design purpose and (+ +) for relatively easy to adapt to a design purpose.

1) *Confidence level:* All mechanisms have literary foundation for their specific applications. For this reason, different criteria are discussed within the relevant literature, this results in not all criteria having been analysed for every mechanism. For this reason, the ratings have been given different confidence levels in the form of different colours. **Green** was chosen for high confidence. In this case, the specific criterion was directly addressed in the literature and hence a definitive rating could be given. It is also possible for it to be green when the same criterion is discussed in a different mechanism but has the same working principle. **Orange** is chosen for moderate confidence. This is used when the rating is indirectly based on literature or not found in literature. Indirect from literature includes cases where there is some mention of it but no real quantification has been given, the relationship to

other criteria, general knowledge of used flexures, or from similarities to other mechanisms. A ? was used when no data was available and no prediction could be made.

III. RESULTS

In this section all mechanisms categorised in Fig. 3 will be rated and explained. They will be rated according to the method shown in Section II-C.

A. Straight Leaf Flexure based Mechanisms

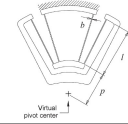
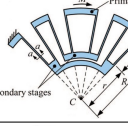
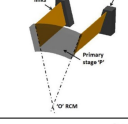
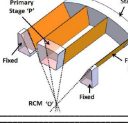
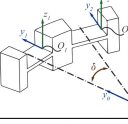
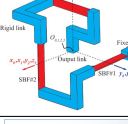
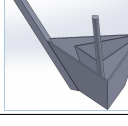
All Straight Leaf Flexure based Mechanisms can be found in Table I.

Mechanism A1[11, 20, 24–29]: The Leaf-type Isosceles-Trapezoid Flexural (LITF) Pivot is composed of an Isosceles-Trapezoid of which the diagonal parts are made of leaf flexures and the parallel parts are rigid bodies. For the mechanism to work, either the top or bottom rigid body can be fixed depending on the application. The angled leaf flexures create an instantaneous center of rotation for the end-effector at the virtual intersection point of the two leaf flexures. Since it is an instantaneous center of rotation, it will only be a Remote Center of Motion for small angular rotations. A variation of the LITF pivot is proposed by Ciblak and Lipkin[11]. This mechanism has 2 extra flexure rods which connect an extra rigid body in the center of the mechanism, these rods change the relative stiffness of the mechanism and shift the Remote Center of Motion upwards.

Mechanism A2[24, 30–32]: The Double Leaf-type Isosceles-Trapezoid Flexural (D-LITF) is a combination of two LITF pivots, similar to Mechanism A1. This mechanism can be seen as a special case of a double parallelogram flexure[33], also known as a folded beam flexure. It can be optimised by adjusting geometric parameters of the single LITF to achieve more range of motion, less center shift, and lower rotational stiffness. The mechanism is, for example, used in "Butterfly" pivots[34] which are also known as a Quadri Leaf-type Isosceles-Trapezoid Flexure (Q-LITF). A variation of this mechanism is shown by Strancz et al.[35], here they showed the same mechanism, however they added reinforcement to the leaf flexures to increase the resistance to buckling and increase the off-axis stiffness. However the rotational stiffness significantly increases when the reinforcement is larger than 70% of the length of the flexure, also the range of motion will be negatively effected.

Mechanism A3[15, 24, 30, 31]: The Multi-stage Compound Radial Flexure (MCRF) has again the same working principle as Mechanism A1. Similar to Mechanism A2 there are LITF mechanisms in series but now 3 or more mechanisms in series. This leads to more range of motion while having a negligible magnitude of center shift. The straight leaf springs in series also result in a reduction in rotational stiffness. A proposed application for this mechanism is in a rotary micro-positioning system driven by a linear voice coil motor[15].

TABLE I: Rating for the Straight Leaf Flexures Mechanisms

		Range of Motion	Center Shift	RCM Distance	Off-Axis Stiffness	Rotational stiffness	Compactness	Adaptability
A1		-	-	0	0	0	+	+
A2		+	+	-	-	+	-	0
A3		+	++	-	--	++	--	-
A4		0	0	+	+	0	0	+
A5		+	+	0	+	+	-	0
A6		+	--	0	-	+	+	-
A7		++	--	0	--	++	0	+
A8		+	?	0	?	?	+	-

Mechanism A4[14, 32, 36]: This is similar to Mechanism A1, with two angled straight leaf flexures. However, the movement is now created by simultaneous twisting and bending rather than just bending of the straight leaf flexures. The mechanism is designed to have minimal center shift while having high off-axis stiffness. It can also increase the off-axis stiffness while keeping the rotational stiffness the same. This mechanism can also be used in a circular arrangement as shown by Gandhi et al.[14]. In this case the center shift is more limited due to the geometric symmetry of the mechanism, this variation could be used in clutch coupling of automobiles for getting a smooth nonlinear

noise-free operation or high-sensitivity torque sensor.

Mechanism A5[14, 32]: This is a variant of Mechanism A4 but an extra motion stage is added in the form of two extra straight leaf flexures in series. This results in a decrease in center shift and lowers the rotational stiffness. The mechanism has a similar concept as Mechanism A2. An application proposed by Gandhi et al.[14] is the use of a hard disk drive arm.

Mechanism A6[37, 38]: The 2R Straight Leaf Flexure based Compliant Chain is used to highlight the added benefits of Mechanism B4. The working principal of this mechanism is by having two straight leaf flexures be chained together with a rigid body. The rigid body angles two identical leaf flexures, which creates a Remote Center of Motion at the virtual intersection of perpendicular lines from the middle of these leaf flexures. This causes the mechanism to rotate around a single point instead of an axis as we have seen with Mechanism A1 to A5. Disadvantages of the use of Straight Leaf Flexures, over Curved Leaf Flexures are worse spherical motion and more parasitic motion and center shift, while the benefits are easier manufacturing.

Mechanism A7[39]: This 3R Straight Leaf Flexure based Compliant Chain mechanism is similar to Mechanism A6 but has an extra flexure added and a different orientation of the flexures. It is also similar to Mechanism B5 but with Straight Leaf Flexures instead of a Spherical Flexures or Circular Curved-Beam Flexures. This will always lead to more parasitic motion and center shift for flexures with identical primary rotational compliance[39].

Mechanism A8: This is a mechanism by J. Rommers¹. No literature has been released on the mechanism at the time of writing. The mechanism is a spherical version of a nested triangle mechanism. One of the arms is considered fixed and the other will be described by a spherical motion around the point at which all flexures virtually intersect. The second stage within the outer triangle reduces the rotational stiffness of the mechanism. The mechanism could be used as a replacement of ball-socket joints in, for example, hexapod robots.

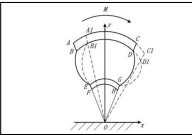
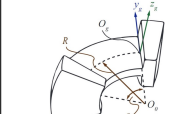
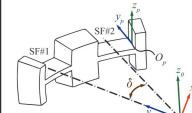
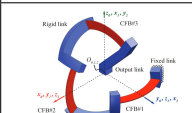
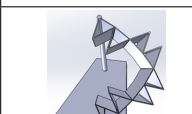
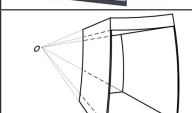
B. Curved Leaf Flexure based mechanisms

All Curved Leaf Flexure based Mechanisms can be found in Table II.

Mechanism B1[32, 40]: This Curved-Isosceles-Trapezoidal Flexure module is similar to Mechanism A1, but uses initially curved leaf flexures instead of straight leaf flexures. This has the advantage of a fixed virtual center while rotating a finite angle[40]. The module is also proposed to be used in a novel

¹Jelle Rommers is a PhD student in the Mechatronic Systems Design group at TU Delft

TABLE II: Rating for the Curved Leaf Flexures Mechanisms

		Range of Motion	Center Shift	RCM Distance	Off-Axis Stiffness	Rotational Stiffness	Compactness	Adaptability
B1		+	0	0	-	+	0	0
B2		+	0	-	-	+	+	-
B3		+	0	0	-	+	++	+
B4		++	+	0	--	++	+	+
B5		++	+	0	--	++	+	+
B6		++	?	0	0	++	+	+
B7		0	0	+	+	0	0	+

annulus-shape flexure, similar to the circular arrangement mentioned for Mechanism A4. This further reduces the center shift and increases the range of motion.

Mechanism B2[41]: An open-section shell building block has the ability to undergo large rotational deformation with significant bending and axial stiffness. Due to the asymmetry of the open shell, the elastic axis is located outside of the mechanism. This mechanism can be altered by using two symmetric open-section shell building blocks which are spatially positioned to share the same elastic axis, which is the locus of the shear centers of the cross section of a shell along its length. This configuration decreases the center shift and parasitic motion significantly and increases off-axis stiffness.

Mechanism B3[38, 42–45]: This mechanism actually consists of two different types of flexures. The first one is a Circular Curved-Beam Flexure and the second is a Spherical

Flexure. A Circular Curved-Beam Flexure features an arc of a circle as the centroidal axis and a rectangular cross section. The Spherical Flexure also features an arc of a circle as a centroidal axis, however, instead of a rectangular cross section this flexure features an annulus sector with the same center as cross-section. For both flexures, the centroidal axis coincides with that of the spherical motion, which is the Remote Center of Motion[42]. For equivalent primary compliance, both mechanisms produce free end deflections that closely resemble a spherical motion around the Remote Center of Motion. However, the Spherical Flexure always outperforms Circular Curved-Beam Flexures in terms of parasitic motion and center shift[44]. Circular Curved-Beam Flexures are more widely used in mechanisms, reasons for that are that the marginally better parasitic motion or center shift is not always necessary. More importantly is that rectangular cross sections are easier to manufacture.

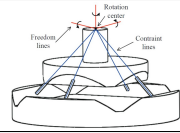
Mechanism B4[37, 38, 44]: The 2R Compliant Chain mechanism is similar to Mechanism A6 with Spherical Flexures or Circular Curved-Beam Flexures replacing the Straight Leaf Flexures. The mechanism works by having the centroidal axis or Remote Center of Motion of both flexures coincide to create a single Remote Center of Motion of this mechanism. Using these flexures in series reduces the parasitic motion and the center shift, it will also increase the range of motion and decrease the rotational stiffness.

Mechanism B5[38, 39, 43, 44, 46]: The 3R Compliant Chain is an extension to Mechanism B4, an extra Spherical Flexure or Circular Curved-Beam Flexure has been added. This further increases the range of motion and decreases the rotational stiffness. The 2R and 3R Compliant Chain could be used for applications such as Cardan's universal joint[47] or Double-Hooke's coupling[48].

Mechanism B6: Similar to Mechanism A8, this is also a mechanism by J. Rommers. Again, no literature has been released at the time of writing. This mechanism is similar to Mechanism B4 with two circular flexures in series. The difference however, is that this mechanism has no rigid body connecting the two flexures. To increase off-axis stiffness of the mechanism while maintaining low rotational stiffness there has been added torsion reinforcement structures[49] to the Circular Curved-Beam Flexures.

Mechanism B7[32]: This mechanism is similar to Mechanism A4, however Circular Curved-Beam Flexures are used instead of the two Straight Leaf Flexures used. This creates a rotational point instead of a rotational axis. For this reason, the motion of the mechanism is also spherical around the Remote Center of Motion.

TABLE III: Rating for the Straight Wire Flexures Mechanisms

		Range of Motion	Center Shift	RCM Distance	Off-Axis Stiffness	Rotational Stiffness	Compactness	Adaptability
C1		-	0	0	-	0	-	+

C. Straight Wire Flexure based mechanisms

All Straight Wire Flexure based Mechanisms can be found in Table III.

Mechanism C1[29, 50]: This mechanism is created with two sets of LITF pivots, similar to Mechanism A1, with wire flexures used in parallel[29]. These wire flexures are uniformly spaced around two circles on the end-effector and base at intervals of $\pi/2$. The mechanism is based on the type synthesis approach Freedom and Constraint topology(FACT)[51] of the parallel flexure system. Four constraint lines intersect in a common point and permit three independent rotations around the intersection. This intersection point is the Remote Center of Motion of the mechanism. An alteration to this mechanism could be to change the interval of the wire flexures to $2\pi/3$, this results in the same permitted rotation at the same location. However, decreasing the number of wires while keeping equivalent primary compliance for these wires will decrease the off-axis and rotational stiffness of the mechanism.

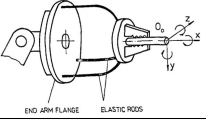
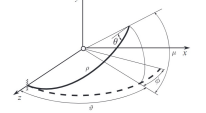
D. Curved Wire Flexure based mechanisms

All Curved Wire Flexure based Mechanisms can be found in Table IV.

Mechanism D1[52, 53]: This mechanism is similar to C1, however the Straight Wire Flexures are replaced by Wire Flexures which are partly curved or circular. Depending on the need, 3 or more of these flexures can be used for different characteristics, mainly in rotational or off-axis stiffnesses. The mechanism has a low off-axis stiffness and can therefore also translate the end-effector, which for some cases could be beneficial. A proposed application for the mechanism is in the use of a self-alignment for a two-phase in a-peg-into-a-hole insertion task[52].

Mechanism D2[54, 55]: This might be the simplest mechanism categorised. The mechanism consists of a single curved or circular wire flexure fixated on one end. The opposite end will follow a spherical motion around the

TABLE IV: Rating for the Curved Wire Flexures Mechanisms

		Range of Motion	Center Shift	RCM Distance	Off-Axis Stiffness	Rotational Stiffness	Compactness	Adaptability
D1		+	-	0	--	+	-	-
D2		+	--	0	--	++	++	+

centroidal axis of the curved wire flexure. The Remote Center of Motion is thus located in this same centroidal axis. The loading however, has to be spherical[55], so the loading direction should be tangent to the surface of the virtual sphere. This is due to the low off-axis stiffness because there is nothing to prevent off-axis movement.

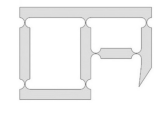
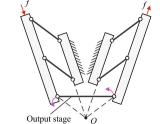
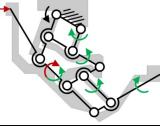
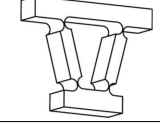
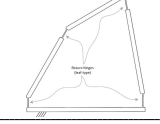
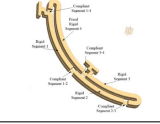
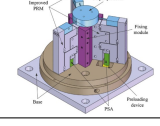
E. Lumped Compliance based mechanisms

All Lumped Compliance based Mechanisms can be found in Table V.

Mechanism E1[56–58]: This parallelogram based Remote Center of Motion mechanism works by having two parallelograms in series. The second parallelogram is smaller than the first one. The second parallelogram has the horizontal bottom link on the midpoint of the vertical side links, this does not effect the motion of both parallelograms. For this reason, there is a Remote Center of Motion created at the virtual intersection of the fixated horizontal bottom link of the first parallelogram and the furthest vertical side link of the second parallelogram. For the mechanism equal input as output it requires the opposite links of each parallelogram to be equal length and parallel. This mechanism is often used with traditional joints and rigid-links. To make the mechanism compliant the traditional joints can be replaced by compliant joints. A variety of compliant joints could be used, a few examples from literature are notch joint[56–58], cruciform flexure[57], cross pivot[57] or a split joint[57]. This mechanism is one of the most used mechanisms in Robot Assisted Minimally Invasive Surgery(RAMIS) for its simplicity and large motion range[5].

Mechanism E2[6, 13, 58, 59]: This symmetric double-parallelogram mechanism is an improved version of Mechanism E1. Two parallelogram mechanisms are used symmetrical to each other. Due to the geometric constraint the rotational precision can be increased by a decreased

TABLE V: Rating for the Lumped Compliance Mechanisms

		Range of Motion	Center Shift	RCM Distance	Off-Axis Stiffness	Rotational Stiffness	Compactness	Adaptability
E1		+	+	++	++	-	--	+
E2		+	++	+	++	-	--	+
E3		+	+	++	++	-	--	+
E4		--	0	0	+	-	0	+
E5		--	0	0	+	-	0	+
E6		+	?	+	0	+	+	0
E7		+	+	0	+	-	-	+
E8		+	++	+	++	-	--	0

center shift. Because of the symmetry, the Remote Center of Motion of both parallelograms intersect at the same location. Notch joints are generally used in this mechanism. In contrast to Mechanism E1 this mechanism is more used for micro-/nanomanipulators in high-precision parallel alignment to eliminate harmful lateral displacement generated at the output platform[6]. This mechanism is used for one degree of freedom alignment. It is often a requirement that the alignment stage has two degrees of freedom, a mechanism which has that capability is Mechanism E8 which will be discussed later.

Mechanism E3[17]: In contrast to Mechanism E1 this mechanism does not have the parallel and equal length constraint[17]. Due to this missing constraint, a mechanism could be developed with four-bar mechanisms of different shapes. This will still be able to create a Remote Center of Motion, however, this mechanism was designed in such a way that the input and output rotation of the mechanism are different. This could be seen as a kind of transmission. This characteristic could open possibilities for increasing the rotation around a point to get a higher output motion with respect to the input motion. The opposite is used by Janssen[17] in the use of an electron microscope, here a smaller output was desired to have a higher degree of precision for the output rotation from the same input rotation.

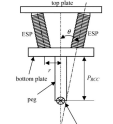
Mechanism E4[26, 60]: This Notch-Type Isosceles-Trapezoid Flexural pivot is the lumped compliant version of Mechanism A1. Notch flexures have a limited angular displacement compared to leaf flexures but have higher precision[26]. However, since the range of motion of Mechanism A1 was already limited due to it only having an instantaneous center of motion the difference in both mechanisms is minimised. Mechanism A1 will have more range of motion outside range for which the instantaneous center of motion can be considered precise, however if high precision is not required, Mechanism A1 will have more range of motion. A proposed application for this mechanism is in the orientation stage of high-resolution imprint lithography machines to provide intimate contact between the template and substrate surfaces[60].

Mechanism E5[61]: This compliant non-parallel four-bar mechanism is similar to Mechanism E4. The only difference is that this is not a trapezoid, therefore there is an extra instantaneous center of motion. This second instantaneous center of motion is located at the virtual intersection of the second set of nonparallel links. The mechanism is optimised to maximise the output rotation with an acceptable amount of deflection.

Mechanism E6[62]: This is a novel fully compliant spherical four-bar mechanism with small length flexural hinges. Initially, all segments are on a parallel plane and all flexures are in their undeformed configuration. The mechanism consists of four arced rigid parts, which have a total combined arc length of 360° , which are connected using small length leaf flexures. All flexures must virtually intersect in the middle of the sphere, this is where the Remote Center of Motion is located.

Mechanism E7[20, 63]: This mechanism is similar to Mechanism C1. However, instead of a flexure over the complete length of the mechanism there are only flexures located at the end points with a rigid body between them. This will increase the resistance to buckling and off-axis stiffness, it will however decrease the range of motion of the

TABLE VI: Rating for the Special Cases

		Range of Motion	Center Shift	RCM Distance	Off-Axis Stiffness	Rotational Stiffness	Compactness	Adaptability
F1		-	-	0	-	0	0	++

mechanism. This is similar to the variation of Mechanism A2 with the added reinforcement. However, for that mechanism the reinforcement was still considered flexible and the flexure parts were a longer portion of the overall length.

Mechanism E8[58, 59]: This mechanism has the same working principle as Mechanism E1 and Mechanism E2. By using three[13] or four[58] parallelogram mechanisms in symmetry, a platform can be created which has two degrees of freedom and rotates around a Remote Center of Motion. It works similar to Mechanism E2 by having parallelogram mechanisms in symmetry around the Remote Center of Motion. By using more than two parallelogram mechanisms, there is an additional degree of freedom in the form of an extra rotation. This allows for better parallel aligning as discussed in the section on Mechanism E2.

F. Special Cases

All Special Cases can be found in Table VI.

Mechanism F1[64–67]: This Variable Remote Center of Compliance mechanism consists of Elastomer Shear Pads(ESPs) and Stiffness Adjusters(SA). The mechanism uses a similar principle as Mechanism A1 by having two "flexures" at an angle to create a remote center of motion at the virtual intersection. However, in this case the "flexures" are not individual flexures but instead are composed of compliant rings in the form of Elastomer Shear Pads(ESPs) in series with rigid washers between them. To make the mechanism have a Variable Remote Center of Compliance, some of the Elastomer Shear Pads can be fixated by either clamping[60], Stiffness Adjusting Rod(SAR)[66] or by controlling the shear stress to change the Elastomer Shear Pad(ESP) stiffness[67]. This changes the stiffness of the Compliant rings and thus shifts the Remote Center of Compliance of the entire mechanism. In this case the Remote Center of Compliance can be considered equivalent to the Remote Center of Motion.

IV. DISCUSSION

When looking at the categorised mechanisms, it can be seen that for the distributed compliance based mechanism the leaf flexures are the most common. Wire flexures are considerably less represented in literature, especially wire flexure based planar motion mechanisms were not found. Leaf flexures are naturally constrained to planar motion, while three wire flexures are required to achieve the same planar motion. Therefore wire flexures are generally not used for planar motion mechanisms. Wire flexures are however used for spherical motion, they generally have low rotational and off-axis stiffness and higher center shift compared to other spherical motion mechanisms. When curved leaf flexures are compared to straight leaf flexures, there are also noticeable differences in the characteristics. It can be seen that straight leaf flexure based mechanisms are generally used for planar motion and curved leaf flexures are predominantly used for spherical motion. Other differences are that curved flexure mechanisms generally have more range of motion, less center shift, are more compact and have lower rotational stiffness compared to straight flexure mechanisms, while straight flexures generally have higher off-axis stiffness compared to curved flexures. Furthermore, using flexures in series will generally result in more range of motion, lower rotational stiffness and off-axis stiffness, which is to be expected. When comparing distributed compliance based mechanisms with lumped compliance based mechanisms, similarities with compliant mechanisms in general can be observed, generally less range of motion, higher rotational stiffness, and higher off-axis stiffness for lumped compliant mechanisms. Furthermore center shift seemed slightly improved for the found mechanisms, while the mechanisms were generally less compact.

While most ratings are based on literature, they remain a relative and subjective rating by the author. The resolution of the rating could also lead to difficulties in comparing the mechanisms. For example while two mechanisms could have the same rating, one of the mechanisms could outperform the other, while not warranting a higher rating.

When looking at the use of Compliant Remote Center of Motion for use in exoskeletons, no relevant literature mentioned its use in exoskeletons. Furthermore, the scale of the found mechanisms is not in a range usable for exoskeleton design, most mechanisms are designed for high precision application and are smaller than would be required for an exoskeleton. However, when looking at the types of mechanisms which would be most suitable for this application, we find that spherical motion with a large range of motion in a compact form factor is often required. For this reason, curved leaf flexure based mechanisms show the most potential for use in exoskeletons. However, particularly for active exoskeletons, it would need reinforcement to increase the off-axis stiffness of the mechanism.

V. CONCLUSION

This literature study set out to achieve three goals: categorise Compliant Remote Center of Motion mechanisms found in literature, compare all found Compliant Remote Center of Motion mechanisms to each other using a rating system, and finally conclude which mechanisms are most suitable for the use in exoskeleton design.

For the first goal, the categorisation, it was found that most Compliant Remote Center of Motion mechanisms could be fitted into the chosen categories. Only one mechanism did not meet the requirements for any category and thus was considered a special case.

For the second goal, the rating system, a rating was established to rate and compare Compliant Remote Center of Motion mechanisms, which was successful. The rating system gave a clear overview of the advantages and disadvantages of the mechanisms and categories in general.

The final goal, regarding the applicability in exoskeleton design, while no mechanisms were found with exoskeletons as an application, a recommendation can be made regarding the types of flexures best suited for the use in exoskeletons. It was found that curved leaf flexures showed the most potential due to their relatively high range of motion and compact form factor.

A. Future Work

Future research could be in the direction of Variable Compliant Remote Center of Motion mechanisms similar to Mechanism F1, which can vary their Remote Center of Motion. Because all people have different lengths and sizes, these types of mechanisms would be beneficial for the use in exoskeletons. This makes the exoskeleton customizable to fit a wide range of people. Secondly, it would be useful to research the effect of scaling up the mechanisms to see if the mechanisms still maintain their properties at larger sizes. Characteristics to consider include a sufficient range of motion, rotational stiffnesses which do not become too large or on the other hand, the off-axis stiffness that are within acceptable margins.

REFERENCES

- [1] R. P. Matthew, E. J. Mica, W. Meinhold, J. A. Loeza, M. Tomizuka, and R. Bajcsy, "Introduction and initial exploration of an Active/Passive Exoskeleton framework for portable assistance," *IEEE International Conference on Intelligent Robots and Systems*, vol. 2015-Decem, pp. 5351–5356, 2015.
- [2] C.-H. Kuo and J. S. Dai, "International Symposium on History of Machines and Mechanisms," *International Symposium on History of Machines and Mechanisms*, no. January 2009, 2009.
- [3] R. C. Locke and R. V. Patel, "Optimal remote center-of-motion location for robotics-assisted minimally-invasive surgery," *Proceedings - IEEE International Conference on Robotics and Automation*, no. April, pp. 1900–1905, 2007.

- [4] M. Fontana, S. Fabio, S. Marcheschi, and M. Bergamasco, "Haptic hand exoskeleton for precision grasp simulation," *Journal of Mechanisms and Robotics*, vol. 5, no. 4, 2013.
- [5] X. Zhou, H. Zhang, M. Feng, J. Zhao, and Y. Fu, "New remote centre of motion mechanism for robot-assisted minimally invasive surgery," *BioMedical Engineering Online*, vol. 17, no. 1, 11 2018.
- [6] J. Qu, W. Chen, and J. Zhang, "A parallelogram-based compliant remote-center-of-motion stage for active parallel alignment," *Review of Scientific Instruments*, vol. 85, no. 9, 2014.
- [7] G. Zong, X. Pei, J. Yu, and S. Bi, "Classification and type synthesis of 1-DOF remote center of motion mechanisms," *Mechanism and Machine Theory*, vol. 43, no. 12, pp. 1585–1595, 12 2008.
- [8] L. L. Howell, *Compliant Mechanisms*. John Wiley & Sons, 2001.
- [9] L. L. Howell, S. P. Magleby, and B. M. Olsen, *Handbook of Compliant Mechanisms*. Wiley, 2 2013.
- [10] M. D. C. Sanchez-Villamañan, J. Gonzalez-Vargas, D. Torricelli, J. C. Moreno, and J. L. Pons, "Compliant lower limb exoskeletons: A comprehensive review on mechanical design principles," 5 2019.
- [11] N. Ciblak and H. Lipkin, "Design and analysis of remote center of compliance structures," *Journal of Robotic Systems*, vol. 20, no. 8, pp. 415–427, 8 2003.
- [12] G. Krishnan, C. Kim, and S. Kota, "An intrinsic geometric framework for the building block synthesis of single point compliant mechanisms," *Journal of Mechanisms and Robotics*, vol. 3, no. 1, 2010.
- [13] J. Qu, W. Chen, J. Zhang, and W. Chen, "A large-range compliant micropositioning stage with remote-center-of-motion characteristic for parallel alignment," *Microsystem Technologies*, vol. 22, no. 4, pp. 777–789, 4 2016.
- [14] P. S. Gandhi, R. S. Bobade, and C. Chen, "On novel compliant mechanisms for remote center motion," *Advances in Mechanical Engineering*, vol. 10, no. 4, 4 2018.
- [15] Q. Xu, "Design and implementation of a novel rotary micropositioning system driven by linear voice coil motor," *Review of Scientific Instruments*, vol. 84, no. 5, 5 2013.
- [16] M. Valentijn, G. Radaelli, and A. A. Nobaveh, "Literature report : Differential mechanism for Remote Center of Rotation applications," 2020.
- [17] J. L. H. M. Janssen, "Department of Precision and Microsystems Engineering Compliant Remote-Center-of-Motion Mechanism Optimized for Energy-Dispersive Spectroscopy," Tech. Rep., 2018.
- [18] J. A. Gallego and J. Herder, "Synthesis methods in compliant mechanisms: An overview," in *Proceedings of the ASME Design Engineering Technical Conference*, vol. 7, no. PARTS A AND B. ASME, 1 2009, pp. 193–214. [Online]. Available: <https://asmedigitalcollection.asme.org/IDETC-CIE/proceedings/IDETC-CIE2009/49040/193/342223>
- [19] P. P. Valentini and E. Pennestrì, "Second-order approximation pseudo-rigid model of leaf flexure hinge," *Mechanism and Machine Theory*, vol. 116, pp. 352–359, 10 2017.
- [20] H. J. Su, H. Shi, and J. Yu, "A symbolic formulation for analytical compliance analysis and synthesis of flexure mechanisms," *Journal of Mechanical Design, Transactions of the ASME*, vol. 134, no. 5, 2012.
- [21] B. T. Edwards, B. D. Jensen, and L. L. Howell, "A pseudo-rigid-body model for initially-curved pinned-pinned segments used in compliant mechanisms," *Journal of Mechanical Design, Transactions of the ASME*, vol. 123, no. 3, pp. 464–472, 2001.
- [22] B. P. Trease, Y. M. Moon, and S. Kota, "Design of large-displacement compliant joints," *Journal of Mechanical Design, Transactions of the ASME*, vol. 127, no. 4, pp. 788–798, 8 2005.
- [23] W. W. Van De Sande and J. L. Herder, "Analysis of parasitic motion in compliant mechanisms using eigenwrenches and eigentwists," in *Proceedings of the ASME Design Engineering Technical Conference*, vol. 5A-2018, 2018. [Online]. Available: <https://proceedings.asmedigitalcollection.asme.org>
- [24] X. Pei, J. Yu, S. Bi, and G. Zong, "A family of butterfly flexural joints: Q-LITF pivots," in *Proceedings of the ASME Design Engineering Technical Conference*, vol. 6, no. PARTS A AND B, 2011, pp. 203–210.
- [25] X. Pei, J. Yu, G. Zong, and S. Bi, "An effective pseudo-rigid-body method for beam-based compliant mechanisms," *Precision Engineering*, vol. 34, no. 3, pp. 634–639, 7 2010.
- [26] X. Pei, Y. Jingjun, Z. Guanghua, B. Shusheng, and Y. Zhiwei, "Analysis of rotational precision for and isosceles-trapezoidal flexural pivot," *Journal of Mechanical Design, Transactions of the ASME*, vol. 130, no. 5, 5 2008.
- [27] S. Awtar, A. H. Slocum, and E. Sevincer, "Characteristics of beam-based flexure modules," *Journal of Mechanical Design, Transactions of the ASME*, vol. 129, no. 6, pp. 625–639, 6 2007.
- [28] A. Zhang, Y. Gou, and X. Yang, "Predicting Nonlinear Stiffness, Motion Range, and Load-Bearing Capability of Leaf-Type Isosceles-Trapezoidal Flexural Pivot Using Comprehensive Elliptic Integral Solution," *Mathematical Problems in Engineering*, vol. 2020, 2020.
- [29] L. J. Lai and Z. N. Zhu, "Modeling and analysis of a compliance model and rotational precision for a class of remote center compliance mechanisms," *Applied Sciences (Switzerland)*, vol. 6, no. 12, 2016.
- [30] E. Sarajlic, C. Yamahata, M. Cordero, and H. Fujita, "Three-phase electrostatic rotary stepper micromotor with a flexural pivot bearing," *Journal of Microelectromechanical Systems*, vol. 19, no. 2, pp. 338–349, 4 2010.
- [31] X. Pei, J. Yu, G. Zong, S. Bi, and Y. Hu, "A novel family of leaf-type compliant joints: Combination of two isosceles-trapezoidal flexural pivots," *Journal of Mecha-*

- nisms and Robotics, vol. 1, no. 2, pp. 1–6, 5 2009.
- [32] J. Yu, X. Pei, M. Sun, S. Zhao, S. Bi, and G. Zong, “A new large-stroke compliant joint & micro/nano positioner design based on compliant building blocks,” in *Proceedings of the 2009 ASME/IFToMM International Conference on Reconfigurable Mechanisms and Robots, ReMAR 2009*, 2009, pp. 409–416.
- [33] R. M. Panas, “Large displacement behavior of double parallelogram flexure mechanisms with underconstraint eliminators,” *Precision Engineering*, vol. 46, pp. 399–408, 2016. [Online]. Available: <http://dx.doi.org/10.1016/j.precisioneng.2016.06.010>
- [34] S. Henein, P. Spanoudakis, S. Droz, L. I. Myklebust, and E. Onillon, “Flexure pivot for aerospace mechanisms,” in *European Space Agency, (Special Publication) ESA SP*, no. 524, 2003, pp. 285–288. [Online]. Available: <https://www.researchgate.net/publication/228802192>
- [35] M. Stranczl, E. Sarajlic, H. Fujita, M. A. Gijs, and C. Yamahata, “High-angular-range electrostatic rotary stepper micromotors fabricated with SOI technology,” *Journal of Microelectromechanical Systems*, vol. 21, no. 3, pp. 605–620, 2012.
- [36] A. Kyusotin, D. Sagawa, and A. Toyama, “Development of Linear and Rotary Movement Mechanisms by Using Leaf Springs,” *Journal of the Japan Society for Precision Engineering*, vol. 53, no. 7, pp. 1092–1096, 1987.
- [37] F. Parvari Rad, G. Berselli, R. Vertechy, and V. Parenti-Castelli, “Stiffness Analysis of a Fully Compliant Spherical Chain with Two Degrees of Freedom,” in *Advances in Robot Kinematics*. Springer International Publishing, 2014, pp. 273–284.
- [38] F. Parvari Rad, V. Parenti Castelli, and G. Berselli, “Design and Characterization of Curved and Spherical Flexure Hinges for Planar and Spatial Compliant Mechanisms,” 2014.
- [39] F. Parvari Rad, G. Berselli, R. Vertechy, and V. Parenti-Castelli, “Design and stiffness analysis of a compliant spherical chain with three degrees of freedom,” *Precision Engineering*, vol. 47, pp. 1–9, 1 2017.
- [40] S. Zhao, S. Bi, J. Yu, M. Sun, and G. Zhong, “A large-deflection annulus-shape flexure hinge based on curved beams,” in *Proceedings of the ASME Design Engineering Technical Conference*, vol. 2, no. PARTS A AND B, 2008, pp. 249–255. [Online]. Available: <https://proceedings.asmedigitalcollection.asme.org>
- [41] S. Hampali, S. Anoosha Pai, and G. K. Ananthasuresh, “A Tunable Variable-Torque Compliant Hinge Using Open-Section Shells,” *Journal of Mechanisms and Robotics*, vol. 12, no. 6, 12 2020.
- [42] F. Parvari Rad, G. Berselli, R. Vertechy, and V. P. Castelli, “Compliance based characterization of spherical flexure hinges for spatial compliant mechanisms,” in *Mechanisms and Machine Science*, vol. 22. Kluwer Academic Publishers, 2014, pp. 401–409.
- [43] F. Parvari Rad, R. Vertechy, G. Berselli, and V. Parenti-Castelli, “Design and stiffness evaluation of a compliant joint with parallel architecture realizing an approximately spherical motion,” *Actuators*, vol. 7, no. 2, 6 2018.
- [44] ———, “Analytical compliance analysis and finite element verification of spherical flexure hinges for spatial compliant mechanisms,” *Mechanism and Machine Theory*, vol. 101, pp. 168–180, 7 2016.
- [45] G. Berselli, F. Parvari Rad, R. Vertechy, and V. Parenti Castelli, “Comparative evaluation of straight and curved beam flexures for selectively compliant mechanisms,” in *2013 IEEE/ASME International Conference on Advanced Intelligent Mechatronics: Mechatronics for Human Wellbeing, AIM 2013*, 2013, pp. 1761–1766.
- [46] F. Parvari Rad, R. Vertechy, G. Berselli, and V. Parenti-Castelli, “Compliant Serial 3R Chain with Spherical Flexures,” 2018, pp. 11–21.
- [47] M. Tanik, V. Parlaktaş, E. Tanik, and S. Kadiolu, “Steel compliant Cardan universal joint,” *Mechanism and Machine Theory*, vol. 92, pp. 171–183, 6 2015.
- [48] D. F. Machekposhti, N. Tolou, and J. L. Herder, “A review on compliant joints and rigid-body constant velocity universal joints toward the design of compliant homokinetic couplings,” 2015.
- [49] J. Rommers, t. M. Naves, D. M. Brouwer, and J. L. Herder, “A flexure-based linear guide with torsion reinforcement structures,” Tech. Rep., 2018.
- [50] J. Ray, V. Gupta, S. Mukherjee, and J. P. Khatait, “Designing compact remote centre of compliance devices for assembly robots,” Tech. Rep., 2015.
- [51] J. B. Hopkins and M. L. Culpepper, “Synthesis of multi-degree of freedom, parallel flexure system concepts via Freedom and Constraint Topology (FACT) - Part I: Principles,” *Precision Engineering*, vol. 34, no. 2, pp. 259–270, 4 2010.
- [52] S. Havlikv, “A New Elastic Structure for a Compliant Robot Wrist,” *Robotica*, vol. 1, no. 2, pp. 95–102, 1983.
- [53] Y. Liu and M. Y. Wang, “Optimal design of remote center compliance devices of rotational symmetry,” *IFIP Advances in Information and Communication Technology*, vol. 435, pp. 161–169, 2014. [Online]. Available: <https://hal.inria.fr/hal-01260756>
- [54] G. Li and G. Chen, “Achieving compliant spherical linkage designs from compliant planar linkages based on PRBM: A spherical Young mechanism case study,” in *2012 IEEE International Conference on Robotics and Biomimetics, ROBIO 2012 - Conference Digest*, 2012, pp. 193–197.
- [55] S. Jagirdar, “Kinematics of curved flexible beam,” Ph.D. dissertation, 2006.
- [56] M. Gaafar, M. Magdy, A. T. Elgammal, A. El-Betar, and A. M. Saeed, “Development of a New Compliant Remote Center of Motion (RCM) Mechanism for Vitreoretinal Surgery,” in *2020 6th International Conference on Control, Automation and Robotics, ICCAR 2020*, 2020, pp. 183–187.
- [57] K. Chandrasekaran, A. Somayaji, and A. Thondiyath, “Realization of a statically balanced compliant planar

remote center of motion mechanism for robotic surgery,” in *Frontiers in Biomedical Devices, BIOMED - 2018 Design of Medical Devices Conference, DMD 2018*. American Society of Mechanical Engineers (ASME), 2018.

- [58] W. Chen, S. Chen, J. Qu, and W. Chen, “A large-range compliant remote center of motion stage with input/output decoupling,” *Precision Engineering*, vol. 51, pp. 468–480, 1 2018.
- [59] J. Qu, W. Chen, J. Zhang, and W. Chen, “A piezo-driven 2-DOF compliant micropositioning stage with remote center of motion,” *Sensors and Actuators, A: Physical*, vol. 239, pp. 114–126, 3 2016.
- [60] B. J. Choi, S. V. Sreenivasan, S. Johnson, M. Colburn, and C. G. Wilson, “Design of orientation stages for step and flash imprint lithography,” *Precision Engineering*, vol. 25, no. 3, pp. 192–199, 2001.
- [61] P. P. Valentini and E. Pennestrì, “Compliant four-bar linkage synthesis with second-order flexure hinge approximation,” *Mechanism and Machine Theory*, vol. 128, pp. 225–233, 10 2018.
- [62] V. Parlaktas, E. Tanik, and M. Tanik, “On the design of a novel fully compliant spherical four-bar mechanism,” *Advances in Mechanical Engineering*, vol. 11, no. 9, 2019.
- [63] X. Wu, Y. Lu, X. Duan, D. Zhang, and W. Deng, “Design and DOF analysis of a novel compliant parallel mechanism for large load,” *Sensors (Switzerland)*, vol. 19, no. 4, 2 2019.
- [64] D. E. Whitney and J. M. Rourke, “Mechanical behavior and design equations for elastomer shear pad remote center compliances,” *Journal of Dynamic Systems, Measurement and Control, Transactions of the ASME*, vol. 108, no. 3, pp. 223–232, 1986. [Online]. Available: <http://www.asme.org/about-asme/terms-of-use>
- [65] S. Choi, S. Lee, and S. Won, “Development of a new variable remote center compliance using stiffness adjusters,” *IEEE International Conference on Intelligent Robots and Systems*, vol. 4, pp. 1860–1863, 2001.
- [66] S. Lee, “Development of a new Variable Remote Center Compliance (VRCC) with modified Elastomer Shear Pad (ESP) for robot assembly,” *IEEE Transactions on Automation Science and Engineering*, vol. 2, no. 2, pp. 193–197, 4 2005.
- [67] —, “Shear control of elastomer shear pads for variable remote center compliance,” *Advanced Robotics*, vol. 23, no. 1-2, pp. 227–237, 1 2009.

B

Concept Generation

This appendix will show some of the designs considered for this thesis. While a lot of concepts have been generated, only a small selection of concepts will be presented, these concepts showed the most potential or were interesting for future works. All concepts try to at least one of the challenges indicated in Chapter 2, the challenge of changing the rotational axis and to reduce the stiffness when walking. The red dotted line and the red dot in the images indicate the axis of rotation of the mechanism.

B.1. Concept A

Concept A consists of a beam fully encircling the user. The warping beam on both sides of the user creates a rotational axis which averages to the middle to align with the rotational axis of the hip joint of the human body. With fixation on the sides of the hip the mechanism can be fixed to the body. The mechanism showed potential in the 3d printed prototype, however the range of motion seemed limited. Furthermore, applying a force on both sides towards each other did show some bistability. This could potentially be used to lower the stiffness of the mechanism. Another problem with this concept is that the mechanism uses a lot of space on the front of the user, which would most likely hinder the user while lifting or bending.

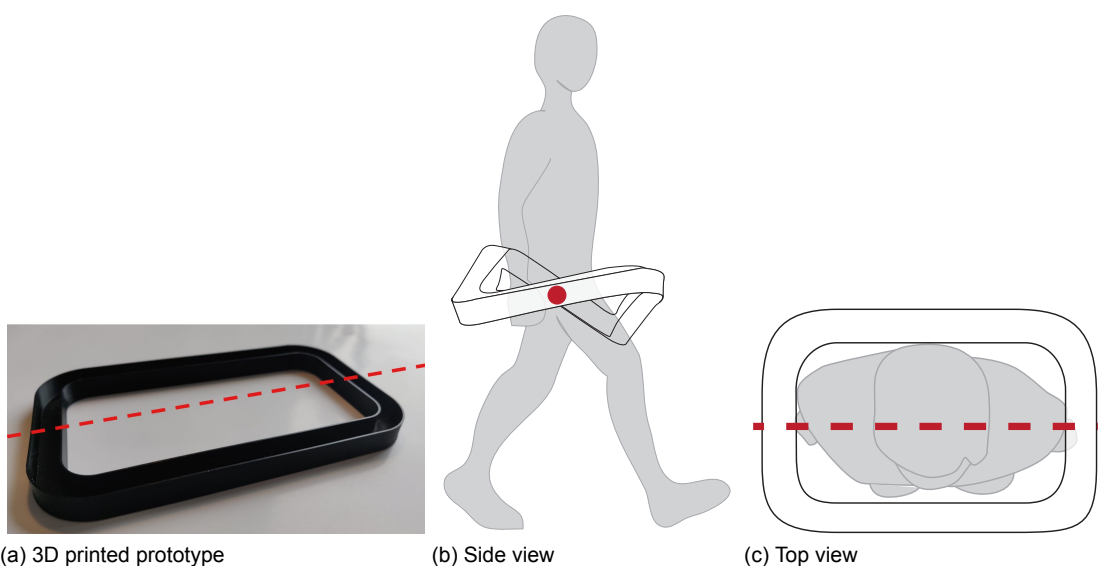


Figure B.1: Concept A

B.2. Concept B

Concept B uses a LITF mechanisms to force a warping beam to have a remote center of motion. More information about this LITF Mechanism can be found in Appendix A. The remote center of motion of this mechanism could be aligned with the rotational axis of the hip joint. The principle worked as expected, however the range of motion was limited due to the way LITF mechanism works. Furthermore, the mechanism was bulky, complex and consists of a lot of different parts. For the mechanism there was also not a clear method found to lower the stiffness of the mechanism. Therefore, while the mechanism showed potential it was rejected as a feasible solution.

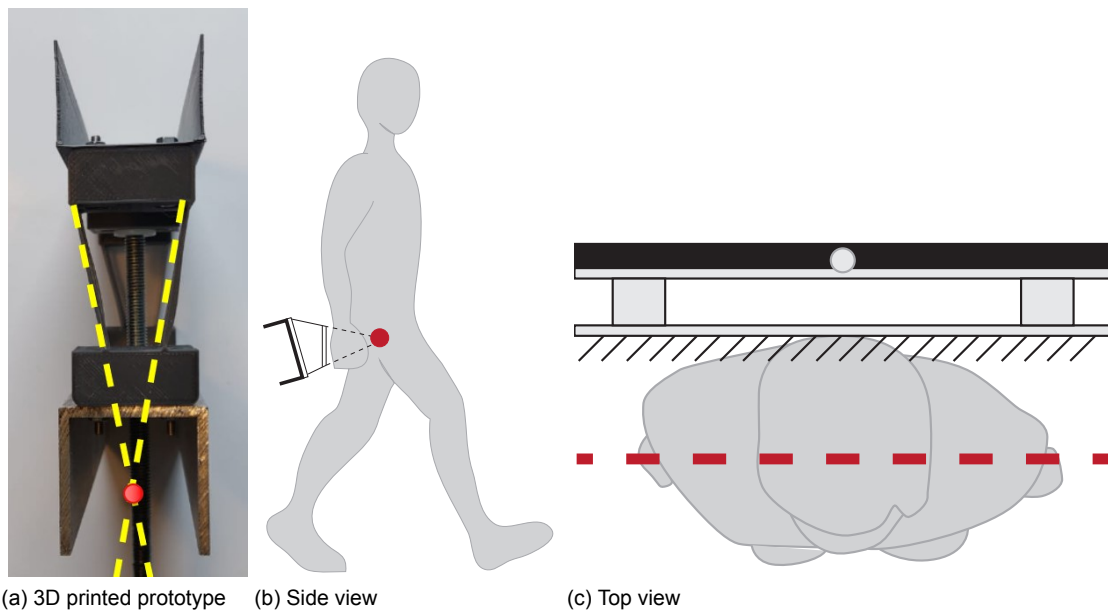


Figure B.2: Concept B

B.3. Concept C

Concept C uses constraints on the side of the hips to force the mechanism to rotate around that axis, this is the same axis as the rotational axis of the hip joint. For this concept 2 points on the side are constrained allow rotation in all directions while only allowing sideways translation in the same axis as the rotational axis of the hip. Furthermore a point on the back is constrained to have the desired differential behaviour. This fixed the challenge of changing the rotational axis, however the stiffness was not reduced. It was quickly discovered that when the two sides at the fixation points were pulled outwards an interesting behaviour occurred, this behaviour was bistability. This bistability indicated that neutral stability could most likely be achieved and that the stiffness of the mechanism could be reduced. This mechanism showed the most potential and was chosen as the concept to further investigate because of the large variety of new concepts to make this mechanism neutrally stable or bistable. A few interesting concepts are Concept C1 to C3

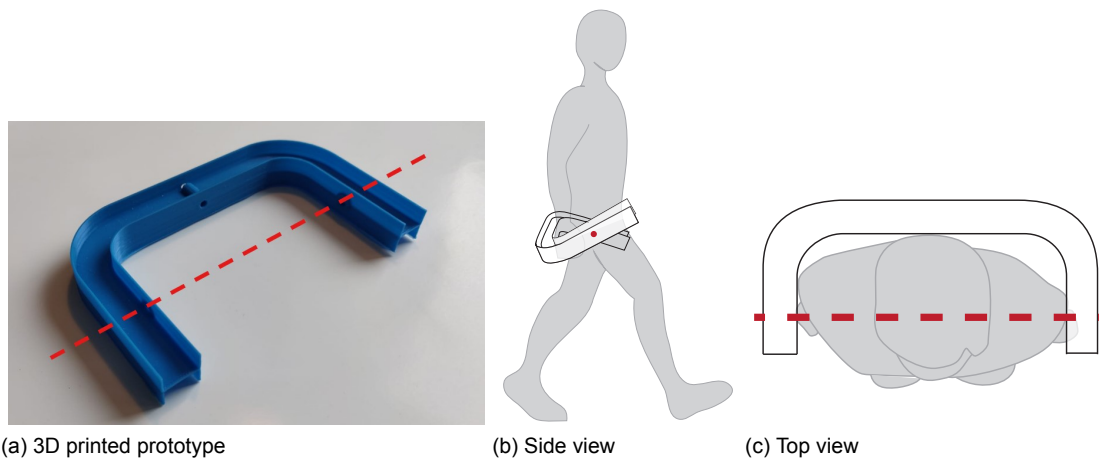


Figure B.3: Concept C

B.3.1. Concept C1

The first idea was to use the force of springs to push outwards as can be seen in Figure. B.4. This showed a lot of promise as I was able to make the 3d printed prototype have both neutrally stable and bistable behaviour by changing the springs. The neutral stability could be achieved over a relatively large range of motion while also rotating around the shifted rotational axis. This was also the case for bistability if the spring force was increased.

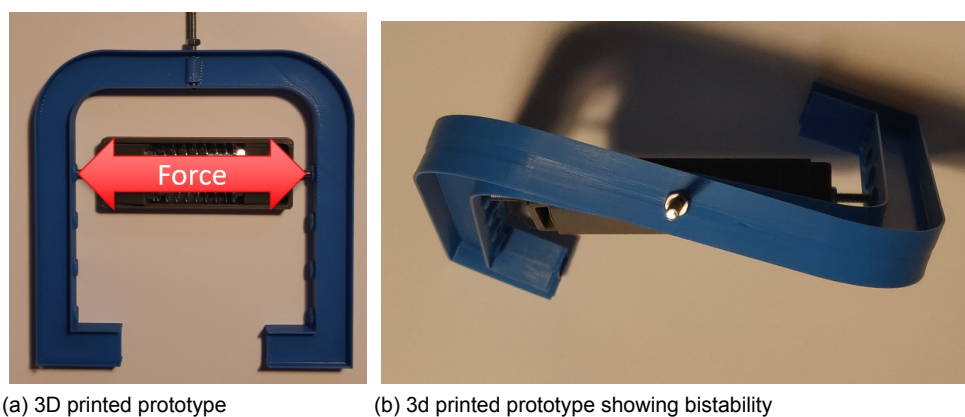
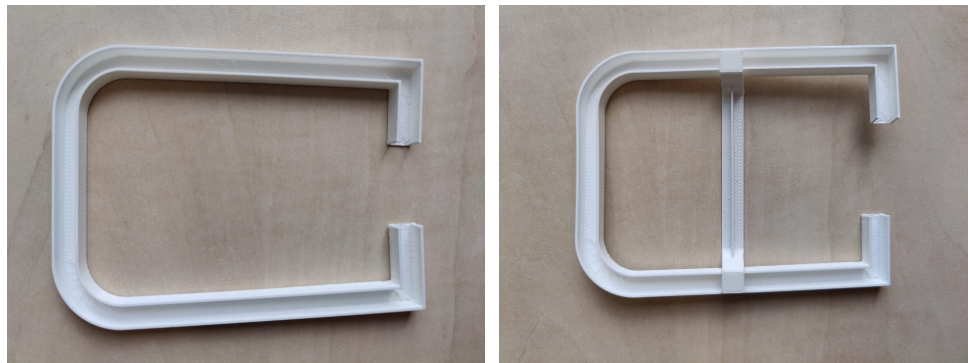


Figure B.4: Concept C1

B.3.2. Concept C2

While Concept C1 showed a lot of potential, using springs was not the preferred solution. The preferred solution would be a mechanism which had a monolithic body, and thus constructed from one single piece of material. Concept C2 uses the "legs" of the mechanism, the parts on the side of the body, as springs. If the mechanism is constructed with "legs" having an inwards angle, we can push the "legs" back to the original position. This forces the "legs" outwards and in a way work like a spring. A prototype for this idea was constructed and indeed showed bistability. However, the mechanism required a very large peak force to switch from one position to the other, this was due to the high bending stiffness of the "legs" in the outward direction. This could be altered by changing the geometry or cross section of the "legs", to make them more flexible. This method was however not chosen in the end, the reason for this was that the method using springs was already quite complex and not well understood. Therefore, this was deemed to be a subsequent project after the mechanism was better understood with fewer variables.



(a) Angels manufactured with inward angle

(b) The inward angle is nullified by a fixation

Figure B.5: Concept C2

B.3.3. Concept C3

Concept C3 had the same idea as Concept C2, Creating a monolithic body while having the benefits of Concept C1. The idea for this concept is to introduce prestresses in the flanges of the mechanism, similar to what Lachenal et al. have done (as discussed in the Paper in Chapter 4). A prototype has been created using this idea, the web (blue) was printed in the straight configuration, while the flanges (white) were printed with an inward angle. These separate components were then glued together, which in theory would introduce prestresses in the flanges which could change the stiffness of the mechanism. In practice, this did not work well, the web was not stiff enough to force the flanges outwards. When the web was reinforced to have the stiffness required to prestress the flanges, the stiffness of the mechanism itself was also increased due to the added material. While in theory this method shows potential, in practise it did not work out in this manner. This concept was not further explored for the same reason Concept C2 was not further explored, concept C1 was deemed a good starting point of the mechanism with less complexity. However, this would be an interesting concept for future research.

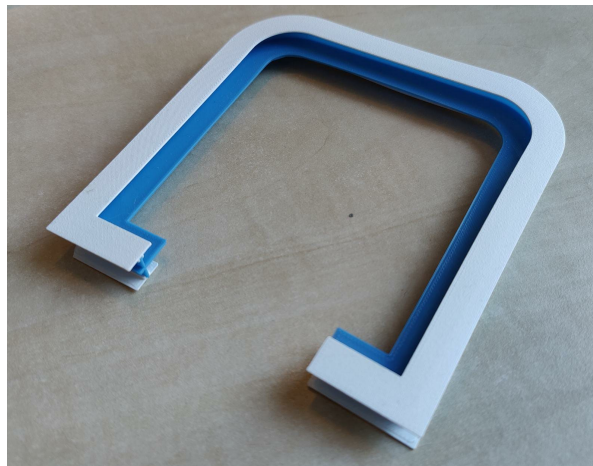
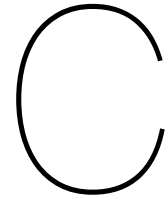


Figure B.6: Concept C3, The web(blue) and flanges(white) have been printed separately



Additional Results

C.1. Linear spring validation

Fig. C.1 shows with the red line the simulated linear springs, following Hooke's law, used for preloading. The initial preload of each preload case is shown with the asterisk at the initial load and compression. The experimental results for validation of the linear spring assumption are shown with the dotted lines for both of the springs. The spring stiffness c is validated to be 1.49 N/mm which was used in the simulations to simulate the spring compression.

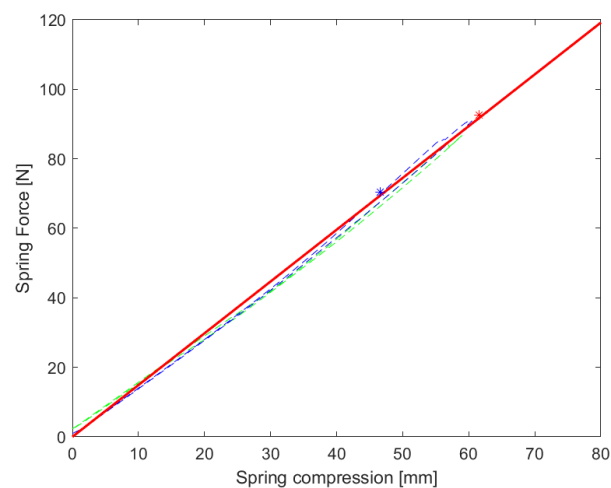


Figure C.1: The Simulated springs(Red) and the measured springs to validate if the used springs follow Hooke's law

C.2. Kinematic Performance Ratio

The kinematic performance ratio of the compliant differential mechanism is calculated by measuring the angle of both the actuated side and the unactuated side. These angles are plotted against each other to find the correlation, as can be seen in Figure C.2. From these data points, a linear regression is taken, for which the slope of this linear regression approximates the average kinematic performance ratio over the complete range of motion. For the experimental results, the slope found for researched mechanism with an initial preload of 70N was 0.9515 as can be seen in Figure C.2a. The data points showed a clear linear trend with only a small deviation. It also shows that the angular deformation does not effect the kinematic performance ratio, thus can be assumed constant for the full range of motion. For the simulated results, the linear trend is even more clear, as can be seen in Figure C.2b. These simulated results do show a slightly higher kinematic performance ratio of 0.9794 for the same initial preload of 70N.

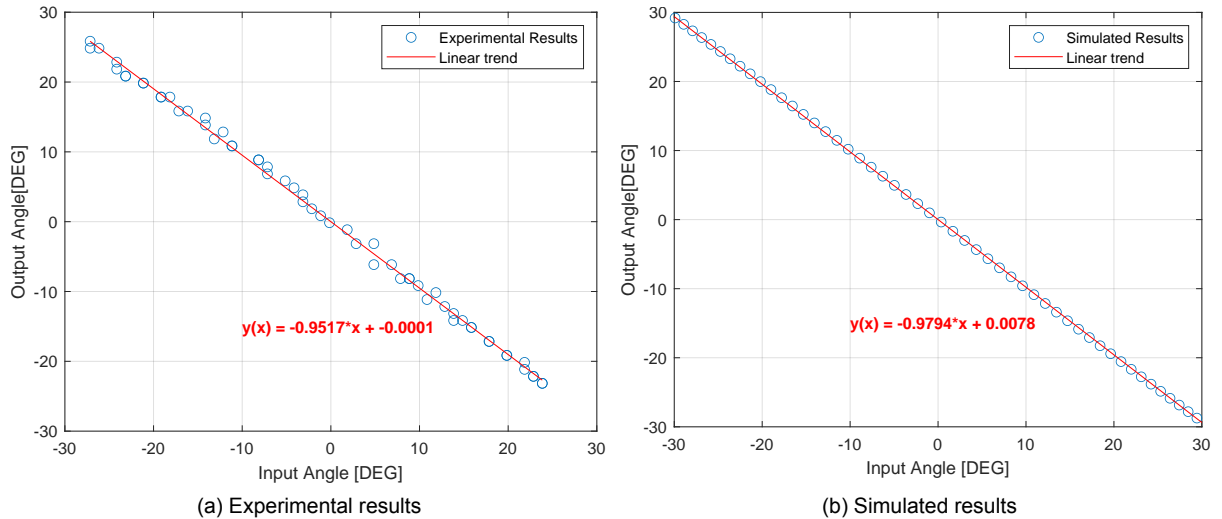


Figure C.2: The kinematic performance ratio calculated by the use of linear regression for both the simulated results and the experimental results

C.3. Stress concentrations

Figure C.3 shows the stresses of the mechanism at the maximum deflection for both the Walking and Bending scenario. For the walking scenario, in Figure C.3a, the main stress distribution can be found on the back side of the mechanism where the main warping of the mechanism occurs. Furthermore, on the inside of the curve at the connection between the web and the flanges, stress concentrations can be observed. These stress concentrations could be lowered by using a larger radius curve. The stresses in the two sides are much lower, this would indicate that these parts do not contribute as much to the behaviour and could therefore be altered. These could be made slimmer to give the user more range of motion around this area. For the Bending scenario, in Figure C.3b, The main stress concentration can be found at the point of actuation. A rotational displacement is applied to a line of nodes at this point, which create high stress concentrations. The two curves also show a higher stress concentration, this could also be more distributed by using a larger radius for the curvature. The stresses in the two sides are again much lower than the rest of the mechanism, this reinforces the idea of optimising the sides of the mechanism more.

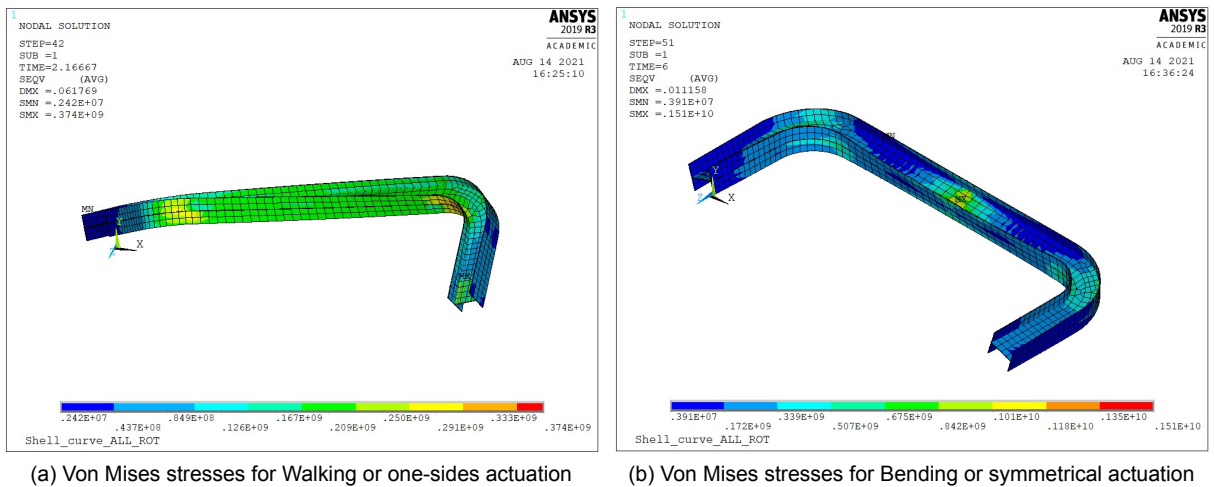


Figure C.3: Von mises stresses at the maximum deflection for both scenarios

C.4. Result unwelded mechanism

Figure C.4 and Figure C.5 show the experimental results of the unwelded mechanism. For this test, the web and flanges were only attached using slots and wedges and not welds were used. This gave a connection which was not a fully rigid connection which led to slightly lower stiffness, this is especially noticeable after 15° degrees of angular rotation. At that point the simulated experimental results how a slightly lower rotational stiffness and thus a lower the actuation moment, this is most noticeable for the 70 N preload and the 85 N preload. After introducing the spotwelds as discussed in Chapter 4, the experimental results showed a much better correlation. The bending scenario has not been tested for this configuration because the fixation mechanism was not deemed sufficient to handle the loads.

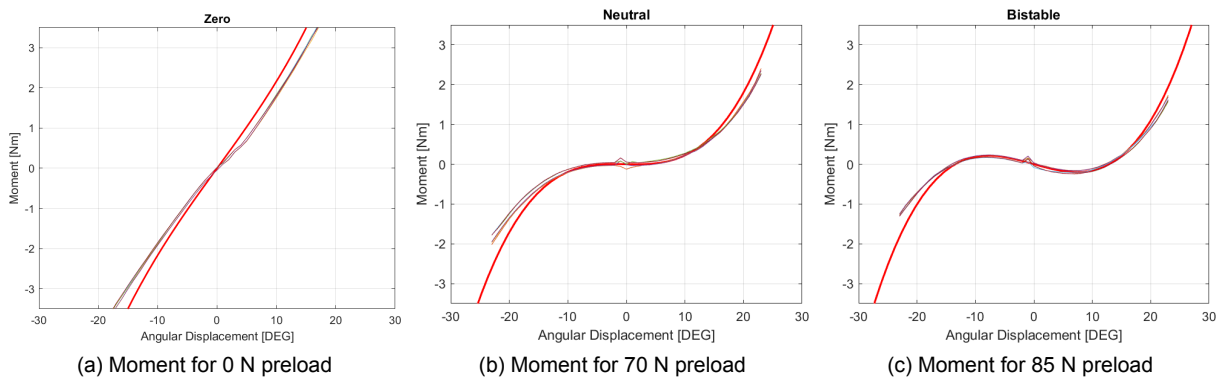


Figure C.4: Moment-Angle curves for the unwelded mechanism. The red line shows the simulated results and the other colour lines show the experimental results of both sides of the mechanism with 3 repetitions

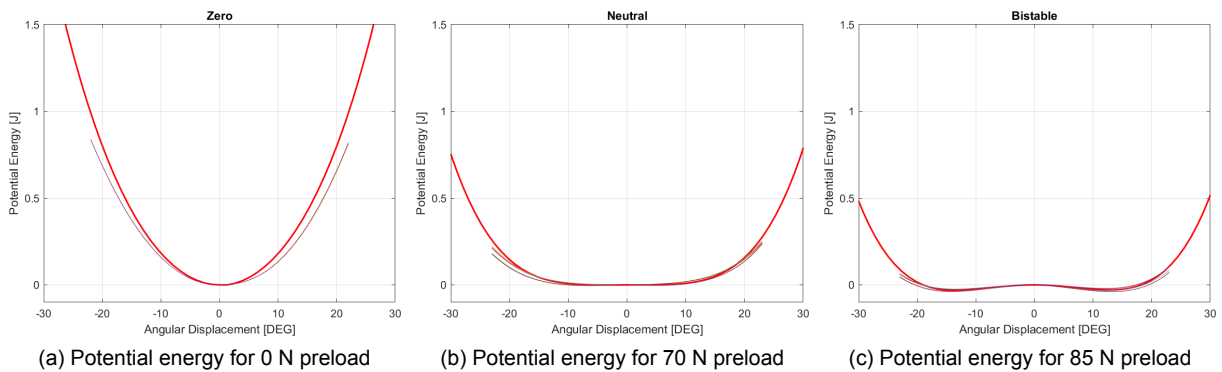


Figure C.5: Potential energy-Angle curves for the unwelded mechanism. The red line shows the simulated results and the other colour lines show the experimental results of both sides of the mechanism with 3 repetitions

C.5. Parameter variation

To find the effect of the bh and bw on the required moments of the mechanism, simulations have been performed. These results can be found in Figure C.6. For these test bh and bw have been varied in steps of 0.1 mm for both the walking and bending scenario after a deformation of 20 N m. For the walking scenario, no preload is applied. If an optimised initial preload was used the required moment would be roughly 3 times lower, however this has not been tested for all dimensions. It was found that an almost linear trend can be observed between 30 mm and 50 mm for both the walking and bending scenario. This also led to a relatively constant ratio between the walking and bending scenario.

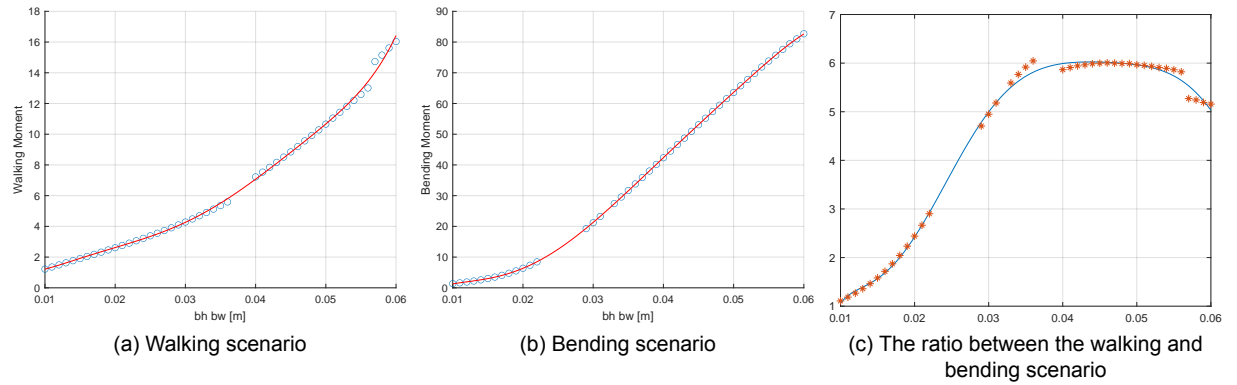
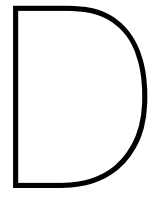


Figure C.6: A parameter variation of bh and bw for both the walking and bending scenario



Exoskeleton Prototype Design



(a) Exoskeleton on a mannequin

(b) Exoskeleton on the human body

Figure D.1: Front view of the Exoskeleton



(a) Exoskeleton on a mannequin

(b) Exoskeleton on the human body

Figure D.2: Rear view of the Exoskeleton



(a) Exoskeleton on a mannequin



(b) Exoskeleton on the human body

Figure D.3: Side view of the Exoskeleton

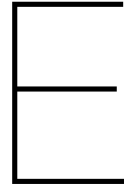


(a) Constraint at point M



(b) Constraint at point R and L

Figure D.4: Constraints



Ansys Parametric Design Language

In this appendix the model, script and choices made for the Ansys model will briefly be explained. The script of the model for Ansys APDL can be found in Appendix G, this is also where all line numbers revert to.

E.1. Initialisation

Because the model is used for optimisation, the model needs to be parametric and conditions of the model should be able to be changed by Matlab. The way this is achieved is by loading a textfile with all the needed conditions and parameters required to control the model. On line 5-10 the used directories are loaded in, these directories are used for loading the parameters, storing log files, and storing the simulated results from the model. On line 32 All the parameters and conditions are loaded in, these parameters determine the dimensions, material property, and the chosen scenario to run. On line 37 the shell model is chosen, The shell model chosen is Shell281. The solid model was too computationally expensive for the use in an optimisation problem therefore a shell model was chosen. The shell is meshed using 8-nodal SHELL281 elements, these elements consist of 8 nodes with each 6 degrees of freedom and is well-suited for linear, large rotation and/or large strain nonlinear applications. 8-nodal SHELL282 elements gave more consistent results than its 4-nodal SHELL181 elements counterpart and was therefore used On line 39-42 the material properties are given to the elements which are used for the web and flanges. Finally on line 45-55 the material properties and element types are attached to the sections used for the flanges and the web, there the thickness of these shells are also defined.

E.2. Model

The model is constructed using keypoints which are located using the parameters defined in Matlab to represent the dimensions of the mechanism. The first thing that is constructed is the overall shape of the mechanism. The mechanism is constructed using lines which are then used to sweep into a surface. The keypoints for the main shape is defined on line 60-74 and the lines are drawn on line 70-85, this line is used on line 118-124 to sweep the cross section into an area. On line 90-114 the cross section for an H cross section is constructed, an If statement is used to check for the requested cross section. For this code the only option is an H cross section to keep the code more condensed, however C cross section can easily be implemented and have been implemented for testing. This cross section is then swept around the main shape mentioned before. this is done on line 117-124 using the ADRAG command. This method of constructing the model is used to create a consistent and stable mesh which can be used reliably for optimisation purposes. The model now consists of 3 surfaces/areas which are merged on line 126. These surfaces are then given the right thicknesses and properties defined on line 45-55, on line 130-140 the surfaces are meshed. On line 160-170 the nodes from which data is required or need to be constrained are defined, this is done using the NODE command, this command selects a node on the location specified. The model is constructed in such a way that that a keypoint is always on the location of which data is required. This ensures that a node will always be on that exact location, this increases the reliability and repeatability of the model for a large range of parameters and dimensions. On line 175-177 the constraints are defined for the nodes

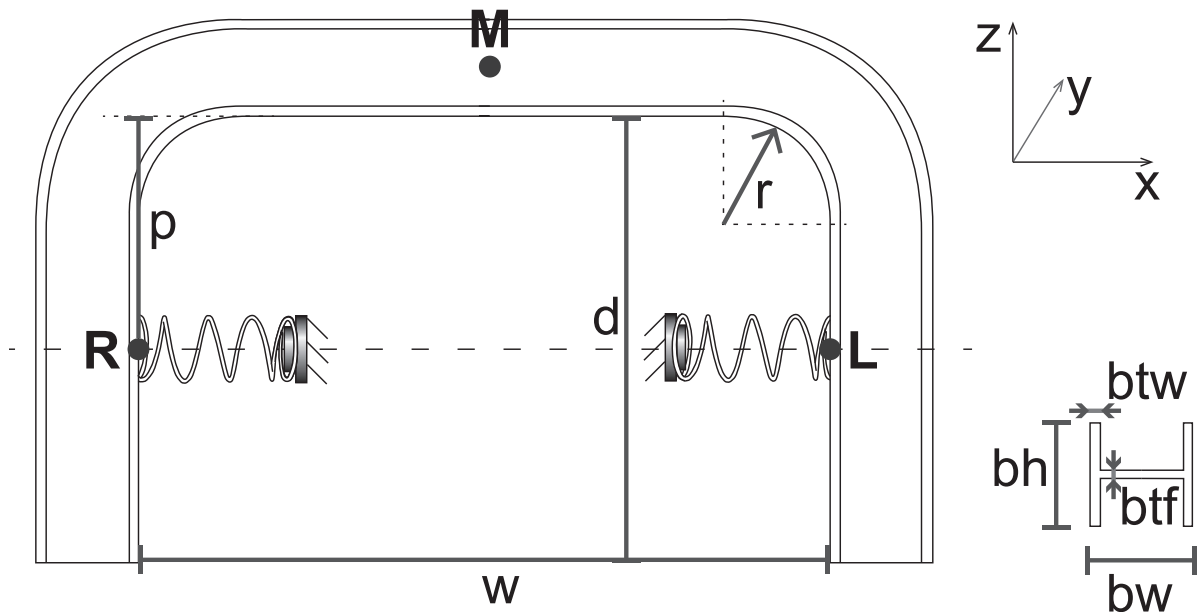


Figure E.1: The model with the dimensions of the mechanism

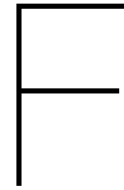
on point R, L and M, for point R and L the translation in the Y and Z direction is constrained. For point M the translation in the Y and X direction are constrained. Rotation around in all directions is allowed.

E.3. Actuation

The actuation of the mechanism is performed by adding a rotation to the centerline of nodes around point R. On line 191-195 this line of nodes is selected, a rotational displacement is applied to these nodes around the x axis. On line 197-205 the mechanism is actuated to the maximum position, then the spring preload force is applied. The preloading of the mechanism is performed by having two forces on points R and L in opposite directions, the force on point R in the positive X direction, and the force on point L in the negative X direction. This force can either be constant or simulating a linear spring in accordance with Hooke's law based on the U_x displacement of points R and L. On line 216-240 the mechanism is then fully actuated to the opposite angle to get results on the full range of motion of the mechanism. This actuation is done using a DO loop, where the solution is solved in small steps. This is not the most elegant solution, however this was found to be the most reliable, applying the full angular displacement in one go did not work reliable enough, even if it was stated the displacement should be performed in a large number of steps. Forcing the solutions to apply only small displacements was very reliable and gave more control over the simulation and was therefore chosen. On line 271-301 the lifting scenario is simulated, a line of nodes spanning a line in the Z direction at point M in the web. These nodes are selected on line 285-290. The rest of the code is similar to the walking scenario, this is again done in small steps.

E.4. Data Storage

After the simulation are done the stored data of all the nodes need to be retrieved and stored for analysis in Matlab. The data stored for individual nodes are retrieved on line 325-354, this data is then stored in variables which are later used to store the data in a .csv file. This was also why it model was modelled in this fashion using the keypoints at predefined locations, this allowed for easy retrieving of the stored data of those specific nodes and keypoints. The data which can be retrieved are displacement, rotational displacement, reaction forces and reaction moments. All data from the specified nodes is then placed into a table format on line 363-387, then the data is written to a .csv file on line 392-396. This .csv file could then be loaded by matlab for post processing.



Optimisation Framework

The optimisation framework consist of two parts. The integration of Matlab and Ansys and the optimisation problem itself which uses the aforementioned integration. The Ansys model itself can be found in Appendix E.

F.1. Matlab and Ansys Integration

The most important part for the optimisation framework is the integration of Matlab and Ansys APDL. The codes used for this can be found in Appendix H.

The integration of Matlab and Ansys can be divided into 3 different stages:

1. Initialising the settings, parameters and directories in Matlab
2. Running the Ansys model
3. Retrieving, analysing and storing the results of the data in Matlab

F.1.1. Initialisation

The first stage is to initialise the settings, parameters, directories which are required for the running of the Ansys model. This stage starts in `Run_ANSYS.m`. On line 12-14 the choice can be made for whether to run the walking scenario, lifting scenario and whether to use a spring or a constant force as the preload. On line 20-25 more initial settings can be selected to chose what will be ran, with regards to plotting, parameters, analysis and/or automatic parameter appointment for Solidworks. On line 27-28 the material choice and cross section of the material can be chosen. line 36-39 set the directory correct, this is done so that it doesn't matter where on the PC the current folder is located it still. In `Setup_Directories.m` a sting is created with the correct directories, which is later used to start the Ansys simulation. On line 27 the parameters are initialised using `Set_Parameters_True_Scale.m` and then stored. All data in this code is stored in a struct called `RESULT` to keep everything accessible in all scripts. Finally on line 55 the script `RUN_Scenario.m` is ran. This script runs the scripts according to the settings set on line 12-14 of `Run_ANSYS.m`. in `Write_Parameters_ANSYS.m` all parameters, settings and configurations are written to a text-file called `ANSYS_input.txt`, this text-file is used to load all information from Matlab to Ansys required for the simulation. This is essential for the integration of Matlab and Ansys and the optimisation. This concludes all initialisation required to run the Ansys model.

F.1.2. Running Ansys model

To start running the Ansys model the script `Run_ANSYS_Batch.m` is ran in `Run_Scenario.m`. On line 8-22 of `Run_ANSYS_Batch.m` the logfiles and memory of previous runs of the Ansys model are deleted. These files sometimes caused errors when the model was ran multiple times in a row, most likely due to a file running out of memory. Therefore these are deleted before each run, this does not

effect the running of the model itself. This increased the robustness and stability of the integration. on line 27 a sting is created which is later used with the `dos` command to run Ansys in batch mode. This `dos` command is used on line 24-27. This starts the Ansys simulations as discussed in Appendix E. Finally on line 22 and line 39-40 the time in which the model ran is calculated and stored, this is later used to calculate if the file with simulated results is recent and from the current run.

F.1.3. Post processing

When the Ansys model finished simulating the post processing of the results is initiated.

In `Load_Store_Results.m` all data in the `.csv` created by the Ansys model is loaded into Matlab. This is preformed on line 33, however before this another important step is taken. on line 10-30 the time difference between when the data was saved and the current time is calculated, this ensures that the data which is loaded is from the most recent run and not a previous run with different parameters. This creates an extra fail safe and is important for the optimisation to run reliably. The rest of this file analyses the data and converts the data to usable/processed data for further analysis and optimisation. In `Analysis.m` the Root Mean Squared Error of various data is calculated to be used in the optimisation problem. Finally, in `Plot_Results.m` the results are plotted to showcase the results of the Ansys APDL simulations.

F.2. Optimisation

For the optimisation itself, the codes can be found in Appendix I. For the optimisation problem in Matlab the `fmincon` function is used, this function is for finding the minimum of constrained nonlinear multi-variable problems. The algorithm used for this problem is interior-point. The main difference between the two preformed optimisations is the difference in design parameters and objective functions. These optimisation problems are run independent and sequentially. The input parameters for both optimisations are the same, they consist of the hip breadth, hip depth, and desired bending moment. The optimisation uses the framework mentioned above to vary the parameters to find an optimum design. The optimisation is started and initialised in `Run_ANSYS_Optimisation_bh_bw_F0.m`. The initialisation on line 1-59 is basically the same as the initialisation in `Run_ANSYS.m`. On line 63 the optimisation is started for `bh` and `bw` in `Optimization_bh_bw_same.m`. On line 8-23 the boundary and starting conditions are initialised and stored. On line 27 the Objective function is defined.

This objective function can be found in `OBJ_FUNC_Run_ANSYS_bh_bw_same.m`, in this script a constant or spring force can be applied on line 7-19. On line 21 the simulation is started with using the `RUN_Scenario.m` discussed earlier. On line 23-37 the values used for the objective function are loaded and calculated, On line 28 the penalty function to optimise the minimum required lifting force is calculated. Line 40-44 checks if the results are recent to not use the results of an earlier simulation using other values. Finally, on line 41 the weighted objective function is calculated to minimize the `bw` and `bh` while minimising the work required for walking and a penalty function to make sure the minimal support is provided.

The optimisation for the initial preload, in `Run_ANSYS_Optimisation_bh_bw_F0.m` on line 69 the same approach is used as for the optimisation of the initial preload. With `OBJ_FUNC_Run_ANSYS_0.m` as the objective function. Notice the weighted function is mainly optimising for the RMSE to approximate zero stiffness.



Ansys Parametric Design Language Code

```

1 ! Robin Mak
2
3 !!!!!!!!!!!!! General info
4
5     *DIM, Dir_Log ,STRING,200
6     *DIM, Dir_Data ,STRING,200
7     *DIM, Dir_Input ,STRING,200
8     Dir_Log(1) = JOIN(Dir(1), 'Logs')
9     Dir_Data(1) = JOIN(Dir(1), 'ANSYS_DATA')
10    Dir_Input(1) = JOIN(Dir(1), 'ANSYS_INPUT')
11
12    /CWD, Dir_Log(1)
13
14    finish
15    /title , Shell_curve_ALL_ROT
16    /FILENAME, Shell_curve_ALL_ROT ,1
17
18    /CONFIG, NRES, 100000 ! assigns values to ansys configuration manager, "nres" is the
19        parameter to be changed
20        ! 100000 is the maximum amount of data sets on result file
21
22    *Abbr, Eplot, eplot ! defines an abbreviation, makes them appear in the tool box bar
23    *Abbr, Gplot, gplot ! defines an abbreviation, makes them appear in the tool box bar
24    *Abbr, Deformed, PLDISP,2 ! dispays the displaced structure, makes them appear in the tool
25        box bar
26
27
28    /units ,SI
29
30    KEYW,PR_STRUC,1
31    PI = ACOS(-1)
32
33    /INPUT, 'ANSYS_input', 'txt', Dir_Input(1) !Load the Parameters specified in matlab
34
35    /PREP7
36    !element selection
37    ET, 1, shell281!shell181! SOLSH190 !shell181 !beam188 ! defines a local element type
38        from the library (ET, ITYPE, Ename, KOP1, KOP2)
39
40    mp, ex, 1, Elastmod !Defines a linear material property as a constant or a function of
41        temperature.
42    mp, nuxy, 1, Poisson
43    !mp, gxy, 1, Gmod
44    mp, dens,1, Density
45
46    ! create crosssection
47    sect,1,shell,, !Inside Flange
48    secdata, btf,1,0,0,3
49    secoffset,USER, -btf/2
50
51    sect,2,shell,, !Outside Flange
52    secdata, btf,1,0,3
53    secoffset,USER, btf/2
54
55    sect,3,shell,, !Web
56    secdata, btw,1,0,3
57    secoffset,MID
58
59    !! CREATE BODY
60    ! Define keypoints SHAPE
61    K,1, 0, 0, 0
62    K,2, 0, 0, -d+r
63    K,3, r, 0, -d
64    K,4, w/2, 0, -d
65    K,5, w-r, 0, -d
66    K,6, w, 0, -d+r
67    K,7, w, 0, 0

```

```

67 |
68 | !Center of arcs SHAPE
69 | K,101, r, 0, -d+r
70 | K,102, w-r, 0, -d+r
71 |
72 | ! extra points for atachment
73 | K,1001, 0, 0, -d+P
74 | K,1002, w, 0, -d+P
75 |
76 | ! define Lines SHAPE
77 | NUMSTR,LINE,100 ! controls the starting number for any subsequently created lines.
78 | L,1,1001
79 | L,1001,2
80 | LARC,2,3,101,r,
81 | L,3,4
82 | L,4,5
83 | LARC,5,6,102,r,
84 | L,6,1002
85 | L,1002,7
86 |
87 | LSEL, S, , , 100, 108
88 | CM, SHAPE, LINE
89 |
90 | *IF, CROSS_SECTION,EQ,'H',THEN
91 | !! Define keypoints crossection
92 | K,201, 0, 0, 0
93 | K,202, -bw, 0, 0
94 | K,203, 0, bh/2, 0
95 | K,204, -bw, bh/2, 0
96 | K,205, 0, bh, 0
97 | K,206, -bw, bh, 0
98 | K,210, -bw/2, bh/2, 0
99 |
100 |
101 | !! Define lines crossection
102 | NUMSTR,LINE,200 ! controls the starting number for any subsequently created lines.\
103 | L,201,203 !Line 100, Inside flange I beam
104 | L,203,205 !Line 101, Inside flange I beam
105 |
106 | NUMSTR,LINE,300 ! controls the starting number for any subsequently created lines.\
107 | L,202,204 !Line 200, Outside Flange I beam
108 | L,204,206 !Line 201, Outside Flange I beam
109 |
110 | NUMSTR,LINE,400 ! controls the starting number for any subsequently created lines.\
111 | L,203,210 !Line 202, web I beam
112 | L,210,204 !Line 202, web I beam
113 |
114 | *ENDIF
115 |
116 | !! Create I beam sweep
117 | NUMSTR,AREA,200 ! controls the starting number for any subsequently created area.\
118 | ADRAG,200,201 , , , ,SHAPE! Sweep inside line , Area
119 |
120 | NUMSTR,AREA,300 ! controls the starting number for any subsequently created area.\
121 | ADRAG,300,301 , , , ,SHAPE
122 |
123 | NUMSTR,AREA,400 ! controls the starting number for any subsequently created area.\
124 | ADRAG,400,401 , , , ,SHAPE
125 |
126 | NUMMRG,ALL !Merges coincident or equivalently defined items.
127 |
128 |
129 | !! Mesh Areas
130 | ASEL, s, , , 200, 216,, 0 ! Mesh inside flange
131 | AATT, 1, , 1, 0, 1
132 | AMESH, 200,216
133 |
134 | ASEL, s, , , 300, 316,, 0 ! Mesh outside flange
135 | AATT, 1, , 1, 0, 2
136 | AMESH, 300,316
137 |

```

```

138 ASEL, s, , , 400, 416,, 0 ! Mesh web
139 AATT, 1, , 1, 0, 3
140 AMESH, 400,416
141
142
143 FINISH
144
145
146 !! SOLUTION
147 /SOLU
148 antype, STATIC !static analysis
149 autots,off
150 nlgeom,on
151 pstres,on
152 arclen,off !on
153 PRED,on
154
155
156 OUTRES,ALL,ALL
157
158 *IF, CROSS_SECTION,EQ, 'H',THEN
159 !! Constraint Nodes
160 N_R_L = NODE(0, bh/2, -d+P) !Node on left side at rotation point
161 N_R_R = NODE(w, bh/2, -d+P) !Node on right side at rotation point
162 N_P_L = NODE(0, bh/2, -d+P) !Node on left side point of force
163 N_P_R = NODE(w, bh/2, -d+P) !Node on right side point of force
164 N_M_M = NODE(w/2, bh/2, -d-bw/2)!Node on middle front side
165 N_M_B = NODE(w/2, bh/2, -d-bw) !Node on middle back side
166 N_M_F = NODE(w/2, bh/2, -d) !Node on middle front side
167 N_A_F_R = NODE(w+bw/2, bh/2, 0) !Node actuation right
168 N_A_F_L = NODE(-bw/2, bh/2, 0) !Node actuation left
169 N_A_F_L_I = NODE(0, bh/2, 0) !Node actuation right on the inside for the angle
170 N_A_F_R_I = NODE(w, bh/2, 0) !Node actuation right on the inside for the angle
171
172 !! Apply constraints
173 ! Original constraint Node by Robin
174
175 D,N_M_M,,,,,UY,UX
176 D,N_R_L,,,,,UY,UZ
177 D,N_R_R,,,,,UY,UZ
178
179
180 *IF, WALK , EQ, 1,THEN
181 !! START WALKING STAGE
182 T=1
183 ROTX_R_RUN = 0
184 ZERO_POINT=ROTX_R_RUN
185 ROTX_INIT_ROT = MAX_Theta_R
186 STEPS = DISP_STEPS/2
187 ROTX_SZ = (ROTX_INIT_ROT-ZERO_POINT)/STEPS
188 T_SZ = 0.5/STEPS
189
190
191 nsel,S,loc,x,w,w+bt
192 nsel,R,loc,y,bh/2
193 nsel,R,loc,z,-d+P,0
194 CM,NODES_ROTX_R,NODE
195 nsel,ALL
196
197 *DO,ROTX_R,ZERO_POINT,ROTX_INIT_ROT, ROTX_SZ
198 TIME,T
199
200 ! Apply outward displacement
201 D,NODES_ROTX_R, ROTX, ROTX_R
202
203 SOLVE
204 T=T+T_SZ
205 *ENDDO
206
207
208 !! complete displacement

```

```

209 ! *GET,UY_R_RUN,node,N_A_F_R,uy ! get displacement
210 T=2
211 STEPS = DISP_STEPS
212 ROTX_SZ = -ROTX_INIT_ROT*2/STEPS
213 T_SZ = 1/STEPS
214
215 ! Y_R =UX_R_RUN
216 *DO,ROTX_R,ROTX_INIT_ROT,-ROTX_INIT_ROT, ROTX_SZ
217     TIME,T
218
219     *IF, SPRING , EQ, 1,THEN
220         *GET,UX_R,NODE,N_R_R,ux ! get displacement
221         *GET,UX_L,NODE,N_P_L,ux ! get displacement
222
223         !Apply Spring Force
224         F_SPRING_L = -F0-UX_L*k
225         F_SPRING_R = F0-UX_R*k
226         F, N_P_L, FX, F_SPRING_L
227         F, N_P_R, FX, F_SPRING_R
228
229     *ELSEIF, SPRING , EQ, 0,THEN
230         F, N_P_L, FX, -F0
231         F, N_P_R, FX, F0
232
233     *ENDIF
234
235     ! Apply outward displacement
236     D,NODES_ROTX_R, ROTX, ROTX_R
237
238     SOLVE
239     T=T+T_SZ
240 *ENDDO
241
242 ! Remove spring force
243 F, N_P_L, FX, 0
244 F, N_P_R, FX, 0
245
246 T=3.5
247 ROTX_INIT_ROT = MAX_Theta_R
248 STEPS = DISP_STEPS/2
249 ROTX_SZ = (ZERO_POINT + ROTX_INIT_ROT)/STEPS
250 T_SZ = 0.5/STEPS
251
252 *DO,ROTX_R, -ROTX_INIT_ROT, ZERO_POINT, ROTX_SZ
253     TIME,T
254
255     ! Apply outward displacement
256     D,NODES_ROTX_R, ROTX, ROTX_R
257
258     SOLVE
259     T=T+T_SZ
260 *ENDDO
261
262     TIME,T
263     DDELETE, NODES_ROTX_R,ROTX
264     ! D,N_R_R,,,,,UY,UZ !! REconstrains de
265
266     SOLVE
267 *ENDIF
268
269
270 !!! LIFTING STAGE
271 *IF, LIFT , EQ, 1,THEN
272     !!! START LIFTING STAGE
273     T=5
274     Theta_LIFT_MAX = Theta_LIFT_MAX_DEG*PI/180
275     ! Theta_LIFT_MAX = PI/2
276     ZERO_POINT = 0
277     ! F_LIFT_MAX= 1
278
279     F, N_P_L, FX, -F0

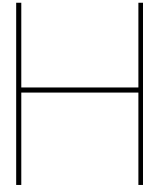
```

```

280 F, N_P_R, FX, F0
281
282 UY_LIFT_SZ = (Theta_LIFT_MAX-ZERO_POINT)/LIFT_STEPS
283 T_SZ = 1/LIFT_STEPS
284
285 ! select web for lifting
286 nsel,S,loc,y, bh/2
287 nsel,R,loc,x, w/2
288 nsel,R,loc,z, -d-bw+btf,-d-btf
289 CM,NODES_ROTX_M,NODE
290 nsel,ALL
291
292 *DO,ROTX_M,ZERO_POINT,Theta_LIFT_MAX, UY_LIFT_SZ
293 TIME,T
294
295 ! Rotation
296 D,NODES_ROTX_M,ROTX, ROTX_M
297
298 SOLVE
299 T=T+T_SZ
300 *ENDDO
301 *ENDIF
302
303
304 FINISH
305
306 /post1
307
308
309 !! Changes the view.
310 /VIEW, All, 1,1,1 !ISO View
311
312 /PBC, ALL, ,1
313 /DSCALE,1,1.0
314 /ESHAPE,1
315
316 EPLOT
317 /REPLOT
318
319 FINISH
320
321 /post26
322 !! Store data to CSV for Matlab
323 NUMVAR, 200
324
325 NSOL,10,N_A_F_L,U,Y,UY_A_L
326 NSOL,11,N_A_F_R,U,Y,UY_A_R
327
328 NSOL,20,N_A_F_R_I,U,Y,UY_A_R_I
329 NSOL,21,N_R_R,ROT,X, ROTX_A_R
330 NSOL,22,N_M_M,ROT,X, ROTX_M_M
331
332
333 NSOL,30,N_R_R,U,X,UX_R
334 NSOL,31,N_R_L,U,X,UX_L
335
336 RFORCE,40,N_A_F_R_I,F,Y, FY_A_R
337 NSOL,41,N_A_F_L_I,U,Y,UY_A_L_I
338
339 !Reaction force on left constraint
340 RFORCE,60,N_R_L,F,Y, FR_L_FY
341 RFORCE,61,N_R_L,F,Z, FR_L_FZ
342
343 !Reaction force on right constraint
344 RFORCE,62,N_R_R,F,Y, FR_R_FY
345 RFORCE,63,N_R_R,F,Z, FR_R_FZ
346
347 NSOL ,70,N_M_M,U,Z, UZ_M_M
348
349 RFORCE,100,N_M_M,F,Y, FR_M_M_FY
350 RFORCE,101,N_M_M,F,X, FR_M_M_FX

```

```
351 RFORCE,102,N_M_F,F,Y, FR_M_F_FY
352 RFORCE,103,N_M_F,F,X, FR_M_F_FX
353 RFORCE,104,N_M_B,F,Y, FR_M_B_FY
354 RFORCE,105,N_M_B,F,X, FR_M_B_FX
355
356
357 STORE,MERGE
358
359
360 !! Save time history variables to file test.txt
361 /CWD, Dir_Data(1)
362
363 *DEL,TO_MATLAB
364 *DIM,TO_MATLAB,TABLE,3000,17!  !! MAXIMUM OF 19 PARAMETERS, OTHERWISE CSV WILL BE CORRUPTED
365 VGET,TO_MATLAB(1,0),1
366 VGET,TO_MATLAB(1,1),10
367 VGET,TO_MATLAB(1,2),11
368
369 VGET,TO_MATLAB(1,3),20
370 VGET,TO_MATLAB(1,4),21
371 VGET,TO_MATLAB(1,5),22
372
373 VGET,TO_MATLAB(1,6),30
374 VGET,TO_MATLAB(1,7),31
375
376 VGET,TO_MATLAB(1,8),40
377 VGET,TO_MATLAB(1,9),41
378
379 VGET,TO_MATLAB(1,10),60
380 VGET,TO_MATLAB(1,11),61
381 VGET,TO_MATLAB(1,12),62
382 VGET,TO_MATLAB(1,13),63
383
384 VGET,TO_MATLAB(1,14),70
385
386 VGET,TO_MATLAB(1,15),100
387 VGET,TO_MATLAB(1,16),101
388
389
390 /OUTPUT, 'ANSYS_DATA_ALL_ROT', 'csv', '.'
391
392 *VWRITE, 'TIME', 'UY_A_L', 'UY_A_R', 'UY_A_R_I', 'ROTX_A_R', 'ROTX_M_M', 'UX_R', 'UX_L', 'FY_A_R', '
    UY_A_L_I', 'FR_L_FY', 'FR_L_FZ', 'FR_R_FY', 'FR_R_FZ', 'UZ_M_M', 'FR_M_M_FY', 'FR_M_M_FX'
393 %C, %C
394 *VWRITE, TO_MATLAB(1,0), TO_MATLAB(1,1), TO_MATLAB(1,2), TO_MATLAB(1,3), TO_MATLAB(1,4), TO_MATLAB
    (1,5), TO_MATLAB(1,6), TO_MATLAB(1,7), TO_MATLAB(1,8), TO_MATLAB(1,9), TO_MATLAB(1,10),
    TO_MATLAB(1,11), TO_MATLAB(1,12), TO_MATLAB(1,13), TO_MATLAB(1,14), TO_MATLAB(1,15), TO_MATLAB
    (1,16)
395 %G, %G
396 /OUTPUT, TERM
397
398
399 /CWD, Dir_Log(1)
400 FINISH
```

Matlab and Ansys APDL integration codes

H.1. Run_ANSYS.m

Run_ANSYS.m

```
1 % Robin Mak
2 clc; clear all; close all;
3 addpath('MATLAB') %Include MAIN folder
4
5 %% INIT
6 RESULT = struct;
7 i=1;
8
9 %% RUN Settings
10 SETTINGS.TYPE = 'ALL_ROT';
11
12 SETTINGS.SPRING = 1; % 1 = Spring, 0 = constant Force
13 SETTINGS.WALK = 1; %1=on , 0=off % Start Walking Senario
14 SETTINGS.LIFT = 0; % 1 =on , 0=off % Start Lifting Senario
15
16 % Run ANSYS
17 SETTINGS.ANSYS = 0; % 1=on , 0=off %Run ansys or not
18
19 % Run Matlab Sections
20 SETTINGS.PARAM_FILE = 1;
21 SETTINGS.LOAD_STORE = 1; % 1=on , 0=off %Run ansys or not
22 SETTINGS.PLOT = 1;
23 SETTINGS.ANALYSIS = 1;
24 SETTINGS.DEL_LOGS = 1; %Deletes all log files , log files can give problems in some
    instances
25 SETTINGS.PARAM_SOLIDWORKS = 1;
26
27 SETTINGS.MATERIAL = 'AISI_301'; %'Steel'; %PLA, Steel
28 SETTINGS.CROSS_SECTION = 'H';
29
30 %% SET ANSYS DIRECTORY!
31 % Things to Check before running:
32 % 1) Locate ANSYS195.exe file and paste below
33 % 2) Make sure the vpn is running
34 % 3) If Ansys does not run properly, delete all files in the Logs folder
35 % 4) Check if first 3 lines are commented of .ANS file
36 PARAM.ANSYS_DIR = "C:\Program Files\ANSYS Inc\v195\ansys\bin\winx64\ANSYS195.exe";
37 PARAM.currentFolder = pwd;
38
39 Setup_Directories(PARAM,SETTINGS) % Fixes all directories!
40
41 %% RUN
42 fprintf('- - START RUNNING %s - -\n',SETTINGS.TYPE)
```

```
43 fprintf('Material Selected: %s\n' , SETTINGS.MATERIAL)
44
45 %% STORE DATA
46 RESULT(i).SETTINGS = SETTINGS; %RUN Settings
47 % fprintf('- - - Step %d/%d - - - \n', i,n );
48
49 %% Dimensions ANSYS model
50 % run MATLAB\Set_Parameters_Small_Scale.m
51 run MATLAB\Set_Parameters_True_Scale.m
52 RESULT(i).PARAM=PARAM; %Store Parameters in results
53
54 %% RUN
55 RESULT = RUN_Scenario(RESULT, i);
56
57 %% SAVE RESULT struct
58 RESULT_Filename = sprintf('MATLAB_Results/Auto_Save_RESULT/RESULT_%s.Mat', datestr(now, 'yyyy-
mm-dd_HH-MM-SS'));
59 save(RESULT_Filename, 'RESULT')
60 fprintf('Storing Data to %s Finished\n',RESULT_Filename)
61 fprintf('- - - RUNNING FINISHED - - - \n')
```

H.2. Setup_Directories.m

Setup_Directories.m

```
1 %% Setup Directories
2
3 function [] = Setup_Directories(PARAM,SETTINGS)
4
5 fprintf('Running from Directory: %s\n' , PARAM.currentFolder)
6
7 % ANSYS_RUN_IN_1 = sprintf('/input, 'Shell_curve_%s', 'ans', '%s', SETTINGS.TYPE,PARAM.
8   currentFolder);
9 % ANSYS_RUN_IN_2 = sprintf('Log_Dir = %s\\Logs',PARAM.currentFolder);
10 % ANSYS_RUN_IN_3 = sprintf('Log_Data = %s\\ANSYS_DATA',PARAM.currentFolder);
11 % ANSYS_RUN_IN_4 = sprintf('Log_Input = %s\\ANSYS_INPUT',PARAM.currentFolder);
12 % ANSYS_RUN_IN_1 = sprintf('/input, 'Shell_curve_%s', 'ans', '%s', SETTINGS.TYPE,PARAM.
13   currentFolder);
14 ANSYS_RUN_IN_1 = sprintf('/clear, START');
15 ANSYS_RUN_IN_2 = sprintf('*DIM, Dir, STRING,200');
16 ANSYS_RUN_IN_3 = sprintf('Dir(1) = %s',PARAM.currentFolder);
17 ANSYS_RUN_IN_4 = sprintf('/input, 'Shell_curve_%s', 'ans', '%s\\ANSYS_INPUT',SETTINGS.
18   TYPE,PARAM.currentFolder);
19
20 ANSYS_RUN_IN_filename = sprintf('%s\\Batch_Folder\\Ansys_matlab_run_in_%s.txt',PARAM.
21   currentFolder,SETTINGS.TYPE);
22 fid = fopen(ANSYS_RUN_IN_filename, 'wt');
23 % fprintf(fid, '%s', ANSYS_RUN_IN_1);
24 fprintf(fid, '%s\n%s\n%s\n%s', ANSYS_RUN_IN_1, ANSYS_RUN_IN_2, ANSYS_RUN_IN_3, ANSYS_RUN_IN_4);
25
26 % fprintf(fid, '%s \n%s \n%s \n%s', ANSYS_RUN_IN_1, ANSYS_RUN_IN_2, ANSYS_RUN_IN_3 );
27 fclose(fid);
28
29 end
```

H.3. Set_Parameters_True_Scale.m

Set_Parameters_True_Scale.m

```

1 %% Set Parameters
2
3 %% Parameters For ANSYS
4 %% Material Properties
5 switch RESULT(i).SETTINGS.MATERIAL
6     case { 'Pla', 'pla', 'PLA' }
7
8         %% Average PLA,
9         PARAM.Density      = 1290;
10        PARAM.Poisson       = 0.331;
11        PARAM.Elastmod      = 2.54e9;
12        %          PARAM.Gmod      = 0.6e9;
13
14        case { 'Steel', 'steel', 'STEEL' }
15            PARAM.CROSS_SECTION = RESULT(i).SETTINGS.CROSS_SECTION;
16
17            %% Average Steel,
18            PARAM.Density      = 7900;
19            PARAM.Poisson       = 0.25;
20            PARAM.Elastmod      = 200e9;
21            %          PARAM.Gmod      = 0.6e9;
22
23        case { 'AISI_301' }
24            PARAM.CROSS_SECTION = RESULT(i).SETTINGS.CROSS_SECTION;
25
26            %% https://www.azom.com/properties.aspx?ArticleID=960
27            PARAM.Density      = 7880;
28            PARAM.Poisson       = 0.275;
29
30            PARAM.Elastmod      = 190e9;
31
32
33            PARAM.UTS           = 185e6;
34            PARAM.YS            = 151e6;
35
36        end
37 %% Dimensions ANSYS model
38 % Shape
39
40 PARAM.P = 0.125; %Outward force point.
41 PARAM.w = 0.45; %Width
42 PARAM.d = PARAM.P + 0.035; %0.145; %Depth
43 PARAM.r = 0.05; %Radus
44
45 %          PARAM.P = PARAM.d/2; %Outward force point.
46
47 %%Cross Section
48 PARAM.bh = 0.034; %Height I Beam
49 PARAM.bw = 0.034; %Width I Beam
50
51
52 PARAM.btw = 0.0008; %Thickness Web
53 PARAM.btf = 0.0008; %Thickness Flange
54
55 %% Spring Constants
56
57 PARAM.F0 = 70; %test
58
59
60 if RESULT(i).SETTINGS.SPRING
61     C = 1.49; %N/mm
62
63     L0 = 86.6; %mm
64     PARAM.L0 = L0*1e-3;
65     PARAM.k = C*1e3; %spring constant
66
67     PARAM.LF = PARAM.L0-(PARAM.F0/PARAM.k); % Voorgespanne lengte voor kracht F0

```

```
68     PARAM.LF_mm = PARAM.LF*1e3;
69
70
71 elseif ~RESULT(i).SETTINGS.SPRING
72     PARAM.dL = 0;
73     PARAM.k = 0; %spring constant
74 end
75
76 %% For SOLIDWORKS
77 PARAM.Wedge_width = 10e-3;
78 PARAM.Wedge_width_TOL = 1e-4;
79
80
81 PARAM.m_balljoint = 17e-3;
82 PARAM.N_balljoint = 3.2e-3;
83 PARAM.h_balljoint = 25e-3;
84
85 PARAM.Lip_Width = 2e-3;
86 PARAM.Lip_Hole_Width_TOL = 15e-4;
87 PARAM.Lip_Hole_Height_TOL = 2e-5;
88 PARAM.Lip_Slot_TOL = -5e-5;
89
90 PARAM.Lip_Hole_Depth_TOL = 1e-4;
91
92
93 %% Matlab Parameters
94 PARAM.Zero_Stiffness_Region_DEG = 7; % Range will be Zero_Stiffness_Region_DEG > x > -
    Zero_Stiffness_Region_DEG
95
96 %% Simulation Parameters
97 PARAM.MAX_Theta_R_DEG = 40; %maximum displacement angle which is checked
98 PARAM.MAX_Theta_R = deg2rad(PARAM.MAX_Theta_R_DEG );
99 PARAM.MAX_UY_R = -(PARAM.d-PARAM.P)*sin(PARAM.MAX_Theta_R); %maximum displacement which is
    checked
100 % PARAM.MAX_UY_R = -0.02; %maximum displacement which is checked
101
102 %% Senarios
103 PARAM.WALK = RESULT(i).SETTINGS.WALK ;
104 PARAM.LIFT = RESULT(i).SETTINGS.LIFT ;
105 PARAM.SPRING = RESULT(i).SETTINGS.SPRING ;
106
107 %% Lifting
108 PARAM.LIFT_STEPS = 50;
109 PARAM.Theta_LIFT_MAX_DEG = 20;
110 PARAM.REQUIREMENT_MAX_MX_LIFT = 30;
111
112 %% Walking
113 PARAM.DISP_STEPS = 60; %EVEN NUMBER
```

H.4. RUN_Scenario.m

RUN_Scenario.m

```
1 %% RUN
2 function [RESULT] = RUN_Scenario(RESULT, i)
3
4 if RESULT(i).SETTINGS.PARAM_FILE || RESULT(i).SETTINGS.ANSYS
5     Write_Parameters_ANSYS(RESULT(i).PARAM)
6
7     if RESULT(i).SETTINGS.PARAM_SOLIDWORKS
8         Write_Parameters_SOLIDWORKS(RESULT(i).PARAM)
9     end
10
11    if RESULT(i).SETTINGS.ANSYS
12        RESULT = Run_ANSYS_Batch(RESULT, i);
13        RESULT = Load_Store_Results(RESULT, i);
14    end
15 end
16
17 if RESULT(i).SETTINGS.LOAD_STORE || RESULT(i).SETTINGS.ANALYSIS
18     if ~RESULT(i).SETTINGS.ANSYS
19         RESULT = Load_Store_Results(RESULT, i);
20     end
21
22     if RESULT(i).SETTINGS.ANALYSIS
23         RESULT = Analysis(RESULT, i);
24     end
25
26     if RESULT(i).SETTINGS.PLOT
27         Plot_Results(RESULT, i)
28     end
29 end
30
31 end
```

H.5. Write_Parameters_ANSYS.m

Write_Parameters_ANSYS.m

```

1 %% Write Parameters for ANSYS
2
3 function [] = Write_Parameters_ANSYS(PARAM)
4
5 fprintf('Creating Parameter file for ANSYS started \n')
6
7 %% Write ANSYS input file
8 Parameter_Filename = 'ANSYS_INPUT/ANSYS_input.txt';
9 fid=fopen(Parameter_Filename, 'wt');
10 fprintf(fid, 'CROSS_SECTION= '%s' \n',PARAM.CROSS_SECTION    );
11
12
13 fprintf(fid, 'Density = %d \n',    PARAM.Density    );
14 fprintf(fid, 'Poisson = %d \n',    PARAM.Poisson    );
15 fprintf(fid, 'Elastmod = %d \n',    PARAM.Elastmod    );
16
17 fprintf(fid, 'w = %d \n',    PARAM.w    );
18 fprintf(fid, 'd = %d \n',    PARAM.d    );
19 fprintf(fid, 'r = %d \n',    PARAM.r    );
20
21 fprintf(fid, 'P = %d \n',    PARAM.P    );
22
23 fprintf(fid, 'bh = %d \n',    PARAM.bh    );
24 fprintf(fid, 'bw = %d \n',    PARAM.bw    );
25 fprintf(fid, 'btw = %d \n',    PARAM.btw    );
26 fprintf(fid, 'btf = %d \n',    PARAM.btf    );
27
28 fprintf(fid, 'k = %d \n',    PARAM.k    );
29 fprintf(fid, 'F0 = %d \n',    PARAM.F0    );
30
31 fprintf(fid, 'MAX_UY_R = %d \n',    PARAM.MAX_UY_R    );
32 fprintf(fid, 'MAX_Theta_R = %d \n',    PARAM.MAX_Theta_R    );
33
34 fprintf(fid, 'LIFT_STEPS = %d \n',    PARAM.LIFT_STEPS    );
35 fprintf(fid, 'Theta_LIFT_MAX_DEG = %d \n',    PARAM.Theta_LIFT_MAX_DEG    );
36
37 fprintf(fid, 'WALK = %d \n',    PARAM.WALK    );
38 fprintf(fid, 'LIFT = %d \n',    PARAM.LIFT    );
39 fprintf(fid, 'SPRING = %d \n',    PARAM.SPRING    );
40
41
42
43 fprintf(fid, 'DISP_STEPS = %d \n',    PARAM.DISP_STEPS    );
44
45
46 fclose(fid);
47 fprintf('Parameters ANSYS written to %s \n', Parameter_Filename)
48 fprintf('Creating Parameter file for ANSYS finished \n')
49 end

```

H.6. Run_ANSYS_Batch.m

Run_ANSYS_Batch.m

```

1 %% Run Ansys
2 function [RESULT] = Run_ANSYS_Batch(RESULT, i)
3 % within starting up ansys, make sure the following is checked:
4 % make sure the vpn is working!!!!
5
6 %% DELETE LOG FOLDER FILES
7
8 try
9     if ~exist('Logs', 'dir')
10         mkdir('Logs')
11     end
12     if RESULT(i).SETTINGS.DEL_LOGS
13         fprintf('Deleting Log Files\n')
14         rmdir('Logs', 's')
15         mkdir('Logs')
16         delete('Logs\*')
17         fprintf('Deleting Log Files Finished\n')
18     end
19 catch ME
20     fprintf('Not all files could be deleted. ERROR:\n%s', ME.message)
21
22 end
23
24 fprintf('START RUNNING ANSYS \n')
25 %% Selecting correct files to run
26 fprintf('Running %s:\n', RESULT(i).SETTINGS.TYPE)
27 BATCH = sprintf('%s" -b -np 6 -d win32 -dir "%s\Logs" -i "Ansys_matlab_run_in_%s.txt" -o "
    Ansys_matlab_run_out.txt"', RESULT(i).PARAM.ANSYS_DIR, RESULT(i).PARAM.currentFolder,
    RESULT(i).SETTINGS.TYPE);
28
29 fprintf('%s\n', BATCH)
30
31 %% STARTING ANSYS IN BATCH MODE
32 tStart = tic; % Find Runtime of ANSYS
33 cd './Batch_Folder'
34 [s, w] = dos('SET ANS_CONSEC=YES', '-echo');
35 [s, w] = dos('SET ANSYS_LOCK=OFF', '-echo');
36 [s, w] = dos('SET KMP_STACKSIZE=4096k', '-echo');
37 [s, w] = dos(BATCH, '-echo');
38 cd('..\')
39 tEnd = toc(tStart); % pair 2: toc
40 RESULT(i).ANSYS_INFO.RUNTIME = tEnd;
41
42 fprintf('Running ANSYS Finished in %4.2f Seconds \n', tEnd)
43 end

```

H.7. Load_Store_Results.m

Load_Store_Results.m

```

1 %% Load and Store Data
2 function [RESULT] = Load_Store_Results(RESULT,i)
3
4 PARAM = RESULT(i).PARAM;
5 Data_File_csv = [ 'ANSYS_DATA/ANSYS_DATA_',RESULT(i).SETTINGS.TYPE, '.csv' ];
6
7 fprintf('Loading File %s\n',Data_File_csv)
8
9 %% CHECKs FOR FILETIME TO SEE IF A NEW FILE HAS BEEN CREATED
10 if RESULT(i).SETTINGS.ANSYS
11     FileInfo = dir(Data_File_csv);
12     FILE_Timestamp = FileInfo.date; %Get timestamp of data file
13     NOW_Timestamp = datetime('now'); %Get timestamp of current moment
14     t_diff = seconds(diff(datetime([FILE_Timestamp; NOW_Timestamp]))); % Get timedifference
15     in seconds
16     RESULT(i).ANSYS_INFO.t_diff = t_diff;
17     fprintf('%s has been modified %4.2f seconds ago\n',Data_File_csv,t_diff)
18     RESULT(i).ANSYS_INFO.Run_Properly = true;
19
20     if t_diff > 5 %checks if the csv file is recent, if not recent then there was probably
21     an error in ansys
22     warning('%s IS NOT A RECENT FILE!!! file is %4.2f Seconds old\nANSYS probably did not
23     run properly. ',Data_File_csv,t_diff)
24     %
25     error('%s IS NOT A RECENT FILE!!! file is %4.2f Seconds old\nANSYS probably
26     did not run properly. ',Data_File_csv,t_diff)
27     %
28     RESULT(i).ANSYS_INFO.Run_Properly = false;
29 end
30
31 if t_diff > RESULT(i).ANSYS_INFO.RUNTIME %checks if the csv file is recent, if not
32 recent then there was probably an error in ansys
33 %
34 warning('%s IS NOT A RECENT FILE!!! file is %4.2f Seconds old\nANSYS
35 probably did not run properly. ',Data_File_csv,t_diff)
36 %
37 error('%s IS NOT A RECENT FILE!!! file is %4.2f Seconds old\nANSYS probably
38 did not run properly. ',Data_File_csv,t_diff)
39 %
40 RESULT(i).ANSYS_INFO.Run_Properly = false;
41 end
42 end
43
44 %% Loading data from ansys
45 ANSYS_DATA_RAW = readtable(Data_File_csv);
46 fprintf('Loading File %s Finished\n',Data_File_csv)
47
48 RESULT_Filename = 'MATLAB_Results/Results.mat';
49 fprintf('Storing Data to %s\n', RESULT_Filename)
50
51 RESULT(i).ANSYS_DATA_RAW=ANSYS_DATA_RAW;
52
53 %% Displacement to angle
54 Theta_R_MAT = asin(-RESULT(i).ANSYS_DATA_RAW.UY_A_R_I/(PARAM.d-PARAM.P));
55 Theta_R_MAT_DEG = rad2deg(Theta_R_MAT);
56 RESULT(i).ANSYS_DATA_RAW.Theta_R_MAT = Theta_R_MAT; %Angle in RAD
57 RESULT(i).ANSYS_DATA_RAW.Theta_R_MAT_DEG = Theta_R_MAT_DEG; %Angle in DEG
58
59 Theta_L_MAT = asin(-RESULT(i).ANSYS_DATA_RAW.UY_A_L_I/(PARAM.d-PARAM.P));
60 Theta_L_MAT_DEG = rad2deg(Theta_L_MAT);
61 RESULT(i).ANSYS_DATA_RAW.Theta_L_MAT = Theta_L_MAT; %Angle in RAD
62 RESULT(i).ANSYS_DATA_RAW.Theta_L_MAT_DEG = Theta_L_MAT_DEG; %Angle in DEG
63
64 %% Get ANSYS angle
65 RESULT(i).ANSYS_DATA_RAW.Theta_R = RESULT(i).ANSYS_DATA_RAW.ROTX_A_R; %Angle in DEG
66 RESULT(i).ANSYS_DATA_RAW.Theta_R_DEG = rad2deg(RESULT(i).ANSYS_DATA_RAW.ROTX_A_R); %Angle
67 in DEG
68
69 %% Ansys Lift angle
70 RESULT(i).ANSYS_DATA_RAW.ROTX_M_M_DEG = rad2deg(RESULT(i).ANSYS_DATA_RAW.ROTX_M_M); %
71 Angle in DEG

```

```

59
60 %% Get Spring Force
61 F0 = PARAM.F0; %Pretention
62 k = PARAM.k; %spring constant
63
64 UX_R = RESULT(i).ANSYS_DATA_RAW.UX_R;
65 UX_L = RESULT(i).ANSYS_DATA_RAW.UX_L;
66
67 F_SPRING_L = -F0-UX_L*k;
68 F_SPRING_R = F0-UX_R*k;
69
70 RESULT(i).ANSYS_DATA_RAW.F_Spring_L = F_SPRING_L; %Spring force Left side
71 RESULT(i).ANSYS_DATA_RAW.F_Spring_R = F_SPRING_R; %Spring force Right side
72
73
74 %% Actuation force to moment
75 RESULT(i).ANSYS_DATA_RAW.M_A_R = RESULT(i).ANSYS_DATA_RAW.FY_A_R.*(RESULT(i).PARAM.P.*cos(
    RESULT(i).ANSYS_DATA_RAW.Theta_R));
76
77 %% ANSYS Lifting Moment
78 RESULT(i).ANSYS_DATA_RAW.MX_LIFT = (RESULT(i).PARAM.P+RESULT(i).PARAM.bw/2-RESULT(i).
    ANSYS_DATA_RAW.UZ_M_M).*(RESULT(i).ANSYS_DATA_RAW.FR_R_FY+RESULT(i).ANSYS_DATA_RAW.
    FR_L_FY);
79
80 %% ANSYS Walking Moment
81 RESULT(i).ANSYS_DATA_RAW.MX_WALK = -(RESULT(i).PARAM.P+RESULT(i).PARAM.bw/2-RESULT(i).
    ANSYS_DATA_RAW.UZ_M_M).*(RESULT(i).ANSYS_DATA_RAW.FR_M_M_FY);
82
83
84 %% Calculate Work, NEEDS TO BE CHECKED, MIGHT BE WRONG
85 RESULT(i).ANSYS_DATA_RAW.Work = RESULT(i).ANSYS_DATA_RAW.MX_WALK.*RESULT(i).ANSYS_DATA_RAW.
    Theta_R_MAT;
86
87
88 %% Remote zeros at the end, Should be fixed later
89 Table_end = min(find(RESULT(i).ANSYS_DATA_RAW.TIME<1e-30));
90 ANSYS_DATA = RESULT(i).ANSYS_DATA_RAW(1:Table_end-1,:);
91 RESULT(i).ANSYS_DATA = ANSYS_DATA;
92
93 %% Force Displacement Range of interest (ROI)
94 ROI_WALK = [2,3];
95 ROI_LIFT = [5,6];
96
97 % RIO for Walking and Lifting
98 RESULT(i).ROI.ROI_WALK = find(RESULT(i).ANSYS_DATA_RAW.TIME>=ROI_WALK(1) & RESULT(i).
    ANSYS_DATA_RAW.TIME<=ROI_WALK(2) );
99 RESULT(i).ROI.ROI_LIFT = find(RESULT(i).ANSYS_DATA_RAW.TIME>=ROI_LIFT(1) & RESULT(i).
    ANSYS_DATA_RAW.TIME<=ROI_LIFT(2) );
100
101 % RIO for No Spring
102 TEMP= find(RESULT(i).ANSYS_DATA_RAW.TIME>=ROI_WALK(1)-1 & RESULT(i).ANSYS_DATA_RAW.TIME<
    ROI_WALK(1));
103 RESULT(i).ROI.ROI_WALK_NOSPRING = [find(RESULT(i).ANSYS_DATA_RAW.TIME>ROI_WALK(2) & RESULT(i)
    .ANSYS_DATA_RAW.TIME<=ROI_WALK(2)+1);TEMP];
104
105 %% ANSYS DATA ROI
106 RESULT(i).ROI.ANSYS_DATA_ROI_WALK = ANSYS_DATA(RESULT(i).ROI.ROI_WALK,:);
107 RESULT(i).ROI.ANSYS_DATA_ROI_LIFT = ANSYS_DATA(RESULT(i).ROI.ROI_LIFT,:);
108 RESULT(i).ROI.ANSYS_DATA_ROI_WALK_NOSPRING = ANSYS_DATA(RESULT(i).ROI.ROI_WALK_NOSPRING,:);
109
110 RESULT(i).PROTOTYPE.Flange.L = 2*(PARAM.d-PARAM.P)+2*(PARAM.P-PARAM.r)+(pi*PARAM.r)+(PARAM.w
    -2*PARAM.r);
111 RESULT(i).PROTOTYPE.Flange.W = PARAM.bh;
112 %% Calculate Potential Energy
113 Theta_E_pot = RESULT(i).ROI.ANSYS_DATA_ROI_WALK.Theta_R_MAT;
114
115 M_E_Pot = RESULT(i).ROI.ANSYS_DATA_ROI_WALK.MX_WALK;
116
117 IDX_Theta_NEG = (Theta_E_pot<0);
118 IDX_Theta_POS = flip(find(Theta_E_pot>=0));
119

```

```
120 E_pot_NEG = cumtrapz(Theta_E_pot(IDX_Theta_NEG),M_E_Pot(IDX_Theta_NEG));
121 E_pot_POS = cumtrapz(Theta_E_pot(IDX_Theta_POS),M_E_Pot(IDX_Theta_POS));
122
123 RESULT(i).ROI.ANSYS_DATA_ROI_WALK.Pot_Energy=[flip(E_pot_POS);(E_pot_NEG)];
124
125 %% Calculating rotational stiffness at Theta = 0
126
127 Theta_k = RESULT(i).ROI.ANSYS_DATA_ROI_WALK.Theta_R_MAT;
128 M_k      = RESULT(i).ROI.ANSYS_DATA_ROI_WALK.MX_WALK;
129
130 k = diff(M_k)./diff(Theta_k);
131
132 RESULT(i).ANALYZED.k_rot =k;
133 RESULT(i).ANALYZED.k_rot_0= min(k);
134
135
136 %% SAVE RESULT to file
137 save(RESULT_Filename, 'RESULT');
138 fprintf('Storing Data to %s Finished\n',RESULT_Filename)
139
140 end
```

H.8. Analysis.m

Analysis.m

```
1 %% Analysis
2 function [RESULT] = Analysis (RESULT, i)
3 %% RMSE
4 RESULT = RMSE_Force (RESULT, i); %Get the Root Mean Squared Error Force
5 RESULT = RMSE_Moment (RESULT, i); %Get the Root Mean Squared Error Moment
6 RESULT = RMSE_Weighted_Force (RESULT, i); %Get the Weighted Root Mean Squared Error Force
7 RESULT = RMSE_Weighted_Moment (RESULT, i); %Get the Weighted Root Mean Squared Error Moment
8
9 RESULT = RMSE_Work (RESULT, i); %Get the Root Mean Squared Error Work
10 RESULT = RMSE_Pot_Energy (RESULT, i); %Get the Root Mean Squared Error
11
12 %% Storing Analysis
13 RESULT_Filename = 'MATLAB_Results/Results.mat';
14 save (RESULT_Filename, 'RESULT');
15 fprintf ('Storing Analysis to %s Finished\n', RESULT_Filename)
16
17 end
```

Optimisation Code

I.1. Run_ANSYS_Optimisation_bh_bw_F0.m

Run_ANSYS_Optimisation_bh_bw_F0.m

```
1
2 % Robin Mak
3 clc; clear all; close all;
4 cd( '..\ ' )
5
6 addpath( 'MATLAB' ) %Include MAIN folder
7 addpath( 'Optimization\Objective_Functions' ) %Include folder
8 addpath( 'Optimization\Constraint_Functions' ) %Include folder
9
10 %% INIT
11 RESULT = struct;
12 i=1;
13
14 %% RUN Settings
15 SETTINGS.TYPE = 'ALL_ROT';
16 SETTINGS.SPRING = 1; % 1 = Spring, 0 = constant Force
17
18 SETTINGS.WALK = 1; % 1=on , 0=off % Start Walking Senario
19 SETTINGS.LIFT = 1; % 1 =on , 0=off % Start Lifting Senario
20
21 % Run ANSYS
22 SETTINGS.ANSYS = 1; % 1=on , 0=off %Run ansys or not
23
24 % Run Matlab Sections
25 SETTINGS.PARAM_FILE = 1;
26 SETTINGS.LOAD_STORE = 1; % 1=on , 0=off %Run ansys or not
27 SETTINGS.PLOT = 0;
28 SETTINGS.ANALYSIS = 1;
29 SETTINGS.DEL_LOGS = 1; %Deletes all log files , log files can give problems in some
30 instances
31 SETTINGS.PARAM_SOLIDWORKS = 1;
32
33 SETTINGS.MATERIAL = 'AISI_301'; %'Steel'; %PLA, Steel
34 SETTINGS.CROSS_SECTION = 'H';
35
36 %% SET ANSYS DIRECTORY!
37 % Things to Check before running:
38 % 1) Locate ANSYS195.exe file and paste below
39 % 2) Make sure the vpn is running
40 % 3) If Ansys does not run properly, delete all files in the Logs folder
41 % 4) Check if first 4 lines are commented of ans file
42 PARAM.ANSYS_DIR = "C:\Program Files\ANSYS Inc\v195\ansys\bin\winx64\ANSYS195.exe";
43 PARAM.currentFolder = pwd;
44 RESULT(i).PARAM=PARAM; %Store Parameters in results
45
```

```
46 Setup_Directories(PARAM,SETTINGS) % Fixes all directories!
47
48 %% RUN
49 fprintf(' - - START RUNNING %s - -\n',SETTINGS.TYPE)
50 fprintf('Material Selected: %s\n' , SETTINGS.MATERIAL)
51
52 %% STORE DATA
53 RESULT(i).SETTINGS = SETTINGS; %RUN Settings
54
55 %% Dimensions ANSYS model
56 % run MATLAB\Set_Parameters_Small_Scale.m
57 run MATLAB\Set_Parameters_True_Scale.m
58
59 RESULT(i).PARAM=PARAM; %Store Parameters in results
60
61
62 %% OPTIMISATION bw bh
63 run Optimization\Optimization_bh_bw_same.m
64
65 RESULT(i).PARAM.bh = x(1);
66 RESULT(i).PARAM.bw = x(2);
67
68 %% OPTIMISATION F0
69 run Optimization/Optimization_F0.m
70 RESULT(i).PARAM.F0 = x(1);
71
72
73 save('MATLAB_Results/optimization_results')
74
75 %% SAVE RESULT struct
76 RESULT_Filename = sprintf('MATLAB_Results/Auto_Save_RESULT/RESULT_OPTIMIZED_%s.Mat', datestr(
    now, 'yyyy-mm-dd_HH-MM-SS'));
77 save(RESULT_Filename, 'RESULT')
78 fprintf('Storing Data to %s Finished\n',RESULT_Filename)
79 fprintf(' - - RUNNING FINISHED - -\n')
```

I.2. Optimization_bh_bw_same.m

Optimization_bh_bw_same.m

```
1 cd( '..\ ' )
2
3
4 %% OPTIMISATION bh bw
5 RESULT(i).PARAM.F0 = 0; %find optimum without spring
6 % initial guess and constraints
7 %Design variables
8 nvars = 2;
9 x0 = [0.04 ];
10 lb =[0.025 ];
11 ub = [0.06];
12 A = [];
13 b = [];
14 Aeq = [];
15 beq = [];
16 nonlcon=[];
17 % F = [0.001];
18
19 %% Store
20 RESULT(i).OPTIMIZATION.bh_bw.x0 = x0;
21 RESULT(i).OPTIMIZATION.bh_bw.lb = lb;
22 RESULT(i).OPTIMIZATION.bh_bw.ub = ub;
23 RESULT(i).OPTIMIZATION.bh_bw.nonlcon = nonlcon;
24
25
26 % fmincon function and its settings
27 Obj_Func_bh_bw = @(X) OBJ_FUNC_Run_ANSYS_bh_bw_same(RESULT,X);
28
29 %% OPTIONS
30 OPTIONS = optimoptions( 'fmincon' , 'Display' , 'iter-detailed' );
31
32 OPTIONS.Algorithm = 'interior-point';
33
34 OPTIONS.MaxIterations = 100;
35 OPTIONS.MaxFunEvals = 200;
36 OPTIONS.DiffMinChange = 0.001;
37 OPTIONS.TolX = 0.0001;
38
39
40 %% Optimization
41 fprintf( 'Starting Optimization bh bw\n' );
42
43 [x, fval, exitflag, output, lambda, grad, hessian] = fmincon( Obj_Func_bh_bw, x0, A, b, Aeq, beq, lb, ub,
44 nonlcon, OPTIONS );
45 fprintf( 'Optimization bw bh finished\n' );
46 save( 'MATLAB_Results/optimization_results_bw_bh' )
47
48 RESULT(i).OPTIMIZATION.bh_bw.OPTIONS = OPTIONS;
49 RESULT(i).OPTIMIZATION_RESULT.bh_bw.x = x;
50 RESULT(i).OPTIMIZATION_RESULT.bh_bw.fval = fval;
51 RESULT(i).OPTIMIZATION_RESULT.bh_bw.exitflag = exitflag;
52 RESULT(i).OPTIMIZATION_RESULT.bh_bw.output = output;
```

I.3. OBJ_FUNC_Run_ANSYS_bh_bw_same.m

OBJ_FUNC_Run_ANSYS_bh_bw_same.m

```

1
2 function [MINIMIZE,RESULT] = OBJ_FUNC_Run_ANSYS_bh_bw_same(RESULT,X)
3 i=1;
4
5 fprintf('Running for bh = %4.6f, bw = %4.6f\n',X(1),X(1))
6
7 switch RESULT(i).SETTINGS.SPRING
8     case 0 %Constant Force
9         %% Varying parameters for Constant Force
10        RESULT(i).PARAM.bh = X(1);
11        RESULT(i).PARAM.bw = X(1);
12
13
14        case 1 %Spring Force
15            %% Varying parameters for Spring
16            RESULT(i).PARAM.bh = X(1);
17            RESULT(i).PARAM.bw = X(1);
18
19 end
20
21 %% RUN
22 RESULT = RUN_Senario(RESULT, i);
23
24 MAX_MX_LIFT = max(RESULT(i).ANSYS_DATA.MX_LIFT);
25 REQUIREMENT_MAX_MX_LIFT = RESULT(i).PARAM.REQUIREMENT_MAX_MX_LIFT;
26
27 P = 1000;
28 PENALTY = P*max(0, REQUIREMENT_MAX_MX_LIFT - MAX_MX_LIFT)^2;
29
30 RMSE_MOMENT = RESULT(i).ANALYZED.RMSE_Moment;
31 W_RMSE_MOMENT = 100;
32
33 BH = RESULT(i).PARAM.bh;
34 W_BH = 0;
35
36 BW = RESULT(i).PARAM.bw;
37 W_BW = 0;
38
39 %% CHECK IF RESULTS BELONG TO THIS RUN
40 if RESULT(i).ANSYS_INFO.RUNTIME > RESULT(i).ANSYS_INFO.t_diff % Check if file is recent and
41     corresponds to this run
42     MINIMIZE = W_RMSE_MOMENT*RMSE_MOMENT + W_BH*BH + W_BW*BW + PENALTY
43 else
44     MINIMIZE = NaN % If file is outdated a NaN will be returned
45 end
46 end

```

I.4. Optimization_F0.m

Optimization_F0.m

```

1 cd('..\')
2
3 %% OPTIMISATION F0
4 % initial guess and constraints
5 %Design variables
6 % X0 = [bh bw f0]
7 nvars = 1;
8 x0 = [1];
9 lb =[0];
10 ub = [120];
11 A = [];
12 b = [];
13 Aeq = [];
14 beq = [];
15 nonlcon = [];
16
17 %% Store
18 RESULT(i).OPTIMIZATION.F0.x0 = x0;
19 RESULT(i).OPTIMIZATION.F0.lb = lb;
20 RESULT(i).OPTIMIZATION.F0.ub = ub;
21 RESULT(i).OPTIMIZATION.F0.nonlcon = nonlcon;
22
23 % fmincon function and its settings
24
25 Obj_Func_F0 = @(X) OBJ_FUNC_Run_ANSYS_F0(RESULT,X);
26 % Obj_Func_F0(x0)
27
28 %% OPTIONS
29 OPTIONS = optimoptions('fmincon','Display','iter-detailed');
30 OPTIONS.Diagnostics = 'on';
31
32 % OPTIONS.Algorithm = 'active-set';
33 % OPTIONS.Algorithm = 'sqp';
34 OPTIONS.Algorithm = 'interior-point';
35
36 OPTIONS.MaxIterations = 100;
37 OPTIONS.MaxFunEvals = 200;
38 OPTIONS.DiffMinChange = 0.1;
39 OPTIONS.ToIX = 0.01;
40
41
42 %% Optimization
43 fprintf('-- Starting Optimization F0 -- \n');
44
45 [x,fval,exitflag,output,lambda,grad,hessian] = fmincon(Obj_Func_F0,x0,A,b,Aeq,beq,lb,ub,
46     nonlcon,OPTIONS);
47 save('MATLAB_Results/optimization_results_F0')
48 fprintf('-- Optimization F0 Finished -- \n');
49
50 RESULT(i).OPTIMIZATION.F0.OPTIONS = OPTIONS;
51 RESULT(i).OPTIMIZATION_RESULT.F0.x = x;
52 RESULT(i).OPTIMIZATION_RESULT.F0.fval = fval;
53 RESULT(i).OPTIMIZATION_RESULT.F0.exitflag = exitflag;
54 RESULT(i).OPTIMIZATION_RESULT.F0.output = output;

```

I.5. OBJ_FUNC_Run_ANSYS_F0.m

OBJ_FUNC_Run_ANSYS_F0.m

```

1
2 function [MINIMIZE,RESULT] = OBJ_FUNC_Run_ANSYS_F0(RESULT,X)
3 i=1;
4
5 fprintf('Running for F0 = %4.6f\n',X(1))
6 %% Variable Parameters; Overwrite values above
7
8 switch RESULT(i).SETTINGS.SPRING
9     case 0 %Constant Force
10         %% Varying parameters for Constant Force
11         RESULT(i).PARAM.F0 = X(1);
12
13
14     case 1 %Spring Force
15         %% Varying parameters for Spring
16         RESULT(i).PARAM.F0 = X(1);
17
18 end
19
20 %% RUN
21 RESULT = RUN_Senario(RESULT, i);
22
23 MAX_MX_LIFT = max(RESULT(i).ANSYS_DATA.MX_LIFT);
24 REQUIREMENT_MAX_MX_LIFT = RESULT(i).PARAM.REQUIREMENT_MAX_MX_LIFT;
25
26 P = 10;
27 PENALTY = max(0, REQUIREMENT_MAX_MX_LIFT - MAX_MX_LIFT)^4;
28
29 RMSE_MOMENT = RESULT(i).ANALYZED.RMSE_Moment;
30 W_RMSE_MOMENT = 100;
31
32 BH = RESULT(i).PARAM.bh;
33 W_BH = 0;
34
35 BW = RESULT(i).PARAM.bw;
36 W_BW = 0;
37
38 %% CHECK IF RESULTS BELONG TO THIS RUN
39 if RESULT(i).ANSYS_INFO.RUNTIME > RESULT(i).ANSYS_INFO.t_diff % Check if file is recent and
40     corresponds to this run
41     MINIMIZE = W_RMSE_MOMENT*RMSE_MOMENT + W_BH*BH + W_BW*BW + P*PENALTY
42 else
43     MINIMIZE = NaN % If file is outdated a NaN will be returned
44 end
45 end

```